Pontifícia Universidade Católica
do Rio de Janeiro

Alexandre Augusto Abreu Almeida

A study on thermal conduction and rectification

Dissertação de Mestrado

Dissertation presented to the Programa de Pós–graduação em Física of PUC-Rio in partial fulfillment of the requirements for the degree of Mestre em Física.

Advisor : Profa. Celia Beatriz Anteneodo de Porto
Co-advisor: Dr. Lucianno Augusto Coddato Antunes e Defaveri

Rio de Janeiro
April 2021

Pontifícia Universidade Católica
do Rio de Janeiro

Alexandre Augusto Abreu Almeida

A study on thermal conduction and rectification

Dissertation presented to the Programa de Pós–graduação em Física of PUC-Rio in partial fulfillment of the requirements for the degree of Mestre em Física. Approved by the Examination Committee:

Profa. Celia Beatriz Anteneodo de Porto
Advisor
Departamento de Física – PUC-Rio

Dr. Lucianno Augusto Coddato Antunes e Defaveri
Co-advisor
Departamento de Física – PUC-Rio

Prof. Carlos Eduardo Fiore dos Santos
USP

Prof. Emmanuel Araújo Pereira
UFMG

Prof. Welles Antônio Martinez Morgado
Departamento de Física – PUC-Rio

Rio de Janeiro, April 23rd, 2021

Alexandre Augusto Abreu Almeida

Majored in Chemical Engineering by Universidade Federal do Rio de Janeiro - UFRJ (Rio de Janeiro, Brazil) in 2017.

Bibliographic data

Almeida, Alexandre A. A.

A study on thermal conduction and rectification / Alexandre Augusto Abreu Almeida; advisor: Celia Beatriz Anteneodo de Porto; co-advisor: Lucianno Augusto Coddato Antunes e Defaveri. – Rio de janeiro: PUC-Rio, Departamento de Física, 2021.

v., 107 f: il. color. ; 30 cm

Dissertação (mestrado) - Pontifícia Universidade Católica do Rio de Janeiro, Departamento de Física.

Inclui bibliografia

1. Física – Teses. 2. dinâmica não linear;. 3. dinâmica estocástica;. 4. condução de calor;. 5. diodo térmico.. I. Anteneodo, Celia. II. Defaveri, Lucianno. III. Pontifícia Universidade Católica do Rio de Janeiro. Departamento de Física. IV. Título.

CDD: 530

Dedicated to my late father, Aderbal Gil de Oliveira Almeida.

Acknowledgments

First, I wish to thank my father, who was my main inspiration in life, and my mother, who is my main support in life. Any accomplishment of mine is thanks to both of you.

Then, I wish to thank my advisor, prof. Celia Anteneodo, who not only proposed me such an interesting research topic as thermal diodes, but also taught me how to do great science, while having patience with all my shortcomings (and there were a lot of them).

I also wish to thank my co-advisor, Dr. Lucianno Defaveri, for all the answers to my questions on the fundamentals of thermodynamics and statistical physics. I finally understand the conceptual difference between Liouville's theorem and the Fokker-Planck equation (I think).

I would like to thank all professors from PUC-Rio whom I had the pleasure of learning from, specially prof. Welles Morgado, who taught me how to "think thermodynamics" (extracting work from information is still mind boggling), and prof. Arman Esmaili, who showed me how physics intuition and mathematics goes hand in hand (and taught me about the monster group).

I wish to thank all my colleagues from the Complex Systems group at PUC-Rio, who have shown me a myriad of interesting problems (including some curious ones, like the C. elegans nervous system).

I would like to thank everyone who worked with me at FGV and in projects Supremo em Números and Regulação em Números, specially Ivar Hartmann, Fernando Correira, Felipe Araújo, Guilherme Almeida, Kaline Santos and José Luiz. If I know anything about programming, it is thanks to you teaching me, whenever I poked you guys in the middle of work (probably because I broke something).

I want to thank all the friends I made in PUC-Rio, whom I had the joy of crossing paths with. You gave me a warm welcome to the physics department and a lot of fun moments afterwards (like getting trapped in the department, due to the rain, for an entire night).

I wish to thank Pedro, Álvaro and Uchôa. You were always there for me for the last twenty years (maybe more, I already lost count).

I also wish to thank my Kling friends, who have supported me for the last fifteen years. I love our many discussions (from politics to disney movie songs), you guys are amazing!

Last, but not least, I would like to thank CNPq and CAPES. This study was financed in part by the Coordenação de Aperfeiçoamento de Pessoal de Nível Superior - Brasil (CAPES) - Finance Code 001.

Abstract

Almeida, Alexandre A. A.; Anteneodo, Celia (Advisor); Defaveri, Lucianno (Co-Advisor). **A study on thermal conduction and rectification**. Rio de Janeiro, 2021. 107p. Dissertação de mestrado – Departamento de Física, Pontifícia Universidade Católica do Rio de Janeiro.

It is a known result in the literature that a one-dimensional chain of particles that interact harmonically with its first neighbors does not conduct heat, and nonlinear forces are needed to reproduce Fourier's law of heat conduction. When asymmetries are introduced in such a conducting system, a rectifying effect is obtained where the thermal current shows different magnitudes depending on which side of the chain has higher temperature, such devices being called thermal diodes. In this work we study both phenomena, heat conduction and thermal rectification, in a one-dimensional chain of particles, with fixed boundary conditions, coupled to two thermal baths, one at each end, modeled as Langevin thermostats. The particles interact with their first neighbors harmonically and have a nonlinear on-site potential, for which we study two types, Frenkel-Kontorova and ϕ^4 potentials. We verify that, for both cases, Fourier's law is observed, where the temperature profile and the thermal conductivity are dependent on the relation between the harmonic and anharmonic amplitudes, and the system's average temperature. Next, to create an asymmetry in the chain, we coupled two different segments of equal lengths. We observed a rectifying effect, where the preferential direction differs for each of the two on-site potentials studied. How the heat-bath temperatures changes the magnitude of rectification was also observed. We also investigated the effect of interfacial nonlinearities through a power-law potential, coupling ϕ^4 segments. By changing the power-law exponent, we looked for the conditions under which optimal rectification is achieved.

Keywords

nonlinear dynamics; stochastic dynamics; heat conduction; thermal diode.

Resumo

Almeida, Alexandre A. A.; Anteneodo, Celia; Defaveri, Lucianno. **Um estudo sobre condução e retificação térmica**. Rio de Janeiro, 2021. 107p. Dissertação de Mestrado – Departamento de Física, Pontifícia Universidade Católica do Rio de Janeiro.

É um resultado conhecido na literatura que uma cadeia unidimensional de partículas, que interagem harmonicamente com seus primeiros vizinhos, não conduz calor, e forças não lineares são necessárias para reproduzir a lei de Fourier da condução de calor. Quando são introduzidas assimetrias em tal sistema condutor, se obtém um efeito retificador onde a corrente térmica apresenta magnitudes diferentes dependendo de qual lado da cadeia tem maior temperatura, tais dispositivos sendo chamados de diodos térmicos. Neste trabalho estudamos os dois fenômenos, condução de calor e retificação térmica, em uma cadeia unidimensional de partículas, com condições de contorno fixas, acopladas a dois banhos térmicos, um em cada extremidade, modelados como termostatos de Langevin. As partículas interagem com seus primeiros vizinhos harmonicamente e estão sujeitas a um potencial localizado externo não linear, para o qual estudamos dois tipos, os potenciais Frenkel-Kontorova e ϕ^4. Verificamos que a lei de Fourier é observada, para ambos os casos, com o perfil de temperatura e a condutividade térmica dependendo da relação entre as amplitudes harmônica e anarmônica, e a temperatura média do sistema. Em seguida, para criar uma assimetria na cadeia, nós acoplamos dois segmentos de mesmo tamanho. Observamos um efeito retificador onde a direção preferencial difere para cada potencial localizado estudado. A forma como as temperaturas dos banhos térmicos mudam a magnitude da retificação também foi observada. Nós também investigamos o efeito de não linearidades interfaciais, por meio de uma lei de potência que acopla segmentos ϕ^4. Alterando o expoente da lei de potência, nós buscamos as condições sob as quais a retificação ótima é atingida.

Palavras-chave

dinâmica não linear; dinâmica estocástica; condução de calor; diodo térmico.

Table of contents

"He fixes radios by thinking!" The whole idea of thinking, to fix a radio - a little boy stops and thinks, and figures out how to do it - he never thought that was possible.

Richard P. Feynman, *Surely you're joking Mr. Feynman!.*

1
Introduction

In 2006, four researchers from the University of California at Berkeley published what was perhaps the first experimental evidence of a thermal diode, a material whose thermal conductivity along a given axis changed depending on the direction of the heat flux along it [1].

They used an experimental apparatus consisting of two pads with platinum resistors that could operate as either a heater - through Joule effect - or as a sensor - through their resistivity variation with temperature.

Each pad was connected to each end of a nanotube which was coated inhomogeneously with trimethyl-cyclopentadienyl platinum ($C_9H_{16}Pt$) and measured the conductivity along its axis with two different configurations, the first one with the heater on the side with more mass and then with the heater on the side with less mass, effectively changing the direction of heat flow, as expected. What was surprising was that the magnitude of the heat flow changed too, with the thermal conductivity of the material changing as much as 7%.

The experiment was repeated with different materials such as carbon nanotubes - CNTs - and boron nitride nanotubes - BNNTs. These materials have high thermal conductivity (compared to the hydrocarbon), dominated by phononic carriers.

Following these results, different research groups were able to devise new ways of obtaining such asymmetric conductivity, with higher and higher differences in the thermal conductivity [2, 3, 4, 5, 6, 7].

Theoretical ways of building such a device were envisioned before this first experimental evidence, being the paper by Terraneo, Peyrad and Casati [8], published in 2002, one of the pioneering works.

In order for us to begin studying this phenomenon, we must first discuss the basic concepts of heat conduction and of the theory of thermal conductivity in solids.

1.1 Basic notions of heat conduction

Before diving into the microscopic understanding of the problem at hand, we need first to look at the basic macroscopic heat conduction problem to develop some intuition [9].

First let us consider a system delimited by a given closed surface $\partial V \in \mathbb{R}^3$ with normal vector $\vec{n}$ pointing outside the system's volume, as in figure 1.1.

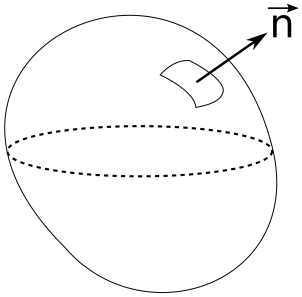

Figure 1.1: Control volume system.

From the first law of thermodynamics, we have that

$$\frac{dU}{dt} = \dot{Q} + \dot{W}, \tag{1-1}$$

where U is the internal energy of the system, $\dot{Q}$ is the rate of heat that enters it, and $\dot{W}$ is the rate of work done by the environment on the system. Assuming no external work is applied, we get a continuity equation, using the internal energy density u and the fact that heat into the system is given by $-\dot{\vec{q}} \cdot \vec{n}$, where $\dot{\vec{q}}$ is the heat flux ($\dot{Q}$ by surface area) into the system, namely,

$$\frac{d}{dt} \iiint_V u \, dV + \iint_{\partial V} \dot{\vec{q}} \cdot \vec{n} \, dS = 0. \tag{1-2}$$

Now assuming the internal energy is sufficiently smooth so that we can put the derivative inside the integral, apply Gauss's theorem on the second term, and rewrite the internal energy density as $u = C\rho T$, using the specific heat capacity C, we have the continuity equation

$$\iiint_V \left[C\rho \frac{\partial T}{\partial t} + \vec{\nabla} \cdot \dot{\vec{q}} \right] dV = 0, \tag{1-3}$$

and hence

$$C\rho \frac{\partial T}{\partial t} + \vec{\nabla} \cdot \dot{\vec{q}} = 0. \tag{1-4}$$

In the XIX century, the mathematician Jean-Baptiste Joseph Fourier coined the phenomenological law that takes his name, Fourier's law of con-

duction, that the flow of heat developed in a material due to a temperature gradient $\vec{\nabla}T$ is proportional to such a gradient [10], so mathematically we have

$$\dot{\vec{q}} = -\kappa\vec{\nabla}T, \tag{1-5}$$

κ being the thermal conductivity, which is always positive. Putting equations 1-4 and 1-5 together, we have a derivation of the famous heat equation

$$\alpha^2\frac{\partial T}{\partial t} - \nabla^2 T = 0, \tag{1-6}$$

where $\alpha = C\rho/\kappa$. This equation describes the dynamics of the temperature of the system with time.

Let us look at a simple one-dimensional case [11]. Suppose we have a solid bar with length L, cross-sectional area A, and thermal conductivity κ, in contact with two thermal baths, one on each side and with temperatures T_L, T_R such that $T_L > T_R$, as illustrated in figure 1.2.

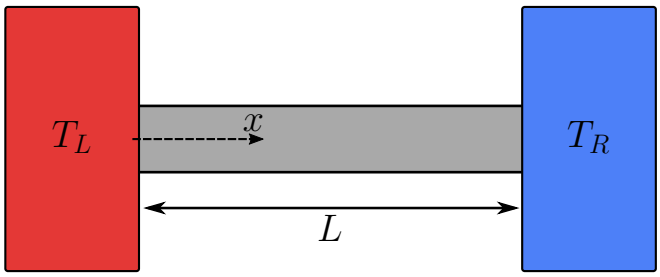

Figure 1.2: One-dimensional heat transport.

We further assume that $L^2 \gg A$, the lateral surface of the bar is isolated from the environment, and κ is homogeneous and does not vary with temperature. In this case, Fourier's law takes the form

$$\dot{q} = -\kappa\frac{dT}{dx}. \tag{1-7}$$

It is expected that, as time goes to infinity, the system approaches a steady state where the heat flux $\dot{q}$ is constant, and as such we can use the boundary conditions $T(x = 0) = T_L$ and $T(x = L) = T_R$ to integrate the temperature and get

$$T = -\frac{(T_L - T_R)}{L}x + T_L, \tag{1-8}$$

showing that the temperature profile along the bar in the steady state is linear, as in figure 1.3. The fact that the system approaches the steady state, with $\dot{q}$ constant in time, can be proven from an analysis of the heat equation [12].

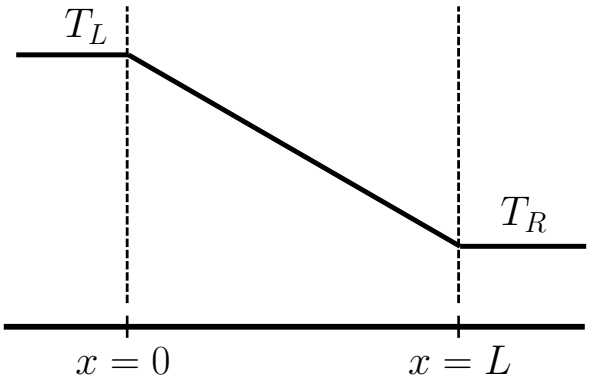

Figure 1.3: Linear temperature profile.

If we replace this result back to Fourier's law we get

$$\frac{\dot{q}}{\Delta T} = -\frac{\kappa}{L}, \tag{1-9}$$

where $\Delta T = T_L - T_R$, showing us that the heat flow is inversely proportional to the length of the bar.

The theoretical proposals for thermal diodes came as a consequence of many works that tried to understand what properties are needed by microscopic models to reproduce, at least approximately, the properties described by equations 1-9 and 1-8.

1.2 Thermal conductivity of solids

Most solids are composed by a regular lattice of atoms or ions that vibrate near their equilibrium positions. The range of their interactions can vary, depending on the nature of the system, from nearest neighbors to more distant ones, with the simplest description given by a chain of atoms interacting harmonically with their first neighbors, such as depicted in figure 1.4.

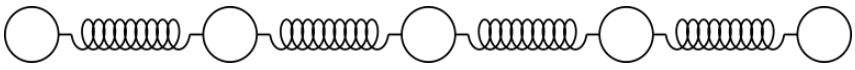

Figure 1.4: Lattice of atoms.

The lattice vibrations affect the thermal conductance of solids differently depending on the material. When looking at their electrical conductivity, solids

are classified as conductors and insulators. Electrical conductors are usually good thermal conductors, for their free electrons act as the main thermal energy carrier in the material. In this case, although the lattice vibrations have to be taken into account to explain some phenomena, they represent generally higher order corrections [13]. Insulators, however, although they do not have such good thermal conductance as they lack electrons in free conducting bands of energy, they do conduct heat with their main carriers being lattice vibrations. These vibrations carry energy on their normal modes, which can interact between them and with other systems such as X-ray electrons, as well as propagate along the crystal as wave packets.

Quantum mechanically, these excitations can be described as quasiparticles called phonons, permitting us to describe the heat transport of insulators by means of a kinetic theory of phonons. In this case, the phononic version of the Boltzmann equation is called Peierls-Boltzmann equation, in honor to sir Rudolf Ernst Peierls who first discovered it [14].

He is also credited with another important discovery, the role of anharmonic interaction terms in the conduction of heat. Perfectly harmonic crystals would have infinite thermal conductivity.

The argument, which can be found in his book [15], first published in 1955, and in ref. [13], goes as follows: in a perfectly harmonic crystal, the distribution of phonons is always composed of stationary modes and, as such, if we prepared them in a way that they were transporting heat, they would remain even without thermal gradient, meaning that the crystal would have infinite thermal conductivity.

In fact, when considering the total potential U on the chain, if we were to expand it as a Taylor series around the lattice equilibrium position as

$$U = U_0 + \frac{1}{2!}\sum_{i,j}\left.\frac{\partial^2 U}{\partial q_i q_j}\right|_{q_i,q_j=0} q_i q_j + \frac{1}{3!}\sum_{i,j,k}\left.\frac{\partial^3 U}{\partial q_i q_j q_k}\right|_{q_i,q_j q_k=0} q_i q_j q_k + \dots , \quad (1\text{-}10)$$

with q_i being the displacement from equilibrium for the i-th particle, we would need to consider terms of order higher than two to overcome the infinite conductivity problem.

These corrections give rise to umklapp processes, which are phonon-phonon collisions that do not conserve total crystal momentum, leading to some thermal resistance in the material.

The fact that the harmonic model does not describe real materials well has also been shown, for one dimensional formulations, from the point of view of classical statistical mechanics by Rieder, Lebowitz and Lieb in [16]. They found the exact form of the temperature profile and the thermal conductivity,

for a harmonic chain of particles, in contact with two heat baths at different temperatures.

They showed that the temperature is approximately flat in the bulk of the chain (with deviations at the extremities [17]), with value $(T_L + T_R)/2$, instead of the linear temperature profile we would expect from Fourier's law (see figure 1.5). They also proved that the heat current in the chain is proportional to the temperature difference between both heat baths $J \propto (T_L - T_R)$, instead of the temperature gradient, as in section 1.1, and hence $\kappa \propto N$ (diverging in the thermodynamic limit $N \to \infty$).

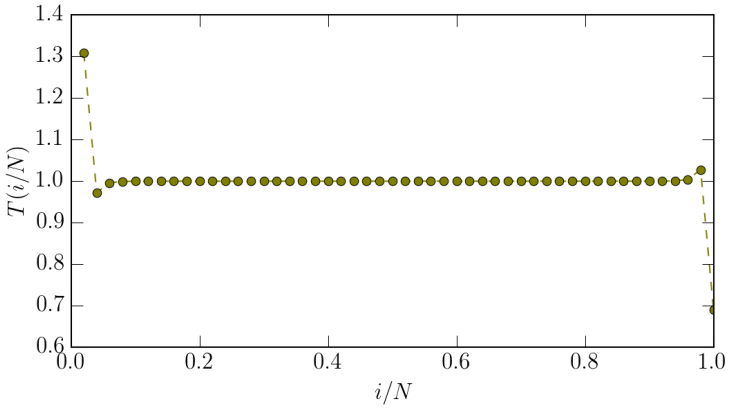

Figure 1.5: Temperature profile calculated using the theoretical results from Rieder, Lebowitz and Lieb [16, 14] for $N = 50$. For the heat conduction, they find $\kappa \propto N$, and so it increases linearly with the number of particles in the chain.

After their work, many others followed on using the framework of classical mechanics to prove that, in general, non conservation of momentum, or of other quantities, is required to reproduce Fourier's law [18].

Many models were able to reproduce these results, such as the ding-a-ling model [19, 20], the ding-dong model [21], the Frenkel-Kontorova model [22] and the ϕ^4 model [23]. Others, like the Fermi-Pasta-Ulam-Tsingou model, does not show the wanted properties, even though it have nonlinearities in the Hamiltonian [24].

All these works culminated in the proposal of thermal rectification using an asymmetric chain of particles.

1.3 Thermal diode

In 2002, Terraneo, Peyrad and Casati [8] published a paper on low-dimensional heat conduction using harmonic interactions between the particles

and a Morse external potential $V(x) = D(\exp(-\alpha x_i) - 1)^2$. They showed that, when D varies along the chain, we could theoretically have a thermal rectifier.

The rationale presented was that changing this parameter, the overlap of the phonon bands in different parts of the chain is lessened, hampering the capacity of the phonons to travel along it.

Following this work, Li, Wang and Casati showed in 2004 [25] such a heat current rectifying mechanism in a 1D nonlinear lattice with a Frenkel-Kontorova potential $A[1-\cos(2\pi x_i)]$ and an harmonic inter-particle interaction by choosing different parameters for the left and right segments of the lattice.

Like we stated previously, the experimental confirmation of a thermal diode came in 2006 [1], albeit with a really small efficiency. Many other papers followed suit with new ways of achieving this asymmetrical thermal conductivity, striving to achieve higher and higher efficiencies, with a work in 2015 by Martínez-Pérez, Fornieri and Giazotto, from the Istituto Nanoscienze-CNR and the Scuola Normale Superiore, showing a heat current in one direction two orders of magnitude higher than the heat current in the opposite direction, when combining normal metals with superconductors [4].

Such devices open the door to very exciting applications.

One option is using thermal diodes for nanoscale refrigeration cycles, where they act as a wall for blocking undesired heat leakages [26]. They could also be applied for solar thermal energy harvesting, by maintaining a temperature difference between two points, even during the night [26]. Such difference would then be used in a heat engine.

Another option are thermal analogs of some electrical circuits could be built [26]. Some examples, by Wehmeyer et. al., are detectors of temperature peaks and DC restorers (also called clampers, they add an offset to oscillatory signals), so that we could avoid freezing materials subject to temperature oscillations. In fact, this open the way for looking at phonons not as wasted energy carriers, but as information carriers, and doing "thermal computations" with them (such control of phonons is studied by an emerging field called phononics) [27, 28].

2
Heat flow in particle chains

The transport of phonons in one dimension is commonly modeled by replacing the bar in figure 1.2, where heat conduction takes place, by a chain of interacting particles (see figure 2.1) and framing the problem in a classical point of view, but interpreting the results with the language of phonons. In accordance to what we discussed in section 1.2, each particle will also be subjected to an anharmonic on-site potential. An in-depth discussion is given in section 2.1.

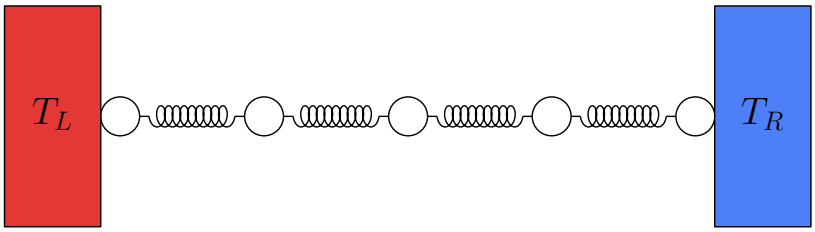

Figure 2.1: Pictorial representation of the mathematical model.

The heat baths also need some kind of microscopic description, and there are two main ways to achieve this. The first one, which we shall use here, is the Langevin thermostat, where a random noise term and a dissipation term are added directly into the equations of motion of the particles in contact with the bath. The second one, called Nosé-Hoover thermostat, adds new terms to the system Hamiltonian that depend on a new degree of freedom s. These will be discussed in section 2.2.

2.1
Particle chain

For the particle chain, we shall always consider the case of first-neighbor interactions. To understand what this means, let us label the particles in figure 2.1 starting from the left and going from 1 to N. Then, each particle n only interacts with particles $n-1$ and $n+1$, where $n = 1, 2, \ldots, N$. For $n = 1, N$, the interactions with $n = 0, N+1$, respectively, are defined by the boundary conditions (discussed at the end of this section).

This is not the only possible case, however, as there is much research on how long-range interactions (for example, if we consider charged particles) would affect thermal conduction [29, 30].

A general chain Hamiltonian can be written as

$$\mathcal{H} = \sum_{n=1}^{N} \frac{1}{2}\frac{p_n^2}{m_n} + \sum_{n=1}^{N} U(x_{n+1} - x_n) + \sum_{n=1}^{N} V(x_n), \tag{2-1}$$

with x_n being the position of the n-th particle (remembering that x_0, x_{N+1} are defined by the boundary conditions), p_n the momentum of particle n and m_n its mass, $U(x_n - x_{n+1})$ the inter-particle potential between particles $n, n+1$, $V(x_n)$ is the on-site potential of particle n.

The equations of motion are derived from 2-1 by means of the Hamilton equations,

$$\dot{p}_n = -\frac{\partial \mathcal{H}}{\partial x_n}, \quad \dot{x}_n = \frac{\partial \mathcal{H}}{\partial p_n}. \tag{2-2}$$

It is common, however, to look at the equations of motion using the displacement from equilibrium $q_n = x_n - na$ for each particle (a is the lattice distance). This is a canonical transformation and as such it does not affect our equations of motion.

In fact, since any function of the position $f(x_n)$ can be rewritten in terms of q_n by substituting $x_n = q_n + na$, the chain rule gives

$$\frac{\partial f}{\partial q_n} = \frac{\partial f}{\partial x_n}\frac{\partial x_n}{\partial q_n} = \frac{\partial f}{\partial x_n}, \tag{2-3}$$

which means we can rewrite the equations of motion in the equivalent form

$$\dot{p}_n = -\frac{\partial \mathcal{H}}{\partial q_n}, \quad \dot{q}_n = \frac{\partial \mathcal{H}}{\partial p_n}. \tag{2-4}$$

Not only are the values of the coordinates (q_n, p_n) much easier to read and interpret than (x_n, p_n), they will also simplify the equations of motion for our chain of particles. Hence, we shall adopt this system of coordinates for much of this work.

All models considered here have harmonic inter-particle interactions, and so their potential energy will be

$$U_{int} = \sum_{i=1}^{N} U(x_{n+1} - x_n) = \sum_{i=1}^{N} \frac{k}{2}(x_{n+1} - x_n - a)^2, \tag{2-5}$$

where a is the distance between the lattice points. Using the displacement q_n, we can rewrite the interaction energy as

$$U_{int} = \sum_{i=1}^{N} \frac{k}{2}(q_{n+1} - q_n)^2. \tag{2-6}$$

We could actually consider more general interactions than just harmonic,

but in general they wouldn't be enough to avoid anomalous heat conduction, since they would conserve momentum due to Newton's third law. Hence, we shall add anharmonicity by means of the on-site potential $V(x_n)$, for which we use the ϕ^4 potential and, alternatively, the Frenkel-Kontorova potential.

2.1.1
ϕ^4 potential

The ϕ^4 potential used here is a special case of the one used in ref. [31]. It is given by

$$V(x_n) = \frac{A_Q}{4}\left(x_n - na\right)^4 , \tag{2-7}$$

or using our variables q_n,

$$V(q_n) = \frac{A_Q}{4} q_n^4 , \tag{2-8}$$

where we set to be zero the coefficient of the quadratic term from the potential definition used in the cited reference. This is exactly the same as in ref. [23]. A graph of the function is given in figure 2.2.

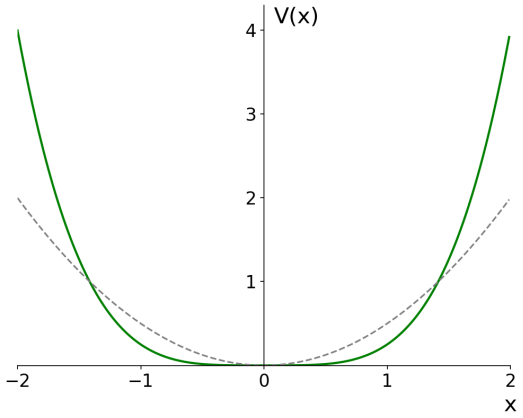

Figure 2.2: The graph of the ϕ^4 potential for $A_Q = 1$ is represented by the solid line. The dashed line is the harmonic potential with $A = 1$, for comparison.

The ϕ^4 potential has been thoroughly studied in the literature, and it is known to generally have normal heat conduction [32, 33, 23, 34, 35, 36].

2.1.2
Frenkel-Kontorova potential

The Frenkel-Kontorova potential [22, 37] is a periodic function with period a_s and amplitude A_{FK},

$$V(x_n) = \frac{A_{FK}}{2\pi}\left[1 - \cos\left(\frac{2\pi x_n}{a_s}\right)\right], \tag{2-9}$$

but we will rewrite it in terms of the displacement from equilibrium for each particle, giving

$$V(q_n) = \frac{A_{FK}}{2\pi}\left[1 - \cos\left(\frac{2\pi na}{a_s} + \frac{2\pi q_n}{a_s}\right)\right]. \tag{2-10}$$

The ratio a/a_s defines the number of particles falling in each potential well and this somewhat corresponds to the degree of disorder in the system, enabling one to simulate different types of solid defects with the model [37].

In our case, we are not interested in studying such defects, and we choose $a/a_s = 1$, so that we have

$$V(q_n) = \frac{A_{FK}}{2\pi}\left[1 - \cos\left(\frac{2\pi q_n}{a_s}\right)\right], \tag{2-11}$$

and with the assumption that $a = 1$,

$$V(q_n) = \frac{A_{FK}}{2\pi}\left[1 - \cos\left(2\pi q_n\right)\right], \tag{2-12}$$

which would be akin to thinking of q_n as a dimensionless variable representing the displacement from equilibrium in terms of the lattice separation [22].

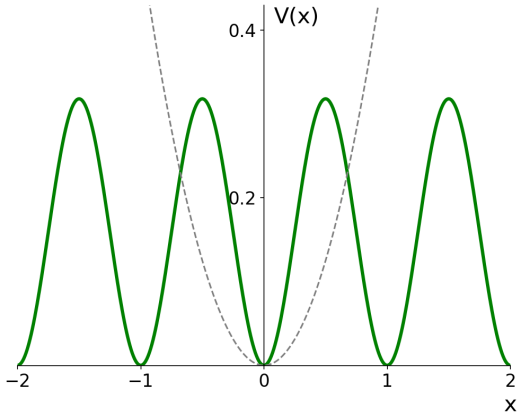

Figure 2.3: The graph of the Frenkel-Kontorova potential for $A_{FK} = a_s = 1$ is represented by the solid line. The dashed line is the harmonic potential with $A = 1$, for comparison.

This model has been already shown to reproduce equations 1-8 and 1-9 [33, 23, 38, 39]. We have to take care, however, to avoid choosing a very high temperature, because when the thermal energy k_BT is of the same order as a threshold energy E_0, the particles will leave their wells and start occupying other wells, giving rise to a transition in the behavior of the transport coefficients [37].

2.1.3 Boundary conditions

The last consideration needed for the chain is on the choice of the boundary conditions.

In analytical calculations, it is common to use periodic boundary conditions, connecting the endpoints of the chain so that $x_{N+1} = x_1$ and $x_0 = x_N$, because they simplify many calculations. However, in this work we will use fixed boundary conditions, such that $x_{N+1} = x_0 = 0$, for all time. This is very common in the literature of heat conduction and is computationally very simple.

It is important to notice that, whenever one simulates heat conduction, temperature discontinuities will appear in the boundaries due to the Kapitza resistance [14]. There are some results in the literature on how the number of particles in the chain, together with the parameters of the heat baths, affects this resistance [40]. Since the dependence on the parameters is highly non-trivial,a systematic analysis of this interface resistance is outside the scope of our thesis.

2.2 Heat baths

For any model used to reproduce a heat bath at constant temperature T, we expect that equilibrium properties are recovered, i.e., the probability density of the velocities must follow the Maxwell-Boltzmann distribution,

$$f(v_x) = \left(\frac{m}{2\pi k_B T}\right)^{1/2} \exp\left(-\frac{m v_x^2}{2k_B T}\right), \tag{2-13}$$

when applied to a system of particles in equilibrium. In this one-dimensional case, the velocity distribution $f(v_x)$ is just a Gaussian distribution with variance $\sigma^2 = k_B T/m$ and zero mean.

The most commonly used thermostats, in the models of low-dimensional heat conduction that we studied, are the Langevin and the Nosé-Hoover thermostat [14]. Their main difference is that the former models the system with stochastic differential equations, while the latter changes the deterministic equations of motion of the system. Any results should be robust under the choice of the thermostat.

2.2.1 Nosé-Hoover thermostat

The Nosé-Hoover thermostat consists of adding one more degree of freedom s, along with its conjugated momentum p_s [41]. Using the same notation as in [42], let $\mathcal{H}_0(\mathbf{q}, \mathbf{p})$ be the many-body Hamiltonian from equation 2-1, the *Nosé Hamiltonian* is then defined as

$$\mathcal{H}_N = \mathcal{H}_0(\mathbf{q}, \mathbf{p}/s) + gKT \ln s + \frac{p_s^2}{2Q}, \tag{2-14}$$

where g is the number of degrees of freedom of the system and Q is a parameter describing the rate at which the fluctuations in the energy are dampened out. Although it is not clear from 2-14 why this additional degree of freedom would give us the expected equilibrium property, it was already proved that we indeed get the desired distribution [41, 43] due to the dynamics of p_s, which maintains the temperature of the system by dissipating or adding energy [14], and it was also shown that it behaves as we would expect when in the linear regime of nonequilibrium [42]. In this work, we shall use the Langevin equation approach to simulate our heat baths.

2.2.2 Langevin bath

In the XIX century, the botanist Robert Brown studied what is now called the *Brownian motion* which is the seemingly random motion of pollen grains in a viscous media such as water or acetone [44]. After Albert Einstein brought forward a microscopical physical intuition of the phenomenon in 1905, Paul Langevin tried to explain it dynamically in 1908 by using Newton's second law and adding a random force, thus devising the Langevin equation [45], whose one-dimensional version can be written as

$$m\ddot{r} = -\gamma'\dot{r} + \eta(t), \tag{2-15}$$

where r is the position of the pollen, $-\gamma\dot{r}$ is a term representing a drag force due to the medium and $\eta(t)$ is called a white noise, i.e., a Gaussian stochastic process defined by having zero mean, $\langle\eta(t)\rangle = 0$ and autocorrelation function

$$\langle\eta(t)\eta(t')\rangle = \Gamma'\delta\left(t - t'\right), \tag{2-16}$$

with $\Gamma' > 0$.

Equation 2-15 was made mathematically precise with the advent of stochastic calculus [46]. In that framework it is known (with the change $\dot{r} = v$) as the Ornstein-Uhlenbeck process, which in differential form is written as

$$dv = -\frac{\gamma'}{m}vdt + \frac{\sqrt{\Gamma'}}{m}dW_t, \tag{2-17}$$

where W_t is the Wiener process [47, 48] with unit variance.

The way this equation can be seen as rigorous is to look at the terms as a sum of infinitesimal variations, so there is an integral on each term, and the integral on the "measure of randomness" (dW_t) is a stochastic integral. There are many types of stochastic integrals, but the main ones are the Itô integral and the Stratonovich integral (also called Itô and Stratonovich prescriptions). The difference between the two are the terms in the summation

(in the definition of the integral). Itô integral sums terms using only the present time $g(x)(W_{t+\Delta} - W_t)$, and Stratonovich integral is a summation of terms $[(g(x+\Delta)+g(x))/2](W_{t+\Delta} - W_t)$, taking a "middle point" between t and $t+\Delta$ [46]. For a given function $g(x)$, the Itô integral is written $g(x) \cdot dW_t$, while the Stratonovich integral is written as $g(x) \circ dW_t$.

Now, it is important to say that from the standpoint of physics, the Langevin equation is more appropriately described by a Stratonovich integral, because its mathematical properties better conforms to our physical intuition [46]. However, since $\sqrt{\Gamma'}/m$ is a constant, both the Itô and the Stratonovich prescriptions give the same results in this case.

From a physical point of view, one can look at this problem as a massive particle in a bath composed of smaller ones. The drag force comes from averaging out the dampening that the motion of the bigger particle suffers from the collisions with the bath, corresponding to slower degrees of freedom, while the random force arises from the many collisions of the lighter bath particles, causing a fluctuation on the speed of the main one, corresponding to the faster degrees of freedom [49].

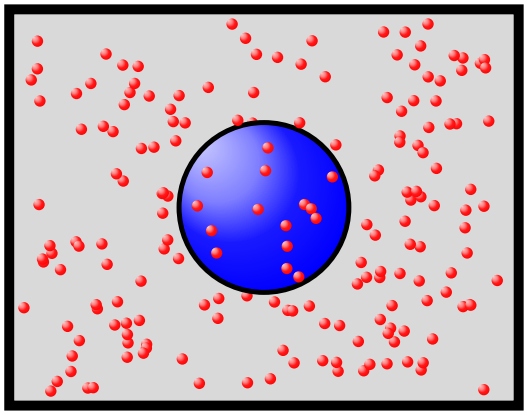

Figure 2.4: Physical representation of a Langevin heat bath. The smaller red particles represents the bath.

It is important to notice that the velocity of the bigger particle $v = \dot{r}$ is being modeled here as a random variable, and the above remarks give us a motivation on why this makes sense. This means that by using the Langevin approach, we are modeling our problem as a stochastic differential equation.

To see how the probability distribution of v is indeed given by equation 2-13 and give a physical meaning to Γ', we follow the derivation by Ornstein and Uhlenbeck [50] (which can be seen in many sources, such as refs [51, 52, 48, 47]), but using the language of Itô integrals [53, 54, 55, 56]. To do this, we need to solve equation 2-15 for the mean, variance and higher order moments.

In order to scale out the mass, let us redefine $\gamma = \gamma'/m$, $\Gamma = \Gamma'/m^2$, so that

$$dv = -\gamma v dt + \sqrt{\Gamma} dW_t. \tag{2-18}$$

Now we multiply $e^{\gamma t}$ on both sides, which after some rearragements gives us

$$e^{\gamma t} dv + \gamma e^{\gamma t} v dt = \sqrt{\Gamma} e^{\gamma t} dW_t. \tag{2-19}$$

For Itô integrals, the chain rule gives way to Itô's lemma [53], which says that for a given function $g(v,t)$, its differential will be

$$dg = \frac{\partial g}{\partial t} dt + \frac{\partial g}{\partial v} dv + \frac{1}{2} \frac{\partial^2 g}{\partial v^2} (dv)^2, \tag{2-20}$$

where $(dv)^2$ is found by using that $dt \cdot dt = 0$, $dt \cdot dW_t = dW_t \cdot dt = 0$ and $dW_t \cdot dW_t = dt$.

Then, from Itô's lemma,

$$d(ve^{\gamma t}) = e^{\gamma t} dv + \gamma e^{\gamma t} v dt, \tag{2-21}$$

which we plug on equation 2-19 to get

$$v(t) = v(0)e^{-\gamma t} + \sqrt{\Gamma} \int_0^t e^{-\gamma(t-s)} dW_s. \tag{2-22}$$

To find the ensemble average and standard deviation of the velocity, we use the property of Itô integrals [53] that

$$\left\langle \int_A^B f(t) dW_t \right\rangle = 0, \tag{2-23}$$

and so we have

$$\langle v(t) \rangle = v(0)e^{-\gamma t}. \tag{2-24}$$

We then substitute back to equation 2-22 and get

$$\left\langle (v(t) - \langle v(t) \rangle)^2 \right\rangle = \Gamma \left\langle \left(\int_0^t e^{-\gamma(t-s)} dW_s \right)^2 \right\rangle. \tag{2-25}$$

Now considering the Itô isometry [53], the property of Itô integrals that

$$\left\langle \left(\int_A^B g(t,v) dW_t \right)^2 \right\rangle = \left\langle \int_A^B g^2(v,t) dt \right\rangle, \tag{2-26}$$

one can show that

$$\left\langle v^2(t) \right\rangle - \langle v(t) \rangle^2 = \Gamma \int_0^t e^{-2\gamma(t-s)} ds, \tag{2-27}$$

and finally,

$$\left\langle v^2(t)\right\rangle - \langle v(t)\rangle^2 = e^{-2\gamma t}\Gamma\int_0^t e^{2\gamma s}ds \tag{2-28}$$

$$= e^{-2\gamma t}\frac{\Gamma}{2\gamma}\left(e^{2\gamma t}-1\right) \tag{2-29}$$

$$= \frac{\Gamma}{2\gamma}\left(1-e^{-2\gamma t}\right). \tag{2-30}$$

When $t\to\infty$, we would expect our system to go to equilibrium, and according to the kinetic theory of gases we should have

$$\frac{1}{2}m\left\langle v^2\right\rangle = \frac{1}{2}k_BT, \tag{2-31}$$

but in this case $\langle v\rangle = 0$ and $\langle v^2\rangle = \Gamma/2\gamma$, thus

$$\Gamma = \frac{2\gamma k_BT}{m}, \tag{2-32}$$

showing that Γ and Γ' define the temperature of the heat bath.

With the mean and the standard deviation, it is possible to calculate the higher-order moments of the velocity [52, 51, 57]. Defining $\Delta v = v(t) - \langle v(t)\rangle$, in equilibrium we have

$$\left\langle(\Delta v)^{2n+1}\right\rangle = 0, \tag{2-33}$$

$$\left\langle(\Delta v)^{2n}\right\rangle = (2n-1)!!\left\langle(\Delta v)^2\right\rangle, \tag{2-34}$$

which are the exact formulae for the moments of a Gaussian distribution, and since this distribution is defined by its moments [58], then v is normally distributed. This means that the probability density function of the velocity v follows a Maxwell-Boltzmann distribution when the system is in equilibrium.

We can use the solution for the velocity to find the mean and variance of the position [52], giving

$$\langle r(t)\rangle = r(0) + \frac{v(0)}{\gamma}\left(1-e^{-\gamma t}\right), \tag{2-35}$$

$$\left\langle\left(r(t)-\langle r(t)\rangle\right)^2\right\rangle = \frac{\Gamma}{\gamma^2}\left[t - \frac{2}{\gamma}\left(1-e^{-\gamma t}\right) + \frac{1}{2\gamma}\left(1-e^{-2\gamma t}\right)\right], \tag{2-36}$$

which for long times tend, respectively, to

$$\langle r(t)\rangle = r(0) + \frac{v(0)}{\gamma}, \tag{2-37}$$

$$\left\langle(\Delta r(t))^2\right\rangle = \frac{\Gamma}{\gamma^2}t. \tag{2-38}$$

For computational purposes, hereafter we will use the forces in equation 2-15 in the form of additional terms in the equations of motion of the particles in contact with the baths, giving a system of two first-order equations, namely,

$$\frac{dv(t)}{dt} = \frac{F}{m} - \gamma v(t) + \sqrt{\Gamma}\epsilon\,(t)\,, \tag{2-39}$$

$$\frac{dr(t)}{dt} = v(t), \tag{2-40}$$

ϵ being somewhat analogous to what would be a term of the form dW_t/dt. This is just an intuitive standpoint, rigorously such a term is impossible since the Wiener process is nowhere differentiable [53], and F being the forces on the particle not related to the bath. This model for a heat bath cannot be written using a Hamiltonian, and so we have to plug the drag and the random forces directly into the equations of motion of the end particles of the chain, located in positions $n = 1, N$, to be able to couple the heat baths with the chain.

2.3 Thermodynamic properties

Interpreting the dynamics of such a mechanical system in thermodynamic terms is not trivial, since Thermodynamics is concerned with macroscopic quantities normally derived in the limit $N \to \infty$ that does not apply to our study here.

The problem of defining temperature and heat current for small systems can be tackled in a rigorous fashion, like what was done by Lepri, Livi and Politi in ref. [14], and by Dhar in ref. [34], but we will simplify the discussion and put forward the intuitions involved and the end result.

Physically we know that the temperature of a system is related to its average energy, while heat is the transport of disordered energy from one point to another. With this in mind, let's define the temperature in terms of the kinetic energy of the particles, and define the heat current from the exchange of energy between particles.

The kinetic temperature of particle n is given by

$$T_n = \left\langle \frac{p_n^2}{m} \right\rangle, \tag{2-41}$$

and for a particle with unit mass it can be rewritten as

$$T_n = \langle v_n^2 \rangle, \tag{2-42}$$

since in this case the numerical value of p_n is equal to v_n.

The heat current transferred from particle n to particle $n+1$ depends

on the inter-particle potential, and is defined as the average rate of work done by the former on the latter,

$$J_n = \langle v_{n+1} F_{n\to n+1} \rangle \,, \tag{2-43}$$

which is the energy that passes through a plane between the particles with

$$F_{n\to n+1} = -F_{n+1\to n} = -\frac{\partial U}{\partial q_n}, \tag{2-44}$$

$F_{n+1\to n}$ being the force that particle $n+1$ applies on particle n.

Now, from Newton's third law, $F_{n+1\to n}$ is a reaction pair to $F_{n\to n+1}$, and so we could question ourselves on the choice of the particle velocity we look at for our definition. However, in the stationary regime, we have

$$\langle v_{n+1} F_{n\to n+1} \rangle = \langle v_n F_{n\to n+1} \rangle, \tag{2-45}$$

and so we can average both terms to get the equivalent definition that we will use,

$$J_n = \left\langle \frac{1}{2} \left(v_n + v_{n+1} \right) F_{n\to n+1} \right\rangle . \tag{2-46}$$

For the harmonic interaction between both particles, definition 2-46 would be written as

$$J_n = \left\langle \frac{1}{2} \left(v_n + v_{n+1} \right) k(q_n - q_{n+1}) \right\rangle , \tag{2-47}$$

where k is the stiffness constant.

An important remark should be made on the signal of the heat current. Consider the axis along which the particles interact as the x-axis. Then, the expression used here considers the positive x-axis being defined to the right (from particle n to particle $n+1$ in figure 2.1), and so $J_n > 0$ when the heat is being transferred from the left to the right ($T_L > T_R$) while $J_n < 0$ in the opposite case ($T_L < T_R$).

It is also important to notice that in the stationary state, we would expect T_n to stop depending on the time, and that implies J_n becomes constant along the chain [14].

One last thermodynamic variable we look at is the conductivity, which for such a system will be defined in the stationary state, when $J = J_n, n = 1, 2, \ldots, N$, as

$$\kappa = \frac{JN}{T_L - T_R}. \tag{2-48}$$

2.4 Homogeneous chain model

With the discussions on the particle chain and the heat baths, we can now describe the working model for heat conduction. To do this, the amplitudes of

the particle-particle interactions and of the on-site potentials will be constant along the chain. We will also consider all particles have the same mass m.

Summarizing, the Hamiltonian is

$$\mathcal{H} = \sum_{n=1}^{N} \frac{1}{2}\frac{p_n^2}{m} + \sum_{n=1}^{N} \frac{k}{2}(q_{n+1} - q_n)^2 + \sum_{n=1}^{N} V(q_n), \tag{2-49}$$

where for $V(q_n)$, we will consider the Frenkel-Kontorova chain (FKC) and ϕ^4 chain (QC) described in section 2.1. The heat bath considered will be a Langevin thermostat

2.4.1 Equations of motion

We apply the discussion at the beginning of this chapter to explicitly write the equations of motion. As said in section 2.2, Langevin heat baths cannot be written as a Hamiltonian and thus only show in ad-hoc terms. One last remark is that we will not use the momentum of each particle, but its velocity, and so we substitute $v_n = p_n/m$.

The equations of motion are then

$$\frac{dq_n}{dt} = v_n, \tag{2-50}$$

for all particles. Now, for the boundaries,

$$\frac{dv_1}{dt} = -\frac{k}{m}q_1 - \frac{k}{m}(q_1 - q_2) - \frac{1}{m}\frac{dV}{dq_1} - \gamma v_1 + \sqrt{\frac{2\gamma T_L}{m}}\,\epsilon_L(t), \tag{2-51}$$

$$\frac{dv_N}{dt} = -\frac{k}{m}q_N - \frac{k}{m}(q_N - q_{N-1}) - \frac{dV}{dq_N} - \frac{1}{m}\gamma v_N + \sqrt{\frac{2\gamma T_R}{m}}\,\epsilon_R(t), \tag{2-52}$$

where $\epsilon_L(t)$ and $\epsilon_R(t)$ are independent white noises with zero mean and autocorrelations $\langle \epsilon_L(t)\epsilon_L(t')\rangle = \delta(t - t')$ and $\langle \epsilon_R(t)\epsilon_R(t')\rangle = \delta(t - t')$. The temperatures T_L and T_R have units of energy, since they are in units of $k_B T$. The remainder of the chain follows

$$\frac{dv_n}{dt} = -\frac{k}{m}(2q_n - q_{n-1} - q_{n+1}) - \frac{1}{m}\frac{dV}{dq_n}, \quad n = 2, \ldots N-1. \tag{2-53}$$

For the ϕ^4 potential, from equation 2-8, we have

$$\frac{dV}{dq_n} = A_Q q_n^3\,, \tag{2-54}$$

and the resulting model will be called ϕ^4 chain (QC), while for the Frenkel-Kontorova potential, from equation 2-11,

$$\frac{dV}{dq_n} = \frac{A_{FK}}{a_s}\sin\left(\frac{2\pi q_n}{a_s}\right), \tag{2-55}$$

the model being called the FK chain (FKC).

With the initial conditions $q_n(0) = q_{n,0}$, $v_n(0) = v_{n,0}$, our working stochastic dynamical system is now fully specified.

2.5 Thermal Diode

With the insights gained in chapter 1 about the possible causes of anomalous heat conduction, we presented in section 2.4 two working models that are known to verify Fourier's law. These models are the basis to construct devices capable of heat rectification, i.e., thermal diodes.

Quoting the words by Terraneo, Peyrard and Casati [8]:

> *Once the general mechanism of the thermal conduction in a composite nonlinear lattice has been understood, this opens many possibilities. For instance, one can design a thermal rectifier[...].*

To change the overlap of phonon bands on the chain according to the direction of the heat current, it is common to introduce a source of asymmetry by dividing the chain in two segments. The amplitude of the potential on each segment (left and right) is different, and a central part connects both segments [8]. Such a device would give a heat current with different magnitudes when the temperature sources in figure 2.1 are exchanged. We then say that our device rectified the thermal current of lower magnitude.

There are a few ways to quantify how good this device is. The most common one used in simulations is the rectification coefficient [26], defined as

$$R = \frac{|J_+ - J_-|}{|J_-|}\,, \tag{2-56}$$

where $J_+ = \max\{|J_{L\to R}|, |J_{R\to L}|\}$ and $J_- = \min\{|J_{L\to R}|, |J_{R\to L}|\}$.

In section 2.5.1, we discuss the modelling of the central (or interfacial) part of the chain. In section 2.5.2, we present the equations of motion that are going to be numerically investigated in the rest of the work.

2.5.1 Interface Interaction

The central part of a thermal diode can be modeled in different ways. It can be a third segment with many particles and a different potential, such as in ref. [59], or the left and right segments can be connected directly through the interaction between the rightmost particle of the left segment and the leftmost particle of the right segment [25]. This is an interesting degree of freedom we are going to explore here.

In our case, the interface interaction will be given by a power-law potential, parameterized by its exponent $\mu > 1$, between particles $N/2$ and $N/2+1$, with even N. This is defined as

$$U\left(x_{\frac{N}{2}+1} - x_{\frac{N}{2}}\right) = \frac{k_\mu}{\mu}\left|x_{\frac{N}{2}+1} - x_{\frac{N}{2}} - a\right|^\mu, \tag{2-57}$$

or, rewritten in terms of q_n,

$$U\left(q_{\frac{N}{2}+1} - q_{\frac{N}{2}}\right) = U_\mu\left(q_{\frac{N}{2}+1} - q_{\frac{N}{2}}\right) = \frac{k_\mu}{\mu}\left|q_{\frac{N}{2}+1} - q_{\frac{N}{2}}\right|^\mu. \tag{2-58}$$

When $\mu = 2$ the harmonic force between both segments is recovered.

2.5.2 Equations of motion

We will change the equations of motion from section 2.4.1 to take into consideration the separation of chain segments. The resulting models will be called the two-segment Frenkel-Kontorova chain (TSFKC) and the two-segment ϕ^4 chain (TSQC). The Hamiltonian is

$$\begin{aligned}\mathcal{H} = \sum_{n=1}^{N}\frac{1}{2}\frac{p_n^2}{m} + \sum_{n=1}^{N/2-1}\frac{k_L}{2}(q_{n+1}-q_n)^2 + \sum_{n=1}^{N}V_L(q_n) \\ + \frac{k_\mu}{\mu}\left|q_{\frac{N}{2}+1} - q_{\frac{N}{2}}\right|^\mu \\ + \sum_{n=\frac{N}{2}+1}^{N}\frac{k_R}{2}(q_{n+1}-q_n)^2 + \sum_{n=\frac{N}{2}+1}^{N}V_R(q_n),\end{aligned} \tag{2-59}$$

which generalizes the diode model defined in ref. [25] (the latter recovered when $\mu = 2$).

The parameters k_L and k_R are the coefficients of the harmonic interaction inside the left and right segments, respectively, k_μ is the strength of the interface interaction, A_L and A_R are the amplitudes of the on-site potentials for the left and right segment, respectively. Like in section 2.4.1, we always substitute $v_n = p_n/m$.

Let us first look at the time derivative of the displacement. Since only the kinetic energy has a dependency on the momenta, we will always have

$$\frac{dq_n}{dt} = v_n, \tag{2-60}$$

for all particles in both segments, $n = 1, 2, \ldots, N$.

For the momenta, there are three cases. First let us look at particles 1 and N, in contact with the heat baths at temperatures T_1 and T_2, respectively. Assuming fixed boundary conditions and remembering the discussion on

Langevin thermostats given in section 2.2, the equations of motion shall be

$$\frac{dv_1}{dt} = -\frac{k_L}{m}q_1 - \frac{k_L}{m}(q_1 - q_2) - \frac{1}{m}\frac{dV_L}{dq_1} - \gamma v_1 + \sqrt{\frac{2\gamma T_L}{m}}\epsilon_L(t), \tag{2-61}$$

$$\frac{dv_N}{dt} = -\frac{k_R}{m}q_N - \frac{k_R}{m}(q_N - q_{N-1}) - \frac{1}{m}\frac{dV_R}{dq_N} - \gamma v_N + \sqrt{\frac{2\gamma T_R}{m}}\epsilon_R(t), \tag{2-62}$$

where $\epsilon_L(t)$ and $\epsilon_R(t)$ are independent white noises with zero mean and autocorrelation $\langle\epsilon_L(t)\epsilon_L(t')\rangle = \delta(t-t')$ and $\langle\epsilon_R(t)\epsilon_R(t')\rangle = \delta(t-t')$, and we assume the temperatures are given in units of the Boltzmann constant k_B (so T_L and T_R have units of energy).

The dynamics of particles $N/2$ and $N/2+1$, at the interface, will be given by the following equations:

$$\frac{dv_{\frac{N}{2}}}{dt} = -\frac{k_L}{m}(q_{\frac{N}{2}} - q_{\frac{N}{2}-1}) - \frac{k_\mu}{m}\mathrm{sgn}\left(q_{\frac{N}{2}} - q_{\frac{N}{2}+1}\right)\left|q_{\frac{N}{2}} - q_{\frac{N}{2}+1}\right|^{\mu-1} - \frac{1}{m}\frac{dV_L}{dq_{\frac{N}{2}}} \tag{2-63}$$

$$\frac{dv_{\frac{N}{2}+1}}{dt} = -\frac{k_R}{m}(q_{\frac{N}{2}+1} - q_{\frac{N}{2}+2}) - \frac{k_\mu}{m}\mathrm{sgn}\left(q_{\frac{N}{2}+1} - q_{\frac{N}{2}}\right)\left|q_{\frac{N}{2}} - q_{\frac{N}{2}+1}\right|^{\mu-1} - \frac{1}{m}\frac{dV_R}{dq_{\frac{N}{2}+1}}. \tag{2-64}$$

In equations 2-63 and 2-64, sgn is the sign function, defined as

$$\mathrm{sgn}(x) = \begin{cases} 1, & \text{if } x > 0, \\ 0, & \text{if } x = 0, \\ -1, & \text{if } x < 0. \end{cases} \tag{2-65}$$

Finally, for the rest of the particles, the differential equations take on much simpler forms,

$$\frac{dv_n}{dt} = -\frac{k_L}{m}(2q_n - q_{n-1} - q_{n+1}) - \frac{1}{m}\frac{dV_L}{dq_n}, \quad n = 2, \ldots \frac{N}{2} - 1, \tag{2-66}$$

$$\frac{dv_n}{dt} = -\frac{k_R}{m}(2q_n - q_{n-1} - q_{n+1}) - \frac{1}{m}\frac{dV_R}{dq_n}, \quad n = \frac{N}{2} + 2, \ldots, N. \tag{2-67}$$

For completeness, we again write the forces due to the ϕ^4 and Frenkel-Kontorova potential,

$$\frac{dV}{dq_n} = A_Q q_n^3, \tag{2-68}$$

$$\frac{dV}{dq_n} = \frac{A_{FK}}{a_s}\sin\left(\frac{2\pi q_n}{a_s}\right). \tag{2-69}$$

The initial conditions, $q_n(0) = q_{n,0},\ p_n(0) = p_{n,0}$, complete the diode model.

3
Heat conduction results

In chapter 2, we discussed the basic components necessary for building simple microscopic models of heat conduction and built the equations of motion in section 2.4.1 for the QC and the FKC.

In appendix A, we raise the problem that obtaining an analytic solution for most nonlinear models is difficult, or even impossible, and thus showed numerical schemes that are used for simulating such systems. Due to having worse convergence properties, the Euler scheme raised there will not be used here. We will use the fourth-order Runge-Kutta scheme, also described in appendix A.

One simulation using stochastic numerical integration is itself just one sample taken from a random distribution of possible paths. Hence to take the thermodynamic average for the kinetic temperature and the heat current, we use many independent sample paths (a proxy of the thermodynamic ensemble) over which we average.

We will do this procedure for the QC and FKC models, calculating a few thermodynamic properties of interest, specifically the temperature, the heat current and the thermal conductivity, for different values of the chain parameters.

The temperature profile of the system is given by the sequence of kinetic temperatures of the particles, $\{T_n, n = 1, 2, \ldots, N\}$. Since we consider a unit lattice distance, the equilibrium point of the i-th particle in the x axis is i, and so we represent all particle positions as i/N, the normalized equilibrium positions. So the temperature profile can also be seen as the graph $T(i/N)$.

Then, we look at the heat current along the chain $\{J_n, n = 1, 2, \ldots, N\}$, again using the graph $J(i/N)$. In the stationary state, J should be approximately constant, $J(n/N) \approx J(m/N)$, $\forall n, m = 1, 2, \ldots, N$.

Finally, we get the average of the heat current along the chain,

$$J = \frac{1}{N} \sum_{n=1}^{N} J_n, \tag{3-1}$$

and use it to calculate the thermal conductivity κ of the system, as defined in equation 2-48, that is,

$$\kappa = \frac{JN}{T_L - T_R}, \tag{3-2}$$

for different parameter values.

The parameters used for the heat baths, as discussed in appendix A, are the average temperature, $T_m = (T_L + T_R)/2$, and the relative temperature difference, $\Delta_{rel} = (T_L - T_R)/T_m$, instead of T_L and T_R. To calculate T_L and T_R back, we use

$$T_L = T_m \left(1 + \frac{\Delta_{rel}}{2}\right), \tag{3-3}$$

$$T_R = T_m \left(1 - \frac{\Delta_{rel}}{2}\right). \tag{3-4}$$

In all cases, here we assume a non-dimensional version of the equations of motion, so all parameters and dynamical thermodynamic quantities are non-dimensional (see appendix A.4).

3.1 Quartic chain

Let us begin with the QC model. The effects of the number of particles in the chain are discussed first. After that, the changes caused by the amplitude of the particle-particle interaction k and the amplitude of the quartic potential A are verified.

All cases are assumed to have total simulation time $t_{max} = 3 \times 10^5$, transient time $t_{trans} = 10^5$, and integration time step $\delta t = 10^{-3}$. The number of copies in the ensemble is $\mathcal{N} = 100$.

Any deviation from these parameters will be raised on a case-by-case basis.

3.1.1 Varying the number of particles

How the number of particles in the chain changes the system properties was first analyzed by setting $k = 1.0$, $A = 1.0$. For the heat baths, $T_m = 1.0$ and $\Delta_{rel} = 1.0$. The results are shown in figures 3.1 and 3.2. Each curve was obtained for a different value of N.

The total simulation time and transient time were changed ($t_{max} = 2 \times 10^5$, $t_{trans} = 5 \times 10^4$).

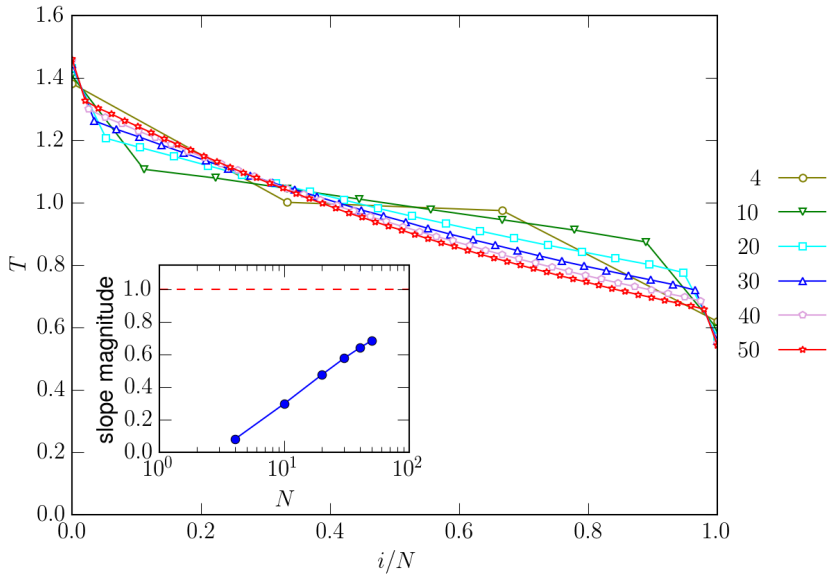

Figure 3.1: Temperature profile along the ϕ^4 chain, varying the number of particles in the chain N. The parameters are $A = 1.0, k = 1.0$, while for the baths we have $T_m = 1.0$ and $\Delta_{rel} = 1.0$. The inset shows the slope of the profile in absolute value (calculated using least squares linear regression, as shown in the appendix) versus N, with the abscissa in logarithmic scale. The dashed red line is the slope of the straight line joining the heat bath temperatures.

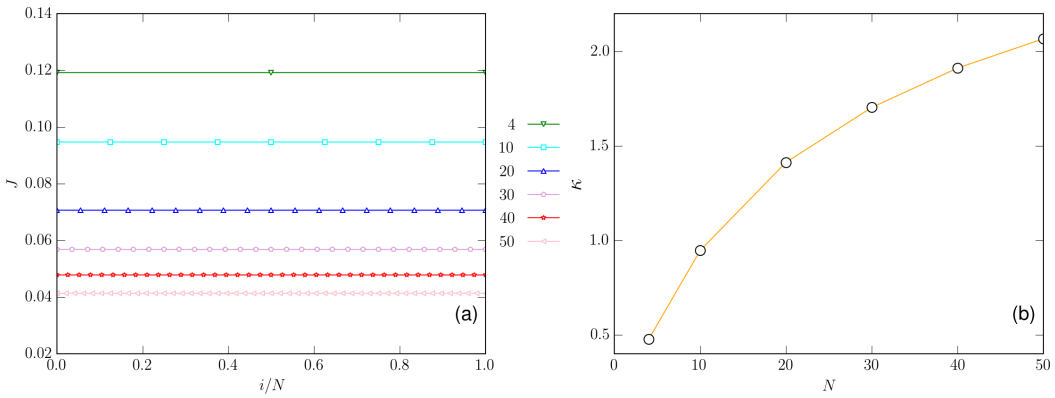

Figure 3.2: Heat current along the ϕ^4 chain, varying the number of particles N. The parameters are $A = 1.0, k = 1.0$, while for the baths we have $T_m = 1.0$ and $\Delta_{rel} = 1.0$. (a) Linear graph of the local heat current and (b) conductivity κ versus N.

From figure 3.1, it appears, due to the almost linear temperature profile, normal heat conduction was achieved with our choice of parameter values. However, a small convexity can be seen. This curvature can be explained with the fact that $\kappa = \kappa(T)$ for the QC model [60]. The linear temperature profile

was derived assuming that the conductivity is constant, but if we assume $\kappa \propto T^{\alpha}$ in equation 1-7, then we would actually get at the steady state [61] (if $\alpha \neq -1$)

$$\dot{q} = -\kappa_0 T^{\alpha}\frac{dT}{dx} \implies T = \left(-\frac{T_L^{\alpha+1} - T_R^{\alpha+1}}{L}x + T_L^{\alpha+1}\right)^{\frac{1}{\alpha+1}}, \tag{3-5}$$

which gives a curved profile. If $\kappa \propto T^{-1}$, the correct profile would be

$$T = T_L\left(\frac{T_R}{T_L}\right)^{x/L}, \tag{3-6}$$

but it also describes a slightly curved profile. In any case, for the general ϕ^4 model, theoretical considerations have been used to argue that $\alpha = -2$ from linear response theory [32, 35], while molecular dynamics simulations have found $\alpha \in [-1.83, -1.35]$ [36, 62].

Since this curvature is very small, we can make a good linear approximation of the profile in the bulk (without the heat baths) by least-square regression (see appendix B). From this we see how the slopes increase with N. Since the Kapitza resistance is defined as the temperature jump in the extremities divided by the heat current [40], the fact that these slopes are getting closer to the slope between the temperatures of the heat baths show this resistance is decreasing with N.

In figure 3.2, the function $\kappa(N)$ does not reach a constant value, as expected for a system with normal conduction. As a matter of fact, larger values of N, $N > 400$ [23], are required.

For different choices of temperature, the amplitude might not be enough to reproduce normal conduction. In fact, when we choose different values of the parameters ($T_m = 0.09, \Delta_{rel} = 0.5, A = 5.0/2\pi$, with the standard simulation times), results for the purely harmonic chain are recovered (that is a flat temperature profile and conductivitity that increases linearly with N, which can be seen in figures 3.3 and 3.4). The reason for such a drastic change with temperature (notice A varies ever so slightly) will be discussed in section 3.1.3. To reproduce normal conduction, smaller values of T_m require higher values of A.

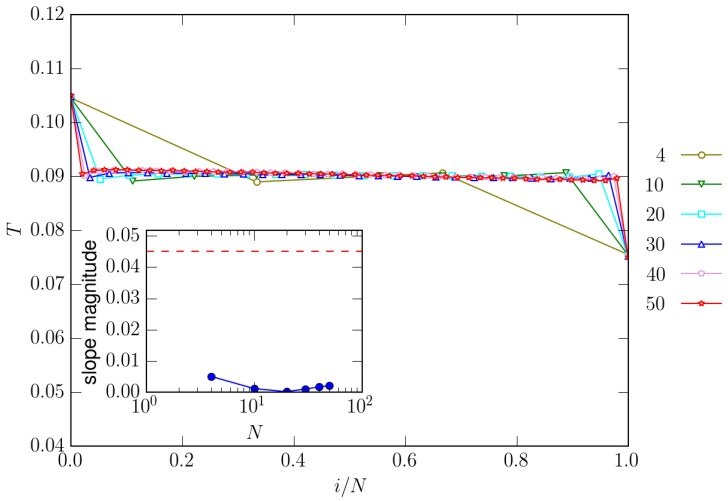

Figure 3.3: Temperature profile along the ϕ^4 chain, varying the number of particles in the chain N. The parameters are $A = 5.0/2\pi, k = 1.0$, while for the baths we have $T_m = 0.09$ and $\Delta_{rel} = 0.5$. The inset shows the slope of the profile in absolute value (calculated using least squares linear regression, as shown in the appendix) versus N, with the abscissa in logarithmic scale. The dashed red line is the slope of the straight line joining the heat bath temperatures.

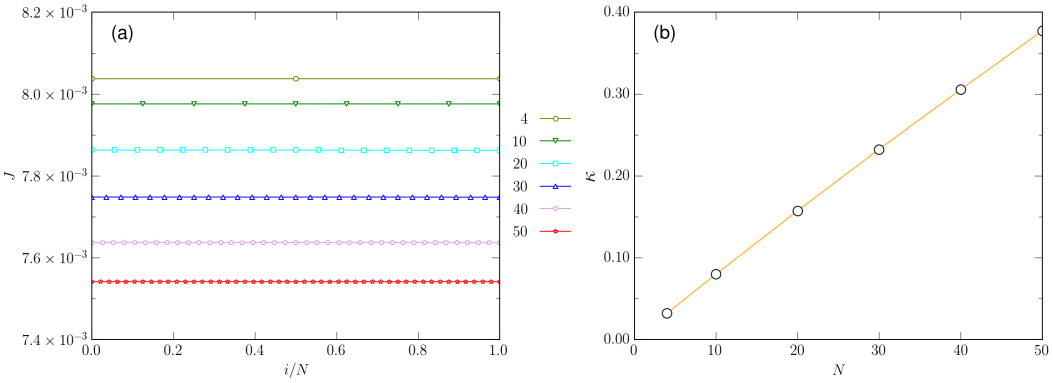

Figure 3.4: Heat current along the ϕ^4 chain, varying the number of particles N. The parameters are $A = 5.0/2\pi, k = 1.0$, while for the baths we have $T_m = 0.09$ and $\Delta_{rel} = 0.5$. (a) Linear graph of the local heat current and (b) conductivity κ versus N.

3.1.2 Varying the interaction strength

To see how the interaction amplitude k affects the thermodynamic properties of the system, we set $A = 5.0, N = 20$. For the heat baths, $T_m = 0.09$

and $\Delta_{rel} = 0.5$. The effect of the interaction strength k is shown in figures 3.6 and 3.5.

The total simulation time and transient time were changed back to the standard set before ($t_{max} = 3 \times 10^5$, $t_{trans} = 10^5$).

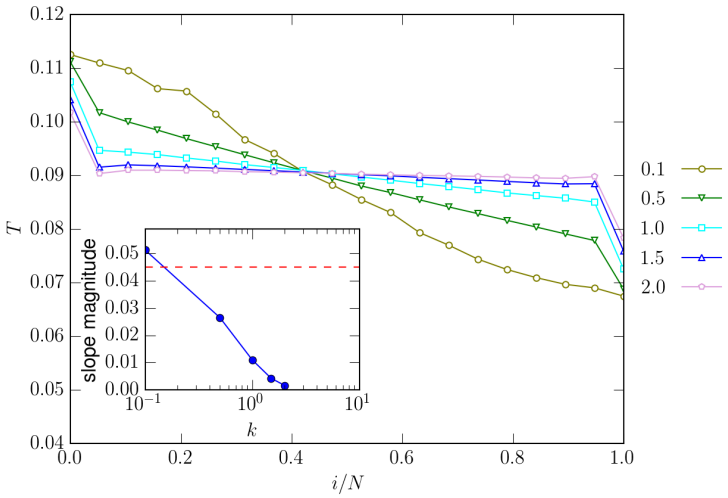

Figure 3.5: Temperature profile along the ϕ^4 chain, varying the interaction strength k. The parameters are $A = 5.0, N = 20$, while for the baths we have $T_m = 0.09$ and $\Delta_{rel} = 0.5$. The inset shows the slope of the profile in absolute value (calculated using least squares linear regression, as shown in the appendix) versus k, with the abscissa in logarithmic scale. The dashed red line is the slope of the straight line joining the heat bath temperatures.

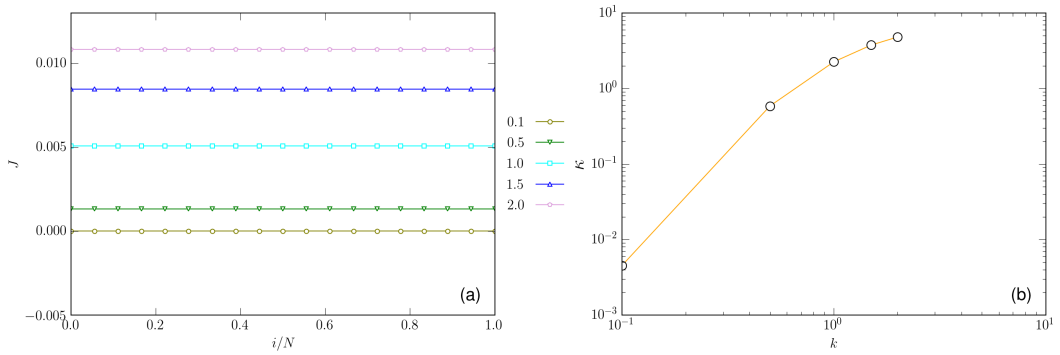

Figure 3.6: Heat current along the ϕ^4 chain, varying the interaction strength k. The parameters are $A = 5.0, N = 20$, while for the baths we have $T_m = 0.09$ and $\Delta_{rel} = 0.5$. (a) Linear graph of the local heat current and (b) Log-log graph of the conductivity κ versus k.

As k increases, for fixed A, the harmonic interaction progressively dominates the dynamics, flattening the temperature profile (see figure 3.5). Con-

cerning the conductivity κ, we see in figure 3.6 that it increases with k, when A and N are fixed. This is consistent with the fact that κ becomes divergent in the thermodynamic limit for the harmonic case.

3.1.3
Varying the anharmonicity strength

When we fix k and N, the effects of varying A can be observed for the system. In this case we set $k = 1.0$ and $N = 20$, while for the heat baths, $T_m = 0.09$ and $\Delta_{rel} = 0.5$.

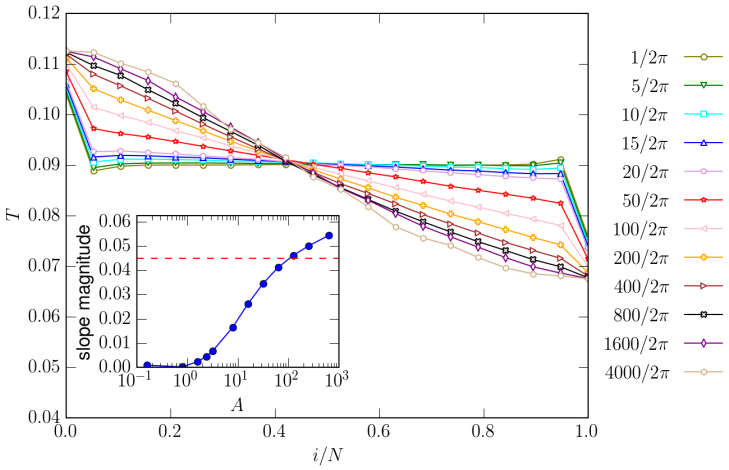

Figure 3.7: Temperature profile along the ϕ^4 chain, varying the anharmonicity strength A. The parameters are $k = 1.0, N = 20$, while for the baths we have $T_m = 0.09$ and $\Delta_{rel} = 0.5$. The inset shows the slope of the profile in absolute value (calculated using least squares linear regression, as shown in the appendix) versus A, with the abscissa in logarithmic scale. The dashed red line is the slope of the straight line joining the heat bath temperatures.

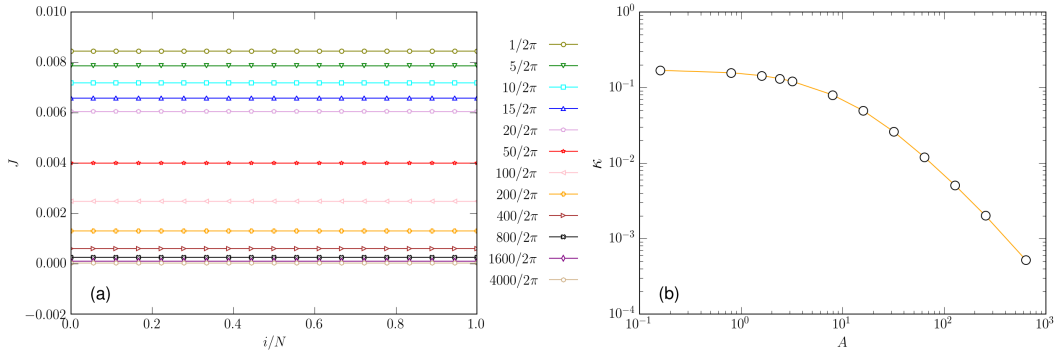

Figure 3.8: Heat current along the ϕ^4 chain, varying the anharmonicity strength A. The parameters are $k = 1.0, N = 20$, while for the baths we have $T_m = 0.09$ and $\Delta_{rel} = 0.5$. (a) Linear graph of the local heat current and (b) Log-log graph of the conductivity κ versus A.

In figure 3.7 it is shown that, for a wide range of amplitudes A, the harmonic potential dominates the dynamics. To understand for which values of A the system presents normal conduction, we see that the harmonic and anharmonic potentials intercept at the point

$$(x, V_Q(x)) = \left(\sqrt{\frac{2k}{A_Q}}, \frac{k^2}{A_Q} \right). \tag{3-7}$$

Since the thermal energy of the particle is of the order T_m (see appendix A), then the quartic potential starts dominating the dynamics near the point $T_m = k^2/A_Q$. The same can be obtained from non-dimensionalization considerations (as shown in appendix A.1).

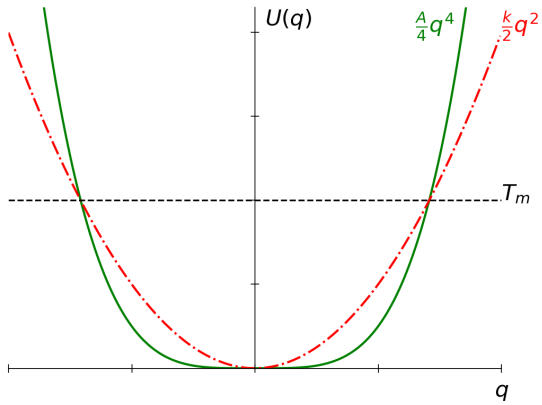

Figure 3.9: Sketch to understand the relation between (T_m, k, A_{FK}) for the ϕ^4 potential.

From this relation, we can estimate the value of A_Q for which the system starts behaving according to Fourier's law. In this case, $A_Q = k^2/T_m \approx 11$. The inset of figure 3.7 shows that indeed there is an inflection point between $A = 10$ and $A = 20$ for the temperature profile slopes.

In figure 3.8, it is shown that the conductivity κ, as a function of A, is almost constant for small enough A, and decays for larger values. The crossover between both regimes is around $A_Q = 10$, as predicted. In the next section we discuss in more depth how the non-dimensional group $A_Q T_m/k^2$ defines when the conduction is normal.

One last remark is that, for very high values of A_Q, the temperature profile seems to follow a sigmoid curve (see figure 3.7).

3.1.3.1 Interplay between anharmonicity and temperature

The previous discussion shows that, when the temperature increases and k is kept constant, we would need smaller values of A_Q to obtain normal conduction (shown by the inflection point of the graph of temperature profile slopes).

To see this effect, we reproduce the previous analysis for different values of T_m, specifically 0.09 (figure 3.10), 0.25(figure 3.11) and 1.0(figure 3.12), while fixing $k = 1.0$ and $\Delta_{rel} = 0.5$.

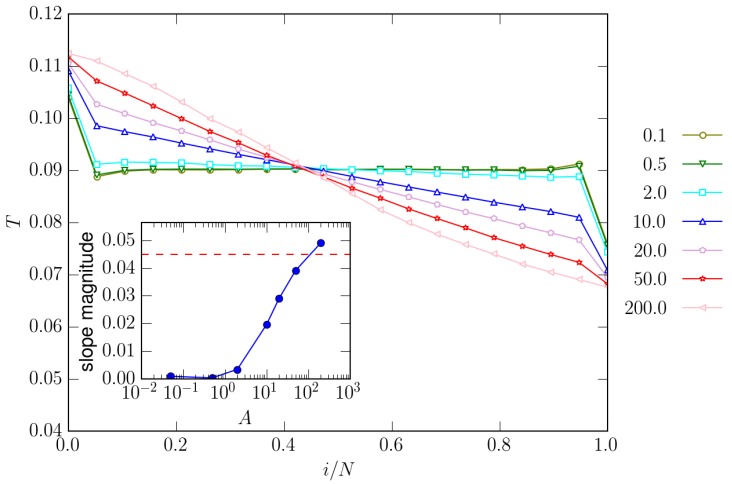

Figure 3.10: Temperature profile along the ϕ^4 chain, varying the anharmonicity strength A. The parameters are $k = 1.0, N = 20$, while for the baths we have $T_m = 0.09$ and $\Delta_{rel} = 0.5$. The inset shows the slope of the profile in absolute value (calculated using least squares linear regression, as shown in the appendix) versus A, with the abscissa in logarithmic scale. The dashed red line is the slope of the straight line joining the heat bath temperatures.

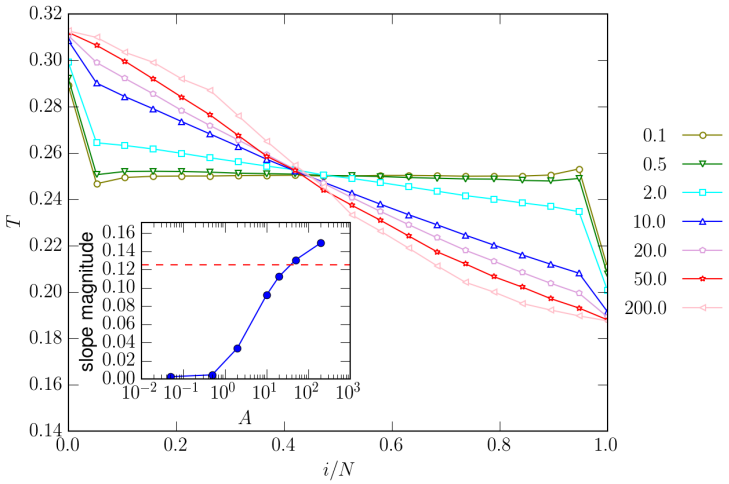

Figure 3.11: Temperature profile along the ϕ^4 chain, varying the anharmonicity strength A. The parameters are $k = 1.0, N = 20$, while for the baths we have $T_m = 0.25$ and $\Delta_{rel} = 0.5$. The inset shows the slope of the profile in absolute value (calculated using least squares linear regression, as shown in the appendix) versus A, with the abscissa in logarithmic scale. The dashed red line is the slope of the straight line joining the heat bath temperatures.

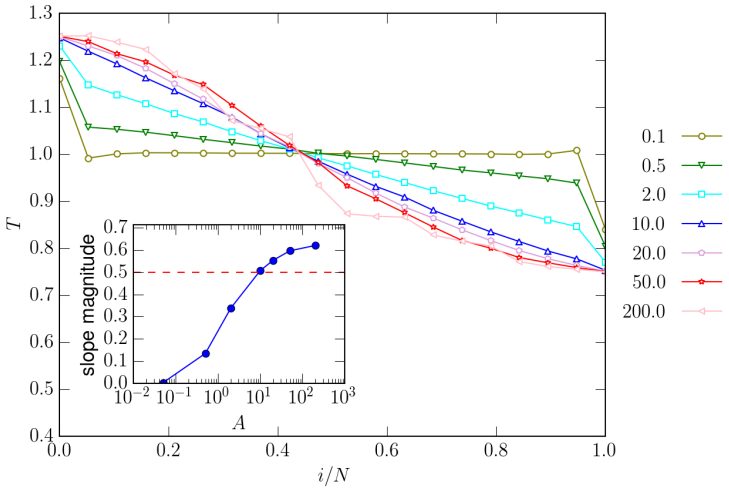

Figure 3.12: Temperature profile along the ϕ^4 chain, varying the anharmonicity strength A. The parameters are $k = 1.0, N = 20$, while for the baths we have $T_m = 1.0$ and $\Delta_{rel} = 0.5$. The inset shows the slope of the profile in absolute value (calculated using least squares linear regression, as shown in the appendix) versus A, with the abscissa in logarithmic scale. The dashed red line is the slope of the straight line joining the heat bath temperatures.

To be able to compare the insets of figures 3.10, 3.11 and 3.12, we divided all the slopes in each inset by the value of the dashed red line (which is the slope between the baths temperatures). The result can be seen in figure 3.13.

There, it is shown that, in fact, the higher the temperature, the smaller the value of A_Q for the inflection point. Since we set $k = 1.0$, then our approximations give $A_Q \approx 11, 4, 1$ for $T_m = 0.09, 0.25$ and 1.0, respectively. In figure 3.13.a, it is shown this is a good approximation. The changes in the conductivity for these values are seen in figure 3.13.b.

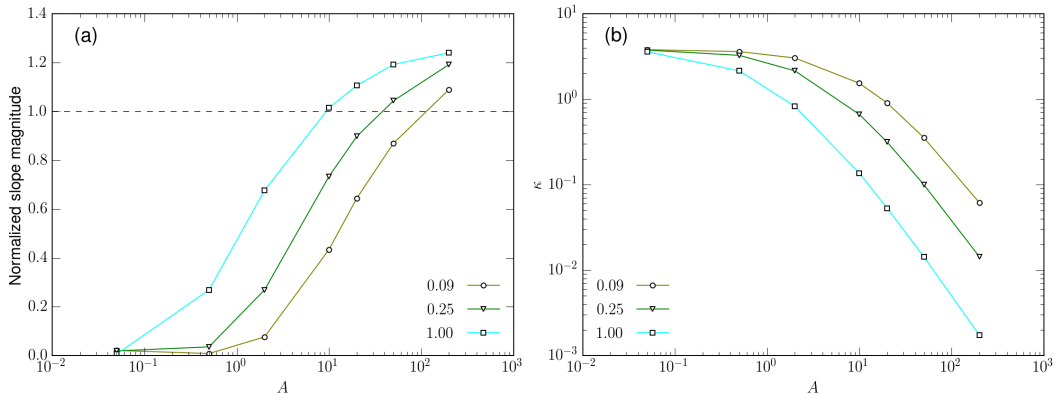

Figure 3.13: ϕ^4 chain model. (a) Comparing the magnitude of the temperature profile slope divided by the slope of the straight line joining the heat bath temperatures, with different T_m. (b) Comparing conductivity for different T_m. In both cases,the parameters are $k = 1.0, N = 20$ and $\Delta_{rel} = 0.5$.

Since we gave an heuristic argument that the relation between (T_m, k, A_Q), which determines if the model behaves as eexpected by Fourier's law, would be $A_Q T_m/k^2$, we then plot the conductivities from figure 3.13 using this variable. The result is that all curves collapse into a single one, as seen in figure 3.14.

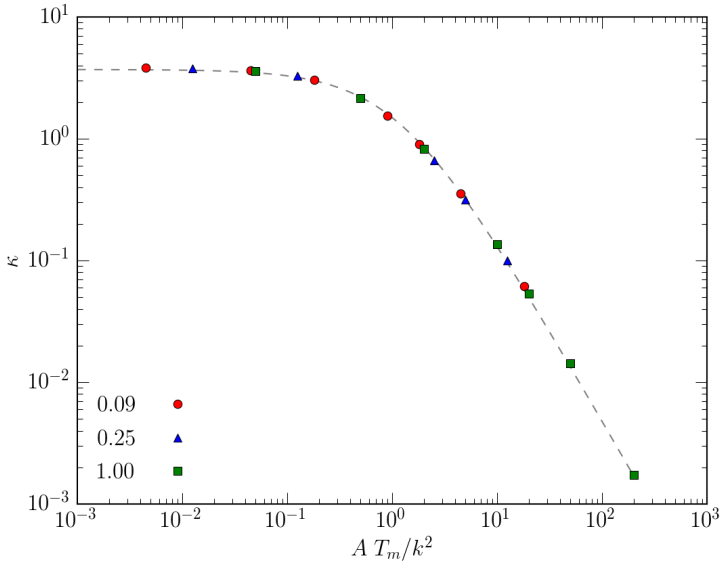

Figure 3.14: The conductivities for varying A_Q and T_m, when written in terms of A_QT_m/k^2, collapse into a single curve. The dashed line was drawn to show how all points fall in the same curve.

The previous results were obtained for $k = 1$. Then, to know what happens otherwise, we repeated the aforementioned simulations, for the same choices of A and T_m, now using $k = 0.5$, 1.5 and 2.0 (see figure 3.15). It can be seen that each value of k gives a different curve. We argue this is due to the harmonic model conductivity depending on k, and so the harmonic regime, obtained for small values of A_QT_m/k^2, show different conductivities. When we account for this dependency, by dividing the entire curve by the harmonic limit conductivity, we again get a common curve for all cases (see figure 3.16).

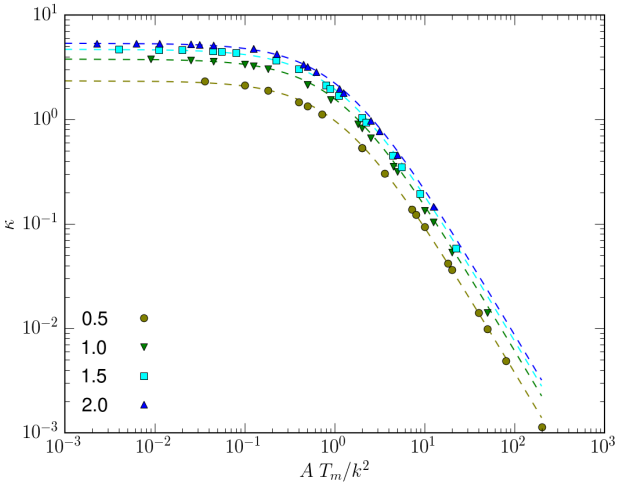

Figure 3.15: Conductitivies written in terms of A_QT_m/k^2, when varying A_Q, T_m and k. The dashed lines were drawn to show how points with the same k fall in the same curve.

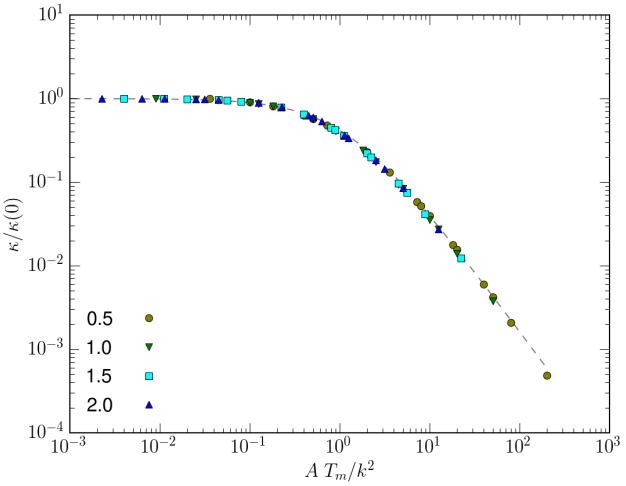

Figure 3.16: Conductitivies divided by the harmonic limit conductivity, written in terms of $A_Q T_m/k^2$, when varying A_Q, T_m and k. The dashed line was drawn to show how all points fall in the same curve.

3.2 Frenkel-Kontorova chain

In the next sections, the effects of each chain parameter on the FKC model will be studied, beginning with the number of particles in the model. Then, we will see how the strength of the harmonic interaction and the strength of the anharmonic potential changes the thermodynamic properties.

In all cases, unless stated otherwise, the bath temperature values are given by $T_m = 0.09$ and $\Delta_{rel} = 0.5$, while the total simulation time was $t_{max} = 3 \times 10^5$, with a transient $t_{trans} = 10^5$, while the integration time step is $\delta t = 10^{-3}$ and $\mathcal{N} = 100$.

3.2.1 Varying the number of particles

In order to see how the number of particles in the chain affects each of the aforementioned properties, we set $k = 1.0$, $A = 5/2\pi$. The results on the temperature profile are shown in figure 3.17, while the heat current and the conductivity are shown in figure 3.18. Each curve was obtained for a different value of N. In this case we used $\mathcal{N} = 100$.

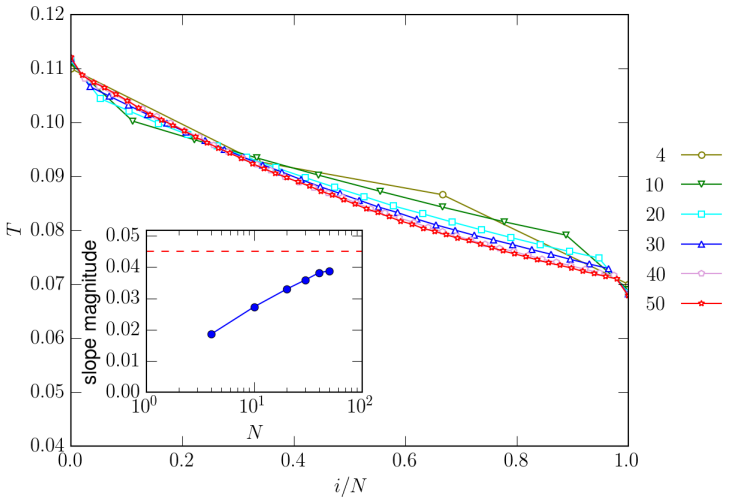

Figure 3.17: Temperature profile along the FK chain, varying the number of particles in the chain N. The parameters are $A = 5/2\pi, k = 1.0$, while for the baths we have $T_m = 0.09$ and $\Delta_{rel} = 0.5$. The inset shows the slope of the profile in absolute value (calculated using least squares linear regression, as shown in the appendix) versus N, with the abscissa in logarithmic scale. The dashed red line is the slope of the straight line joining the heat bath temperatures.

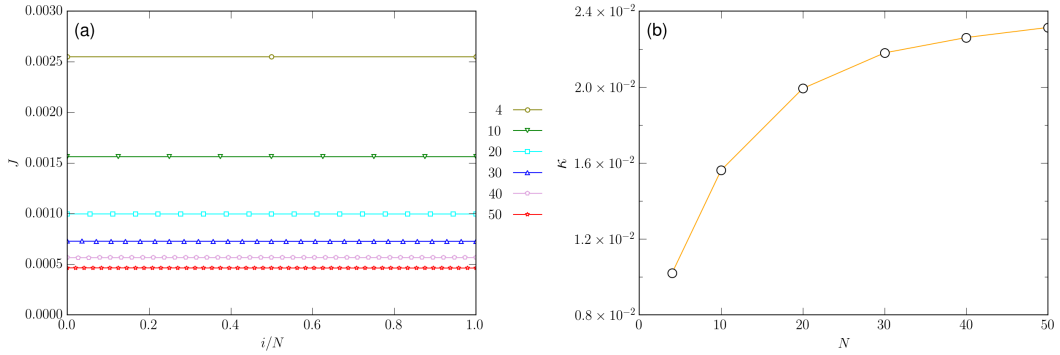

Figure 3.18: Heat current along the FK chain, varying the number of particles N. The parameters are $A = 5/2\pi, k = 1.0$, while for the baths we have $T_m = 0.09$ and $\Delta_{rel} = 0.5$. (a) Linear graph of the local heat current and (b) conductivity κ versus N.

We can observe that the heat currents are constant along the chain within the precision shown in figure 3.18. This is a clear indication that the system has reached a stationary state.

As N grows, the discontinuity in the boundary of the temperature profile gets smaller, something that has already been shown extensively in

the literature [63]. This shows that the Kapitza resistances decrease with N. The profile slope, calculated using least squares linear regression, seems to be increasing up to a maximum value (see inset of figure 3.17), as does the conductivity (see figure 3.18.b).

According to Fourier's law, κ should become independent of N, for large N. However, depending on the temperature of the system, the range of N for which κ is constant changes, generally being higher than $N = 200$ [22]. This is consistent with our results slowly approaching a limiting value.

Now, although the slope of $T(i/N)$ increases together with κ when varying N, we will see this is not the case when varying A and k, so it should not be seen as a general rule.

Also, for higher values of N, a small curvature appears for the temperature profile, which gets slightly convex. A closer look at the graphs of the linear regression show this convexity (see appendix B), but as was the case for the ϕ^4 model, this can be explained by the fact that the thermal conductivity of the FKC model depends on the local temperature of the particles [64, 63, 33, 39]. In ref. [22] the profile is also curved (albeit it is concave). This is due to the range of temperatures is large relative to T_m.

The behavior of κ as a function of T_m (not shown in this work) is complex, decreasing until a minimum value and then increasing [64, 63, 33]. Qualitatively, this is consistent with $\kappa \propto T^\alpha$ if, for small T_m, $\alpha < 0$, while $\alpha > 0$ otherwise.

3.2.2
Varying the interaction strength

When varying k, we will fix $A = 5$ and $N = 20$. The resulting temperature profiles are shown in figure 3.19, while the heat current and the conductivity are shown in figure 3.20. Each curve is for a different value of k.

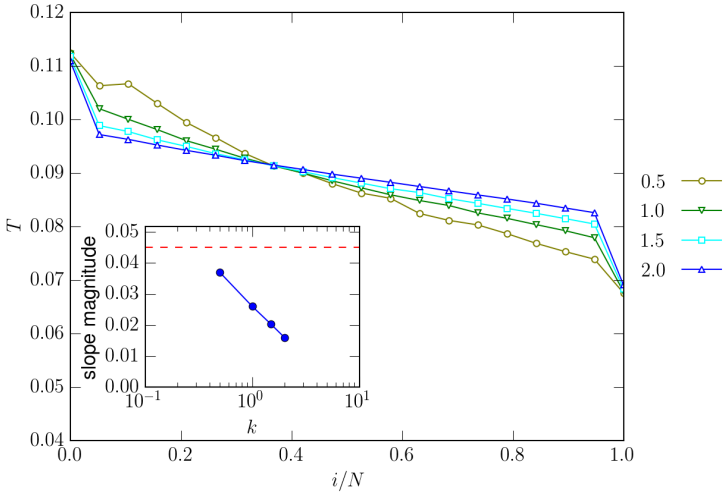

Figure 3.19: Temperature profile along the FK chain, varying k. The parameters of the chain are $A = 5.0/2\pi$, $N = 20$, while for the baths we have $T_m = 0.09$ and $\Delta_{rel} = 0.5$. The inset shows the slope of the profile in absolute value (calculated using least squares linear regression) versus k, with the abscissa in logarithmic scale. The dashed red line is the slope of the straight line joining the heat bath temperatures.

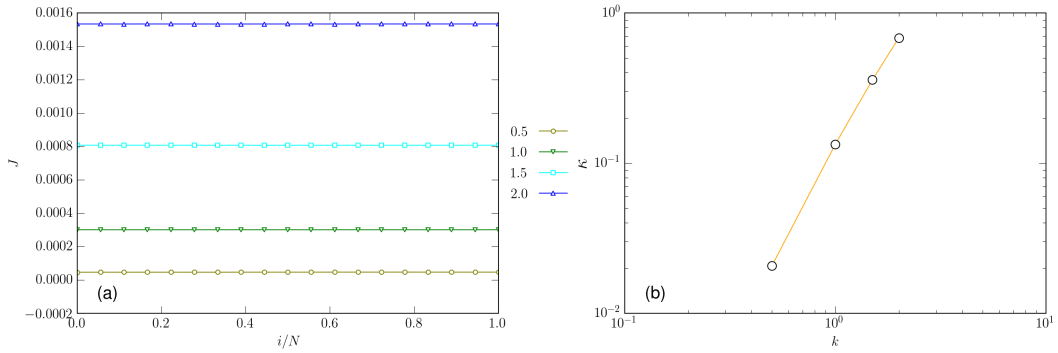

Figure 3.20: Heat current along the FK chain, varying the strength of interaction k. The parameters are $A = 5.0/2\pi$, $N = 20$, while for the baths we have $T_m = 0.09$ and $\Delta_{rel} = 0.5$. (a) Linear graph of the local heat current and (b) Log-log graph of the conductivity κ versus k.

In figure 3.19, the slope of the profile get smaller with higher values of k. This is to be expected, since in this case the harmonic interaction would be the dominating term in the dynamics, and a purely harmonic chain has a flat temperature profile. Thus higher values of k, relative to A, should result in flatter temperature profiles. The heat conductivity κ increases with k, in agreement with the results for QC discussed in the section 3.1.2.

3.2.3
Varying the anharmonicity strength

When varying A, we will set $k = 1.0$ and $N = 20$. The resulting temperature profiles are shown in figure 3.21, while the heat current and the conductivity are shown in figure 3.22. Each curve is for a different value of A.

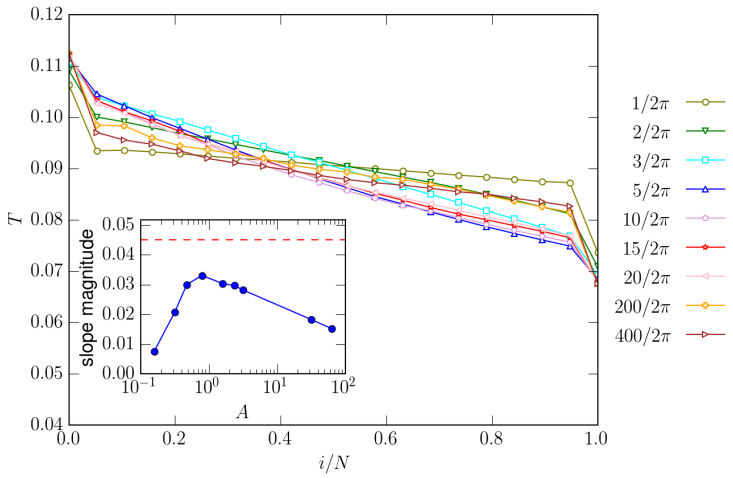

Figure 3.21: Temperature profile along the FK chain, varying A. The parameters are $N = 20, k = 1.0$, while for the baths we have $T_m = 0.09$ and $\Delta_{rel} = 0.5$. The inset shows the slope of the profile in absolute value (calculated using least squares linear regression, as shown in the appendix) versus A, with the abscissa in logarithmic scale. The dashed red line is the slope of the straight line joining the heat bath temperatures.

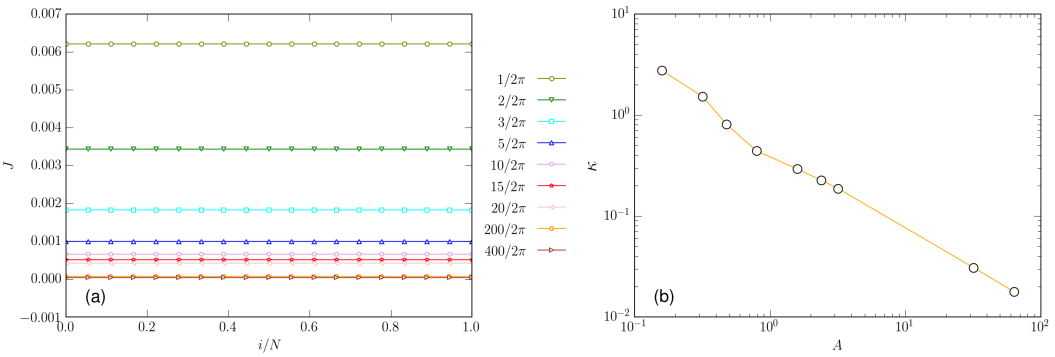

Figure 3.22: Heat current along the FK chain, varying A. The parameters are $N = 20, k = 1.0$, while for the baths we have $T_m = 0.09$ and $\Delta_{rel} = 0.5$. (a) Linear graph of the local heat current and (b) Log-log graph of the conductivity κ versus A

When we increase the strength of the periodic anharmonic potential in the FK chain, the slope of the temperature profile increases up to a maximum, and then decreases (see the inset of figure 3.21).

In the case of small A, the harmonic particle-particle interaction dominates the dynamics, resulting in a flat profile. As we increase A, the Frenkel-Kontorova potential starts dominating. At this point, we need to compare the quadratic and higher-order terms of the Taylor expansion for the cosine,

$$A\left[1-\cos(x)\right] = A\left[\frac{x^2}{2!} - \frac{x^4}{4!} + \ldots\right]. \tag{3-8}$$

The thermal fluctuations of the particle depend on the mean temperature of the baths, T_m, and on the strength of the anharmonic potential, A. Now if the displacement q_n is near zero most of the time, the cosine can be well approximated by a parabola, while the quartic term is important for higher q_n.

When A is too big, relative to T_m, the particle thermal fluctuations are confined to the potential well near equilibrium and the quadratic term dominates the dynamics, thus flattening the temperature profile. For A not as big, q_n varies enough for the particle to feel the quartic term, thus showing the expected linear profile.

Looking at figure 3.22 (b), we see that κ decreases with A, in accordance with ref. [63]. This makes sense in the context of our discussion on the temperature profile slope. Higher values of A would make each particle vibrate less, thus making the thermal current smaller. The conductivity then decreases.

Because the potential is bounded, the relation between T_m, k and A_{FK} that produces normal conduction is not as clear as before. When T_m is higher than the periodic potential amplitude, $T_m > A_{FK}/\pi$, the particles have enough energy to hop between the potential wells and as we increase T_m, the harmonic interactions tend to dominate the dynamics [25]. For $T_m < A_{FK}/\pi$, depending on the relative values of (T_m, k, A_{FK}), either the harmonic or the anharmonic terms can dominate.

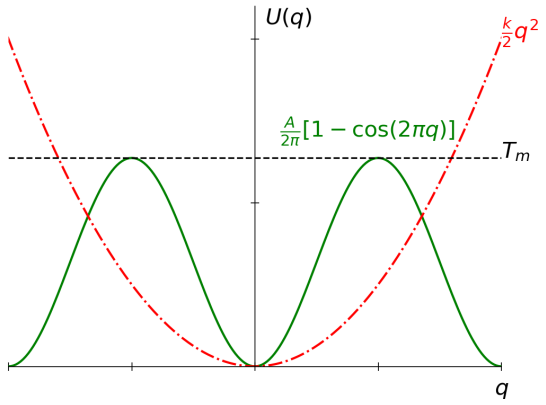

Figure 3.23: Sketch to understand the relation between (T_m, k, A_{FK}) for the Frenkel-Kontorova potential. Notice the amplitude of the periodic potential is A_{FK}/π, due to the fact that $0 < 1 - cos(2\pi q) < 2$.

If we use nondimensionalization arguments for the Frenkel-Kontorova model (analogous to the ones used for the ϕ^4 model), we would find that the adimensional anharmonic amplitude is

$$A^*_{FK} = \frac{A_{FK}}{a}\sqrt{\frac{1}{kT_m}}. \tag{3-9}$$

The relation between (T_m, k, A_{FK}) will be further discussed in the next section.

3.2.3.1 Interplay between anharmonicity and temperature

To understand the interplay between the parameters (T_m, k, A_{FK}) that reproduces normal conduction, we will fix $k = 1.0$, while varying A for different values of T_m. Like in the QC model, we use the values 0.09, seen in figure 3.24, 0.25, seen in figure 3.25, and 1.0, in figure 3.26

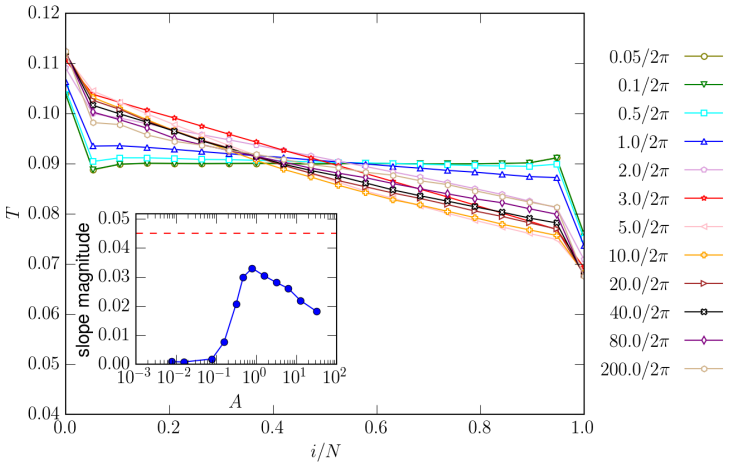

Figure 3.24: Temperature profile along the FK chain, varying the anharmonicity strength A. The parameters are $k = 1.0, N = 20$, while for the baths we have $T_m = 0.09$ and $\Delta_{rel} = 0.5$. The inset shows the slope of the profile in absolute value (calculated using least squares linear regression, as shown in the appendix) versus A, with the abscissa in logarithmic scale. The dashed red line is the slope of the straight line joining the heat bath temperatures.

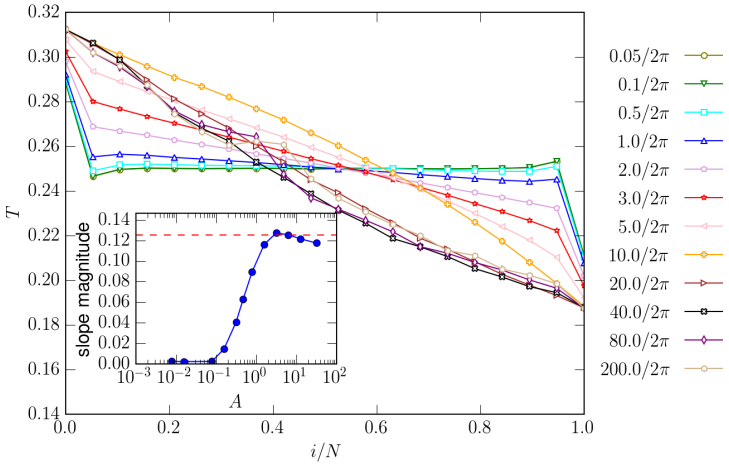

Figure 3.25: Temperature profile along the FK chain, varying the anharmonicity strength A. The parameters are $k = 1.0, N = 20$, while for the baths we have $T_m = 0.25$ and $\Delta_{rel} = 0.5$. The inset shows the slope of the profile in absolute value (calculated using least squares linear regression, as shown in the appendix) versus A, with the abscissa in logarithmic scale. The dashed red line is the slope of the straight line joining the heat bath temperatures.

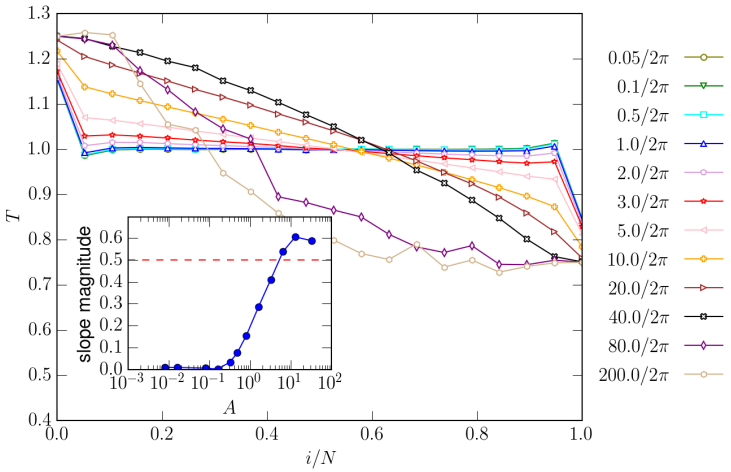

Figure 3.26: Temperature profile along the FK chain, varying the anharmonicity strength A. The parameters are $k = 1.0, N = 20$, while for the baths we have $T_m = 1.0$ and $\Delta_{rel} = 0.5$. The inset shows the slope of the profile in absolute value (calculated using least squares linear regression, as shown in the appendix) versus A, with the abscissa in logarithmic scale. The dashed red line is the slope of the straight line joining the heat bath temperatures.

As discussed previously, when T_m is increased above A_{FK}/π, the harmonic interactions tend to dominate the dynamics. By the same argument, if T_m is fixed, it must be $A_{FK} > \pi T_m$ to avoid this harmonic regime. In figure 3.27.a, we see that this is a good approximation for the inflection point of the slope. For $T_m = 0.09$, 0.25 and 1.0, the expected values of A_{FK} would be 0.28, 0.79 and 3.14, respectively. When $T_m < A_{FK}/\pi$, increasing A_{FK} makes the particle dynamics be dominated by the quadratic term of the anharmonic potential, and so the slope tends to zero.

Similar to the ϕ^4 model, κ, as a function of A (figure 3.27), is approximately constant for small values of A, and then decreases (see figure 3.13.b). However, for values of A_{FK} bigger than the plateau one (in the slope graph), the conductivity decreases more slowly.

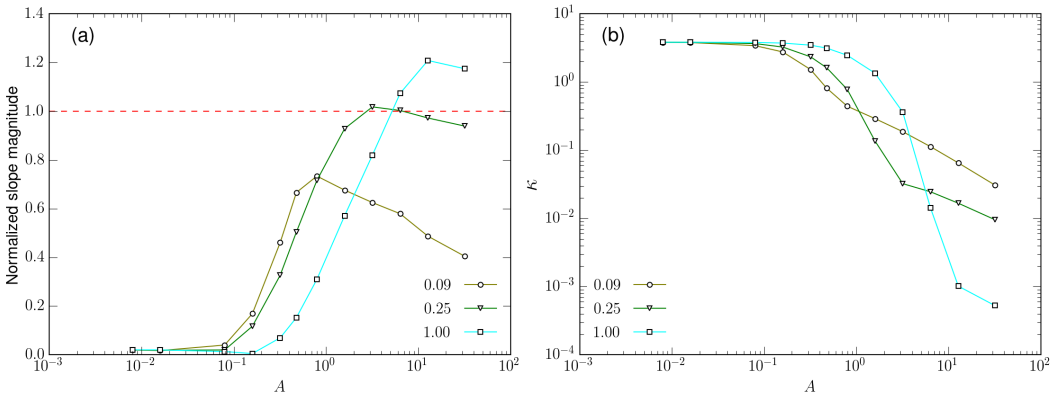

Figure 3.27: FK chain model. (a) Comparing the magnitude of the temperature profile slope divided by the slope of the straight line joining the heat bath temperatures, with different T_m. (b) Comparing conductivity for different T_m. In both cases,the parameters are $k = 1.0, N = 20$ and $\Delta_{rel} = 0.5$.

Like we did for the ϕ^4 model, we try to redraw the graphs in terms of a relation between the amplitudes and the temperature. In this case, we use the parameter achieved from nondimensionalization, and the result, which is not as good as the aforementioned case, can be seen in figure 3.28.

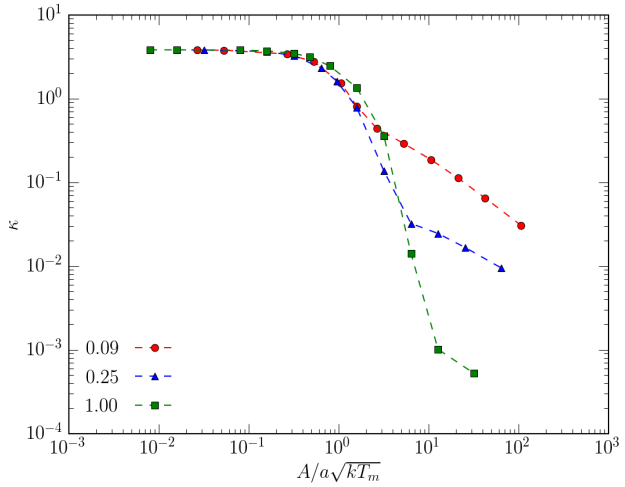

Figure 3.28: Collapsing the conductivities of the Frenkel-Kontorova model in a single curve.

3.3 Final Remarks

In this chapter, we made a preliminary study about heat conduction, in order to familiarize ourselves with this subject in order to study the more complex problem of heat current rectification in the next chapter.

For this study, we addressed two different models, with the minimal requirements for the validity of Fourier's law (an anharmonic potential that does not conserve momentum). We considered two potentials, one bounded (Frenkel-Kontorova potential) and one unbounded (ϕ^4 potential), for comparison.

As a control for choosing the parameters of the thermal diode models, we performed numerical simulations to verify how changing the parameters of both models changed the thermodynamic properties of the system.

We studied the relation between the harmonic interaction amplitude, k, the anharmonic on-site potential amplitude, A, and the average system temperature, T_m, to obtain normal heat conduction, and how they affect the system thermal conductivity. It was discussed how the conductivity depends on the temperature, $\kappa = \kappa(T)$.

4
Thermal diode results

In chapter 3, we showed numerical results for heat conduction in the FKC and QC models. There we discussed how the magnitudes of k and A, relative to T_m, affect the temperature profile and conductivity, and tried to get insights by zooming in the dynamics of the system.

In this chapter, we will investigate how non-homogeneity and the interface interaction, in the TSFKC and TSQC models, bring forth the rectification of the heat current along the chain.

Here we use the same numerical schemae as before, the stochastic fourth-order Runge-Kutta method. All thermodynamic properties are also calculated in the same way. The difference is that now we have to define the parameters of both left (k_L, A_L) and right (k_R, A_R) segments, as well as those of their interaction (μ, k_μ).

Since we have seen in the previous chapter that the ratio of the amplitudes dictates if the conductivity of each segment is normal, following Fourier's law, we shall always consider $k_L/A_L = k_R/A_R$. To do this, the parameter $\lambda = k_R/k_L = A_R/A_L$ was defined in section A.4.

To be able to observe the rectification of the heat current, we will need to always compare the cases $T_L > T_R$ and $T_L < T_R$, with $|T_L - T_R|$ and T_m being kept constant. As discussed in chapter A, instead of using the temperature difference, we will use the relative difference $\Delta_{rel} = (T_L - T_R)/T_m$. When $\Delta_{rel} > 0$, $T_L > T_R$, and when $\Delta_{rel} < 0$, $T_L < T_R$. In this case, we define $J_{L\to R}$ as the heat current when $\Delta_{rel} > 0$, and $J_{R\to L}$ as the heat current when $\Delta_{rel} < 0$.

The rectification coefficient was defined in equation 2-56 as

$$R = \frac{|J_+ - J_-|}{|J_-|}\,, \tag{4-1}$$

where J_+ and J_- were the absolute values of the higher and lower heat currents, respectively.

This chapter will be separated in two parts. First, we discuss how inhomogeneity, $\lambda \neq 1$, changes the system dynamics,creating thermal rectification. In the sequence, we will change the exponent μ of the interfacial interaction and see its effects.

4.1 Varying the asymmetry

To look at how $\lambda \neq 1$, compared with the previous chapter where $\lambda = 1$, affects the rectification of the TSQC and TSFKC models, we keep $\mu = 2.0$ and change the values of the parameters of the chains and thermal baths. Unless stated otherwise, we will always assume the chain is small, with $N = 4$. The quartic chains will be discussed first, before moving on to the Frenkel-Kontorova chains.

In order to compare the magnitude of the forward and backward currents, we always consider both positive and negative values of Δ_{rel}, but with the same absolute value, thus we represent both cases using $|\Delta_{rel}|$.

In both cases, we use a total simulation time of $t_{max} = 2 \times 10^5$, transient time $t_{trans} = 5 \times 10^4$, and integration time step $\delta t = 10^{-3}$, with $\mathcal{N} = 100$ samples.

4.1.1 Two-segment ϕ^4 chain

From the definition of λ, the difference between the on-site potential amplitudes of the left and right segments is given by $|A_L - A_R| = A_L|1 - \lambda|$. Because of this, we will now look how λ and A_L alter the rectification coefficient for the ϕ^4 chain.

Let us first look at varying λ. The parameters of the left segment of the chain are $k_L = 1.0, A_L = 10.0$, while the parameters of the right segment depend on λ. The parameters of the baths are $T_m = 0.25$ and $\Delta_{rel} = 0.5$.

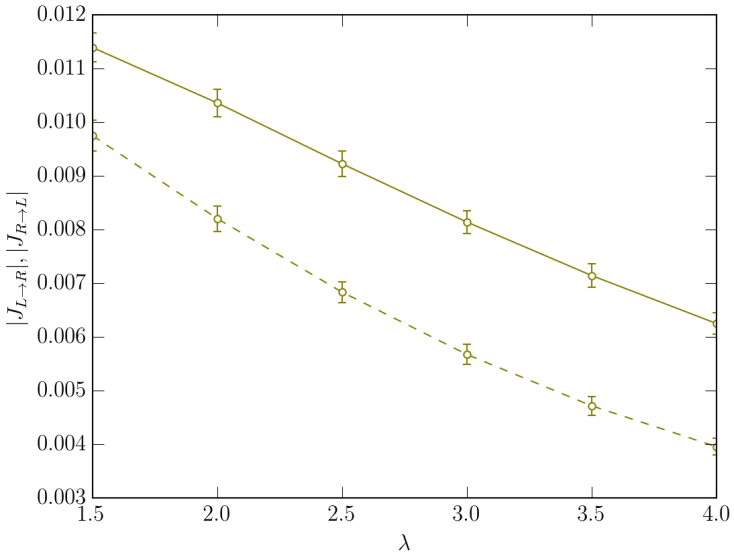

Figure 4.1: Magnitude of the heat current as a function of λ, for the TSQC. The dashed and solid lines correspond to $|J_{R\to L}|$ and $|J_{L\to R}|$, respectively. The parameters of the chains are $k_L = 1.0$, $A_L = 10.0$, $k_\mu = 1.0$, $\mu = 2.0$, while for the baths we have $T_m = 0.25$, $|\Delta_{rel}| = 0.5$.

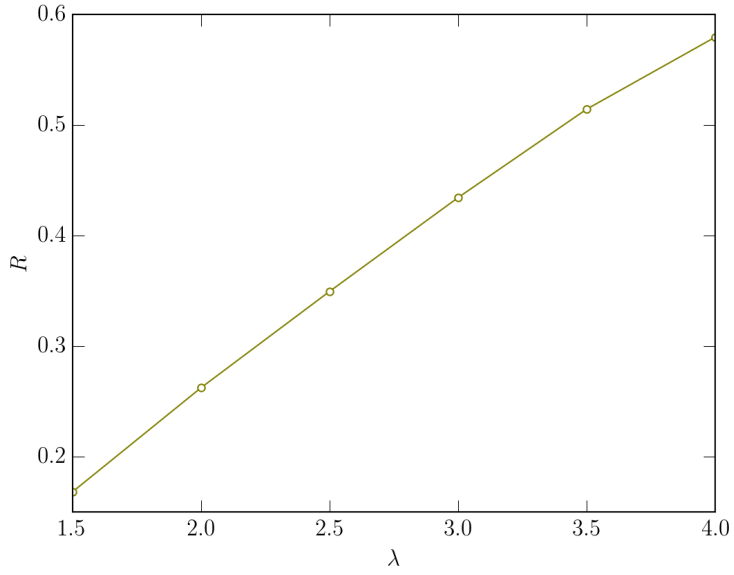

Figure 4.2: Rectification coefficient against λ, for the TSQC. The parameters of the chains are $k_L = 1.0$, $A_L = 10.0$, $k_\mu = 1.0$, $\mu = 2.0$, while for the baths we have $T_m = 0.25$, $|\Delta_{rel}| = 0.5$.

We will set $\lambda > 1.0$, because we can increase $|A_L - A_R|$ with no bounds, for fixed A_L. In this case, we have $|J_{L\to R}| > |J_{R\to L}|$. This shows that the heat current is bigger when going from the segment whose on-site potential has lower amplitude to the one with higher amplitude. In section 4.2, we will see how this

is the opposite of the TSFKC model. We notice that when λ increases, the heat current decreases, which makes sense, since the on-site potential amplitudes will increase and restrain the particle vibrations.

The rectification coefficient increases with λ, indicating that it enhances (dampens) the phonon bands overlap for $\Delta_{rel} > 0$ ($\Delta_{rel} < 0$), as seen in [25].

To understand the role of the amplitude difference $|A_L - A_R|$ in the rectification R, we fix $\lambda = 2.0$ and vary the values of A_L.

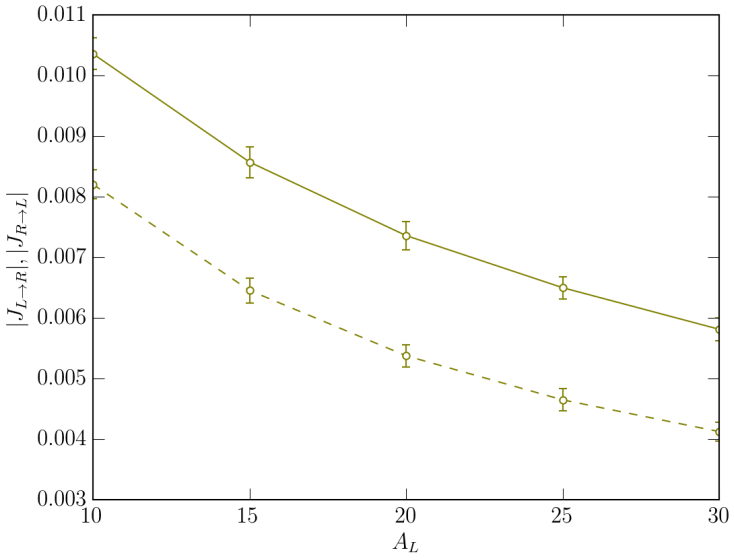

Figure 4.3: Magnitude of the heat current as a function of A_L, for the TSQC. The dashed and solid lines correspond to $|J_{R\to L}|$ and $|J_{L\to R}|$, respectively. The parameters of the chains are $k_L = 1.0$, $\lambda = 2.0$, $k_\mu = 1.0$, $\mu = 2.0$, while for the baths we have $T_m = 0.25$, $|\Delta_{rel}| = 0.5$.

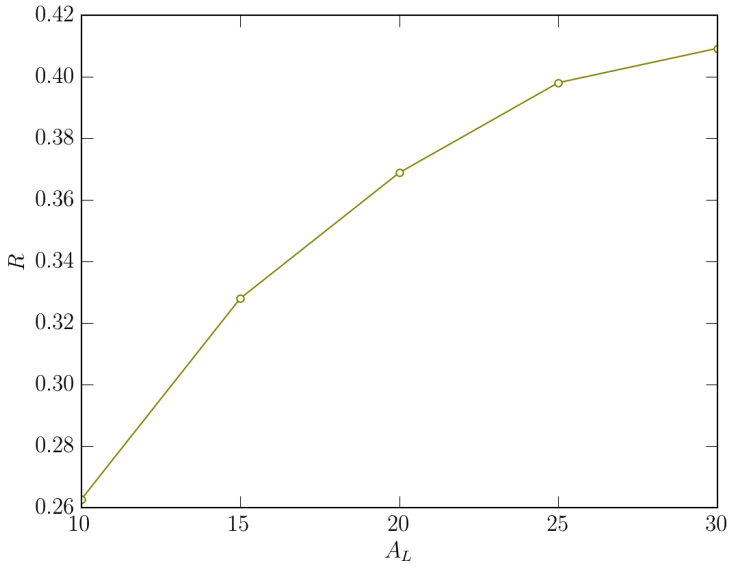

Figure 4.4: Rectification coefficient against A_L, for the TSQC. The parameters of the chains are $k_L = 1.0$, $\lambda = 2.0$, $k_\mu = 1.0$, $\mu = 2.0$, while for the baths we have $T_m = 0.25$, $|\Delta_{rel}| = 0.5$.

Again, as the amplitudes increases, the heat current decreases while R increases. However, now it seems as if R is approaching a plateau.

4.2 Varying the temperatures of the heat baths

Now that we understand how λ brings the rectification effect, we look how the bath temperatures affects it. In all cases, we use a total simulation time of $t_{max} = 3 \times 10^5$, transient time $t_{trans} = 10^5$, and integration time step $\delta t = 10^{-3}$, with $\mathcal{N} = 100$ samples.

4.2.1 Two-segment ϕ^4 chain

The first results are the variation of the rectification with T_m and Δ_{rel} for the TSQC. The parameters of the left segment of the chain are $k_L = 1.0, A_L = 5/2\pi$, while the parameters of the right segment are calculated using $\lambda = 0.2$.

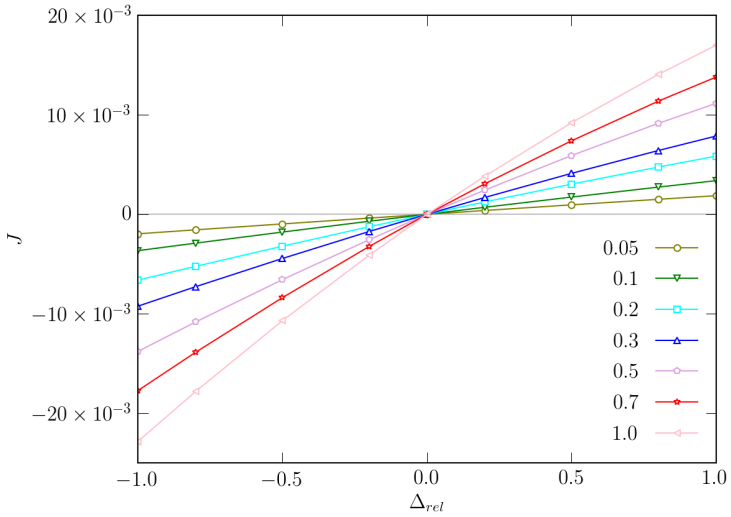

Figure 4.5: Heat current of the chain against Δ_{rel} for different values of T_m for the TSQC. The parameters of the chains are $k_L = 1.0, A_L = 5.0/2\pi, \lambda = 0.2, k_\mu = 1.0, \mu = 2.0$.

Figure 4.5 shows how the heat current changes with the variation of the bath parameters. When $\Delta_{rel} < 0$, we have $T_L < T_R$, while $\Delta_{rel} > 0$ implies $T_L > T_R$.

Although our choice of parameter values does not show much difference in the magnitude of heat currents for positive and negative Δ_{rel}, it is still possible to see a slight asymmetry. Figure 4.6 makes this clearer, by looking only at the magnitudes of the heat currents against the same absolute value of temperature difference, $|\Delta_{rel}|$.

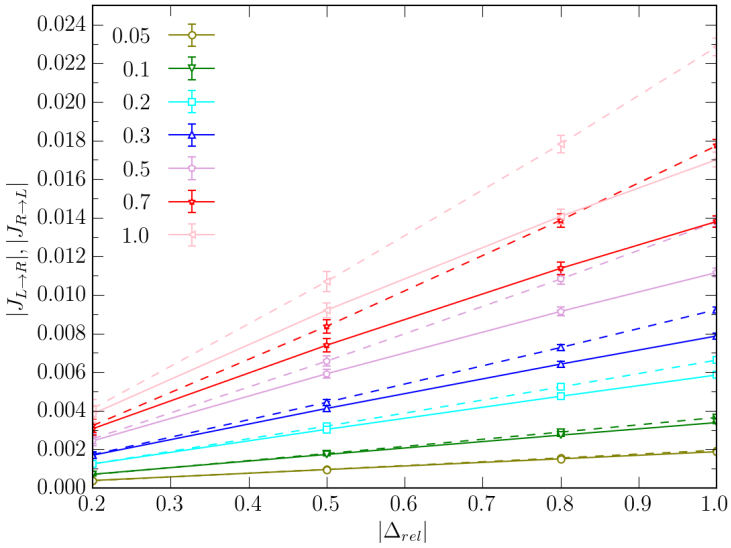

Figure 4.6: Magnitude of the heat current as a function of $|\Delta_{rel}|$, for different values of T_m, for the TSQC. The dashed and solid lines correspond to $|J_{R\to L}|$ and $|J_{L\to R}|$, respectively. The parameters of the chains are $k_L = 1.0, A_L = 5/2\pi, \lambda = 0.2, k_\mu = 1.0, \mu = 2.0$.

The value of $|J_{R\to L}|$ is bigger than $|J_{L\to R}|$, showing the rectification effect. Since $\lambda = 0.2$, $k_L = 1.0$ and $A_L = 5/2\pi$, the chain is such that $k_R = 0.2$ and $A_R = 1/2\pi$, in accordance with section 4.1. We can also observe that the heat currents increase with the average temperature of the baths and with the temperature difference.

The discrepancy between $|J_{L\to R}|$ and $|J_{R\to L}|$, measured through the rectification factor R, depends on T_m and $|\Delta_{rel}|$, as shown in figure 4.7. Notice that, for sufficiently large values of T_m and $|\Delta_{rel}|$, the rectification increases with both parameters, while for small values, that monotonic tendency changes.

A closer look on the behavior of the rectification coefficient is presented in figures 4.8 and 4.9, that represent different cuts of figure 4.7.

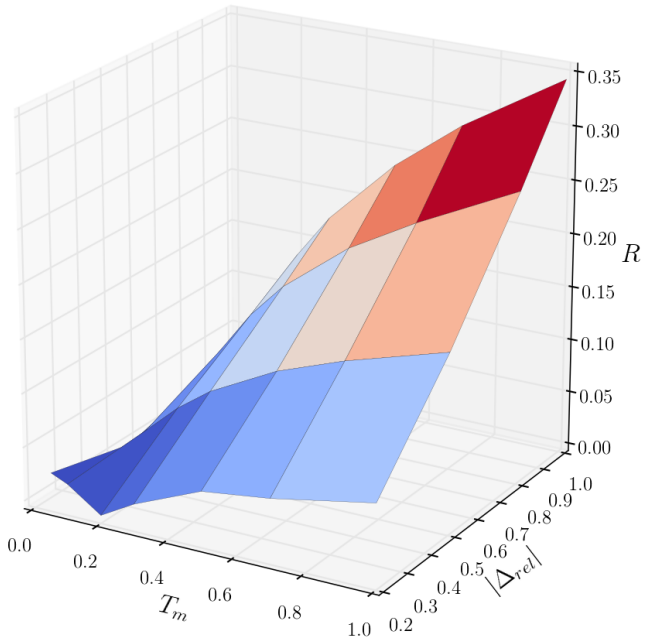

Figure 4.7: Surface of the rectification coefficient for different values of T_m and $|\Delta_{rel}|$ for the TSQC. The parameters of the chains are $k_L = 1.0, A_L = 5.0/2\pi, \lambda = 0.2, k_\mu = 1.0, \mu = 2.0$.

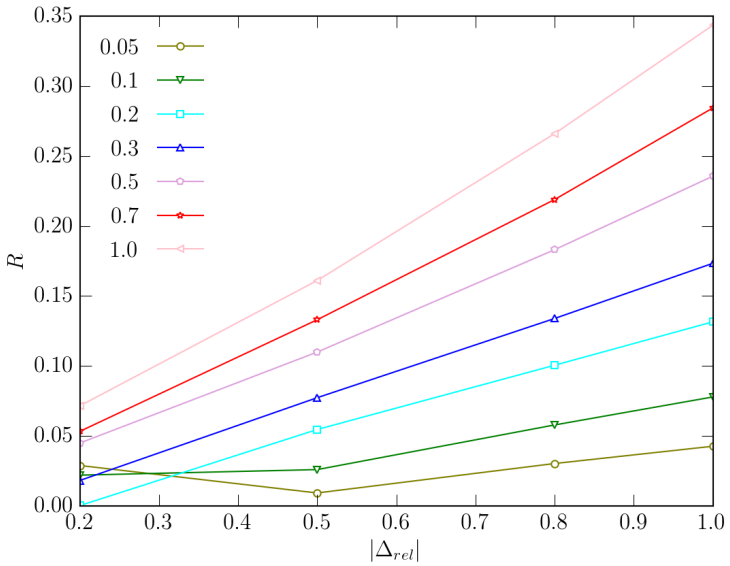

Figure 4.8: Rectification coefficient against $|\Delta_{rel}|$ for different values of T_m for the TSQC. The parameters of the chains are $k_L = 1.0, A_L = 5.0/2\pi, \lambda = 0.2, k_\mu = 1.0, \mu = 2.0$.

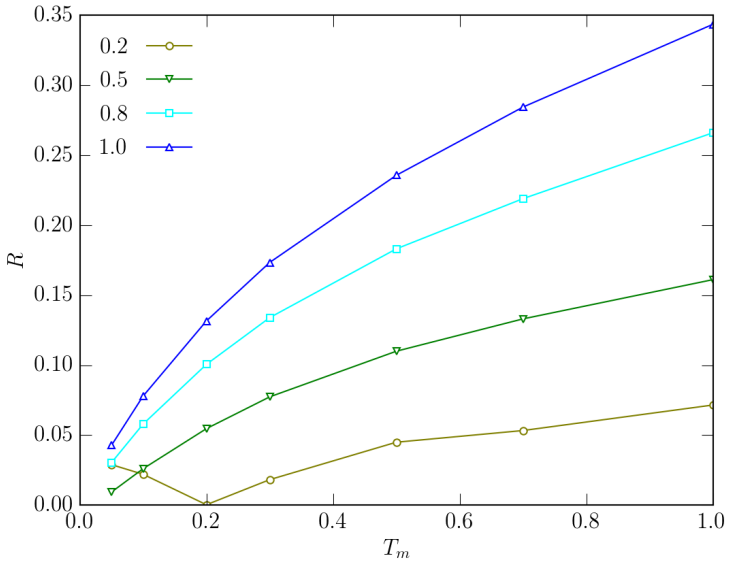

Figure 4.9: Rectification coefficient against T_m for different values of $|\Delta_{rel}|$ for the TSQC. The parameters of the chains are $k_L = 1.0, A_L = 5.0/2\pi, \lambda = 0.2, k_\mu = 1.0, \mu = 2.0$.

The interplay between T_m and $|\Delta_{rel}|$ is highly non-trivial. In figure 4.8, notice that for fixed T_m, R has a local minimum for $|\Delta_{rel}| = 0.5$ when T_m takes the lowest investigated value, while for higher values of the average temperature, R is an increasing function of $|\Delta_{rel}|$.

In figure 4.9, the rectification increases with T_m for $|\Delta_{rel}| > 0.2$. However, it decreases for $|\Delta_{rel}| = 0.2$.

4.2.2 Two-segment Frenkel-Kontorova chains

Now we study the impact of T_m and Δ_{rel} on the rectification R, for the TSFKC model. Again the parameters of the left segment of the chain are $k_L = 1.0, A_L = 5.0/2\pi$, while the parameters of the right segment are calculated using $\lambda = 0.2$.

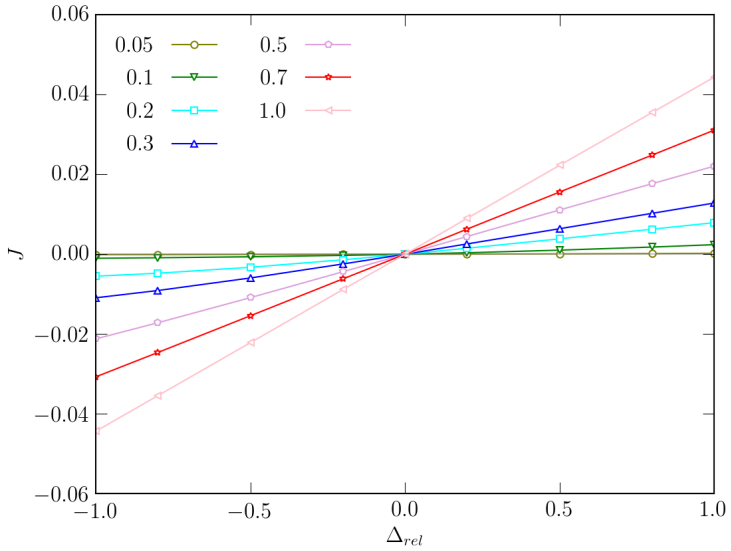

Figure 4.10: Heat current of the chain against Δ_{rel} for different values of T_m for the TSFKC. The parameters of the chains are $k_L = 1.0, A_L = 5.0/2\pi, \lambda = 0.2, k_\mu = 1.0, \mu = 2.0$.

The asymmetry, present in figure 4.10 but mitigated by the scale, becomes far more evident in figure 4.11.

Also in figure 4.12 we see that, as T_m increases, the difference between $|J_{R\to L}|$ and $|J_{L\to R}|$ first increases and then decreases.

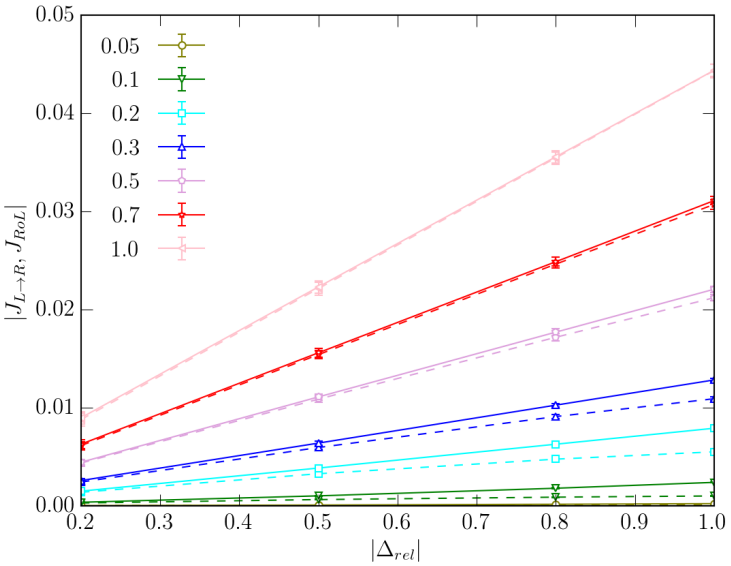

Figure 4.11: Magnitude of the heat current against $|\Delta_{rel}|$, for different values of T_m, for the TSFKC. The dashed and solid lines correspond to $|J_{R\to L}|$ and $|J_{L\to R}|$, respectively. The parameters of the chains are $k_L = 1.0, A_L = 5.0/2\pi, \lambda = 0.2, k_\mu = 1.0, \mu = 2.0$.

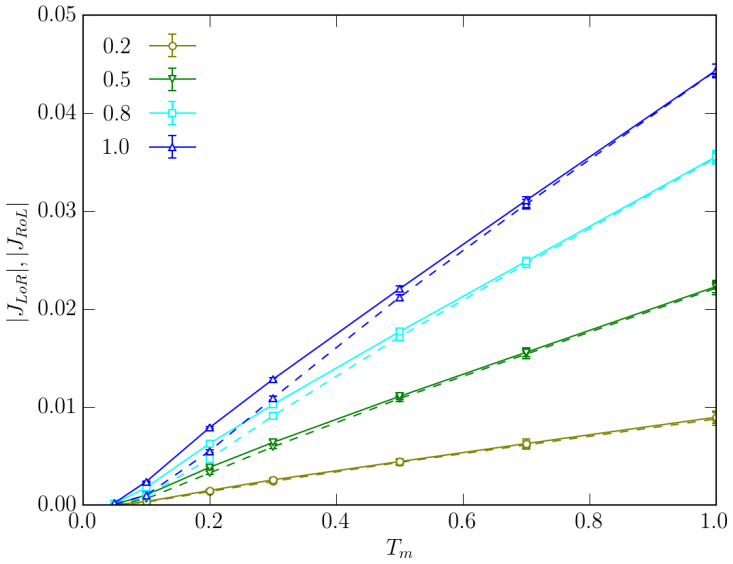

Figure 4.12: Magnitude of the heat current against T_m, for different values of $|\Delta_{rel}|$, for the TSFKC. The dashed and solid lines correspond to $|J_{R\to L}|$ and $|J_{L\to R}|$, respectively. The parameters of the chains are $k_L = 1.0, A_L = 5.0/2\pi, \lambda = 0.2, k_\mu = 1.0, \mu = 2.0$.

Unlike the quartic potential, the current in the Frenkel-Kontorova chain is stronger from the larger to the smaller potential amplitudes.

How much the currents, $|J_{R\to L}|$ and $|J_{L\to R}|$, differ is seen by the rectification coefficient variation with the temperatures in figures 4.13, 4.14 and 4.15.

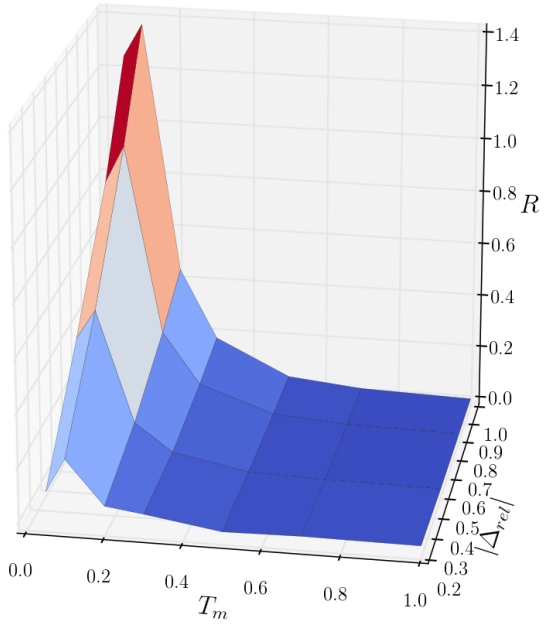

Figure 4.13: Surface of the rectification coefficient, as a function of T_m and $|\Delta_{rel}|$, for the TSFKC. The parameters of the chains are $k_L = 1.0, A_L = 5.0/2\pi, \lambda = 0.2, k_\mu = 1.0, \mu = 2.0$.

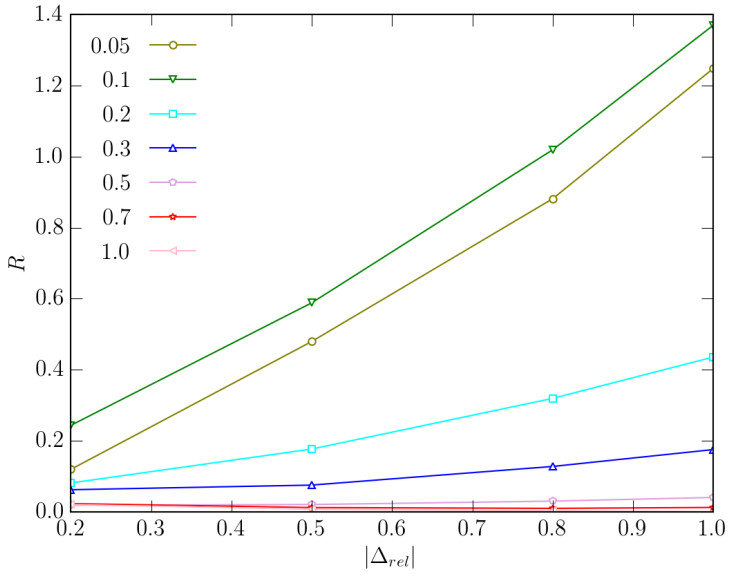

Figure 4.14: Rectification coefficient against $|\Delta_{rel}|$, for different values of T_m, for the TSFKC. The parameters of the chains are $k_L = 1.0, A_L = 5.0/2\pi, \lambda = 0.2, k_\mu = 1.0, \mu = 2.0$.

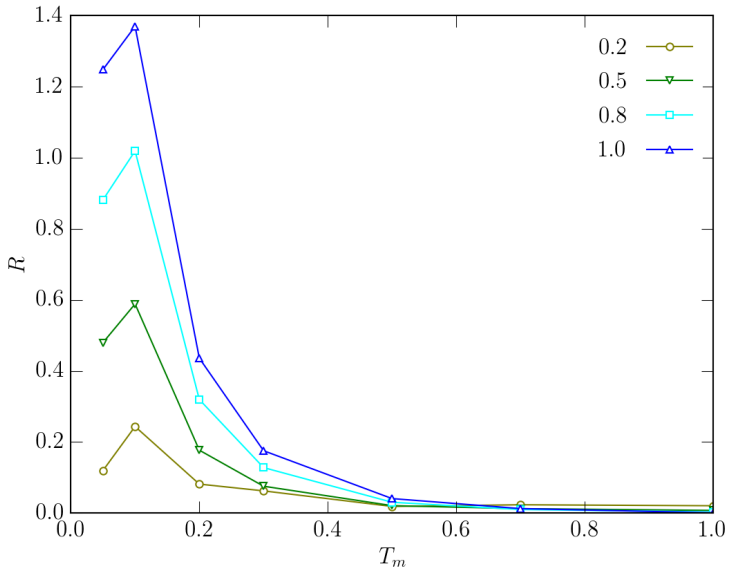

Figure 4.15: Rectification coefficient against T_m for different values of $|\Delta_{rel}|$ for the TSFKC. The parameters of the chains are $k_L = 1.0, A_L = 5.0/2\pi, \lambda = 0.2, k_\mu = 1.0, \mu = 2.0$.

In figure 4.15, we see that as the temperature increases, the rectification coefficient tends to zero, and the diode effect is lost. It shows a maximum near $T_m = 0.1$, and also increases with higher $|\Delta_{rel}|$.

The fact that R decreases as T_m increases is not surprising. For sufficiently high T_m, the Frenkel-Kontorova potential becomes negligible, and the particles are able to freely hop between the potential wells. In this regime, the dynamics is mainly governed by the harmonic potential. Then the rectification would depend only on the asymmetry of the particle-particle linear interactions. A purely harmonic chain is such that κ does not depend on the temperature, and so is not expected to show rectification [65].

4.3 Nonlinear interfacial interaction

Now we want to understand how changing the interaction between both segments of the two-segment models affects our previous results. To achieve this, we will be using the power-law potential defined in equation 2-58, namely

$$U_\mu\left(q_{n+1} - q_n\right) = \frac{k_\mu}{\mu}\left|q_{n+1} - q_n\right|^\mu, \; n = N/2, \tag{4-2}$$

and vary its parameter μ. For each exponent chosen, we will see the effects of changing k_μ, T_m and $|\Delta_{rel}|$.

As before, we use $N = 4$ in all cases. The quartic chains will be the focus, and the Frenkel-Kontorova chains will not be considered. Like in the

inhomogeneous case, we use the notation $|\Delta_{rel}|$ to show we are using both the positive and negative values of Δ_{rel}.

4.3.1 Impact of k_μ and μ

We start by looking at how k_μ changes the rectification, for different values of μ. We choose $k_L = 1.0$, $A_L = 1.0$ and $\lambda = 5.0$, meaning that the right-side potential has bigger amplitude than the left-side one.

For the baths, $T_m = 1.0, |\Delta_{rel}| = 1.0$, and the results are shown in figures 4.16 and 4.17.

The total simulation time is $t_{max} = 10^5$, while the transient time is $t_{trans} = 10^3$, and the integration time step is $\delta t = 10^{-3}$. We always simulate $\mathcal{N} = 100$ samples.

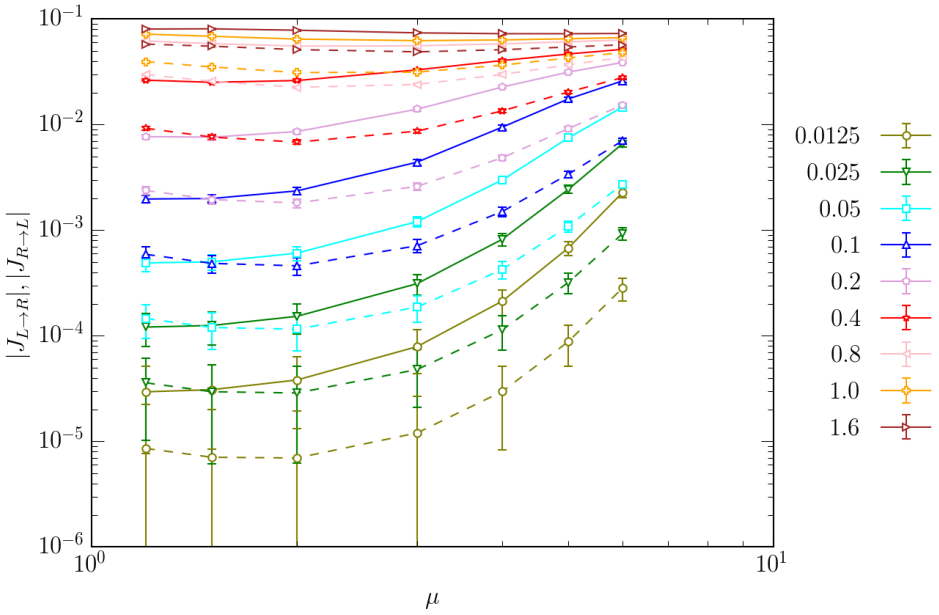

Figure 4.16: Log-log plot of the heat current against μ for different values of k_μ for the TSQC. The parameters of the chains are $k_L = 1.0$, $A_L = 1.0$, $\lambda = 5.0$, while for the baths we have $T_m = 1.0$, $|\Delta_{rel}| = 1.0$. The solid and dashed lines correspond to $|J_{R\to L}|$ and $|J_{L\to R}|$, respectively.

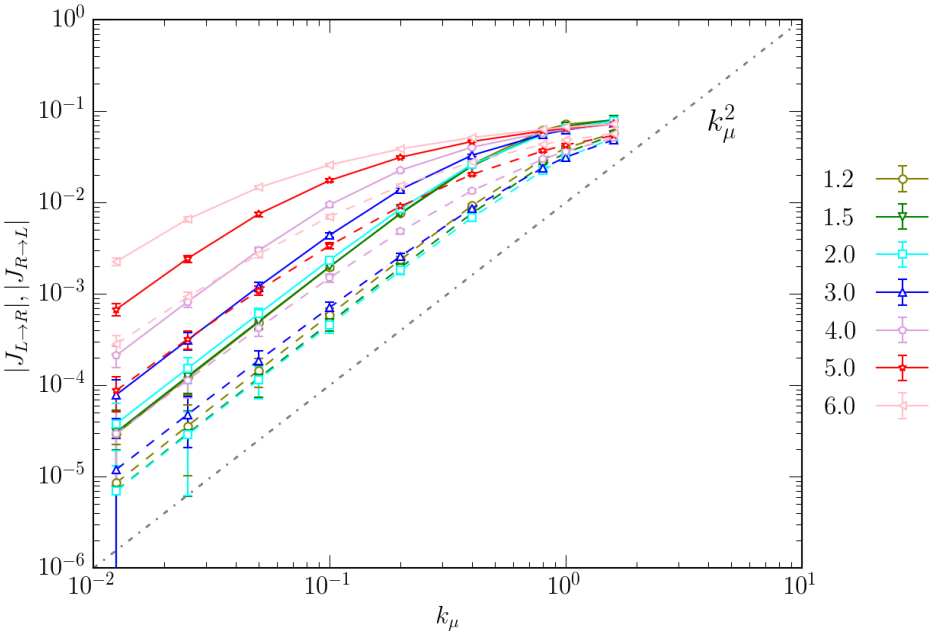

Figure 4.17: Log-log plot of the heat current against k_μ for different values of μ for the TSQC. The parameters of the chains are $k_L = 1.0$, $A_L = 1.0$, $\lambda = 5.0$, while for the baths we have $T_m = 1.0$, $|\Delta_{rel}| = 1.0$. The solid and dashed lines correspond to $|J_{R\to L}|$ and $|J_{L\to R}|$, respectively.

In these figures, we notice that the heat currents in both directions ($R \to L$ and $L \to R$) increase non-linearly with μ and k_μ, although for the case $L \to R$ we notice a minimum for $\mu = 2.0$.

The values of $|J_{L\to R}|$ and $|J_{R\to L}|$ become closer for higher values of k_μ, which indicated that the interplay between the potential amplitudes becomes hampered and the interfacial interaction U_μ dominates the dynamics. A closer look at the rectification shows this is indeed the case, as depicted in figures 4.18, 4.19 and 4.20.

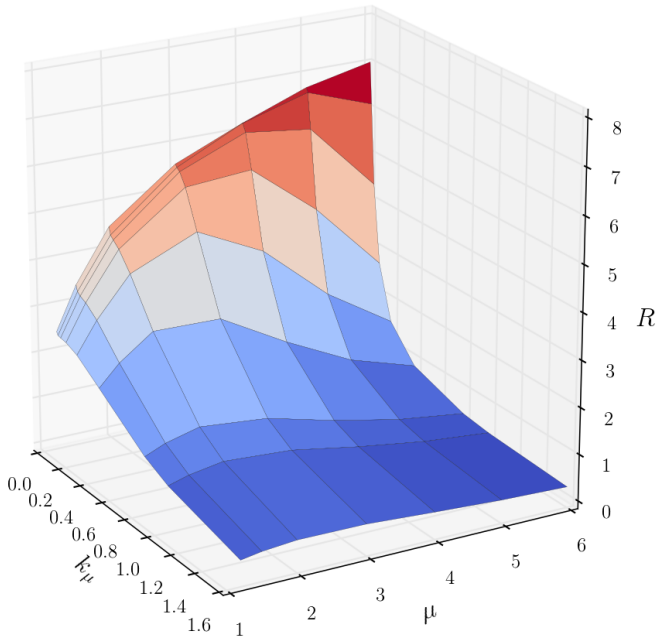

Figure 4.18: Surface plot of rectification coefficient against (k_μ, μ) for the TSQC. The parameters of the chains are $k_L = 1.0$, $A_L = 1.0$, $\lambda = 5.0$, while for the baths we have $T_m = 1.0$, $|\Delta_{rel}| = 1.0$.

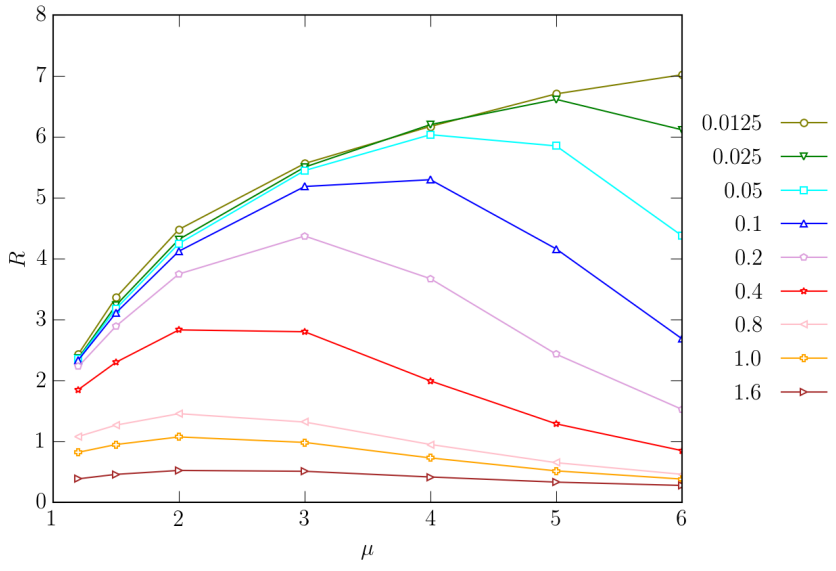

Figure 4.19: Linear plot of the rectification coefficient against μ for different values of k_μ for the TSQC. The parameters of the chains are $k_L = 1.0$, $A_L = 1.0$, $\lambda = 5.0$, while for the baths we have $T_m = 1.0$, $|\Delta_{rel}| = 1.0$.

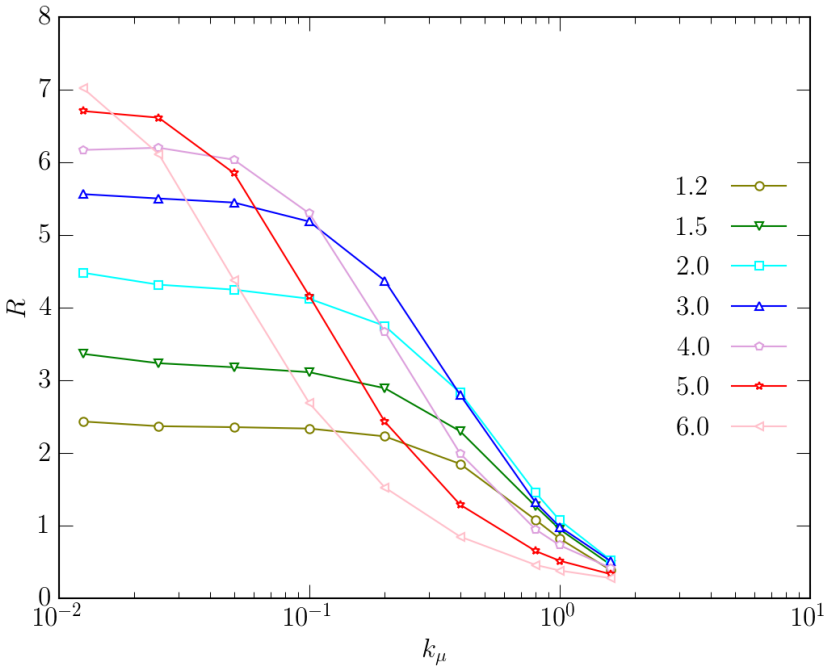

Figure 4.20: Log-linear plot of the rectification coefficient against k_μ for different values of μ for the TSQC. The parameters of the chains are $k_L = 1.0$, $A_L = 1.0$, $\lambda = 5.0$, while for the baths we have $T_m = 1.0$, $|\Delta_{rel}| = 1.0$.

We can clearly see in figure 4.19 that for higher k_μ, R is an extremum for $\mu \approxeq 2.0$, and for smaller values the extremum is achieved for higher μ.

4.3.2 Impact of the heat-bath temperatures

Now for simulations varying Δ_{rel}, we choose $k_L = 1.0$, $A_L = 1.0$, $\lambda = 5.0$, $k_\mu = 0.1$, $T_m = 1.0$. The parameters of the numerical integration are the same as for the previous section. In this case, the results for the heat currents are shown in figures 4.21 and 4.22.

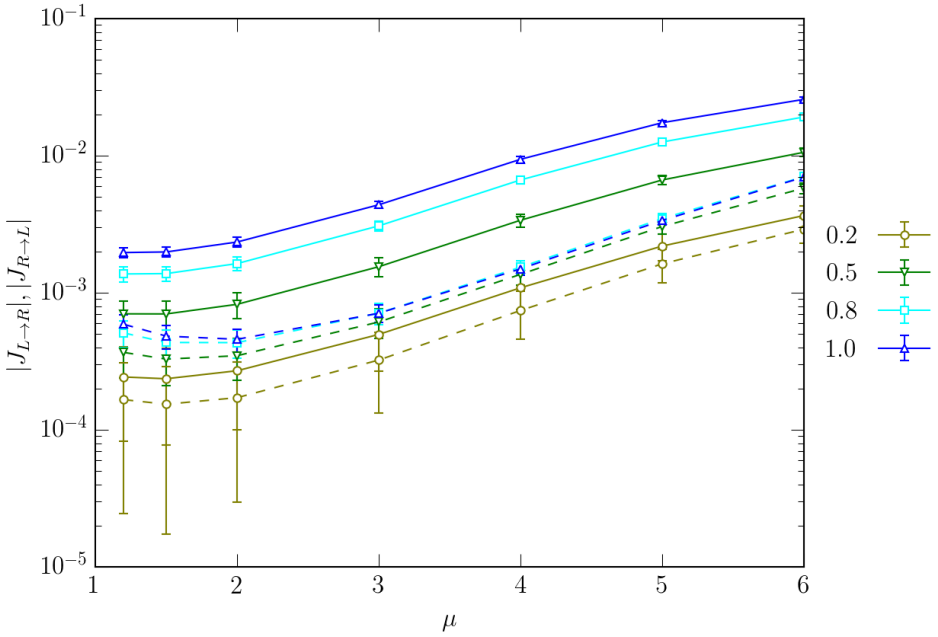

Figure 4.21: Linear-log plot of the heat current against μ for different values of $|\Delta_{rel}|$ for the TSQC. The parameters of the chains are $k_L = 1.0$, $A_L = 1.0$, $\lambda = 5.0$, $k_\mu = 0.1$, while for the baths we have $T_m = 1.0$. The solid and dashed lines correspond to $|J_{R\to L}|$ and $|J_{L\to R}|$ respectively.

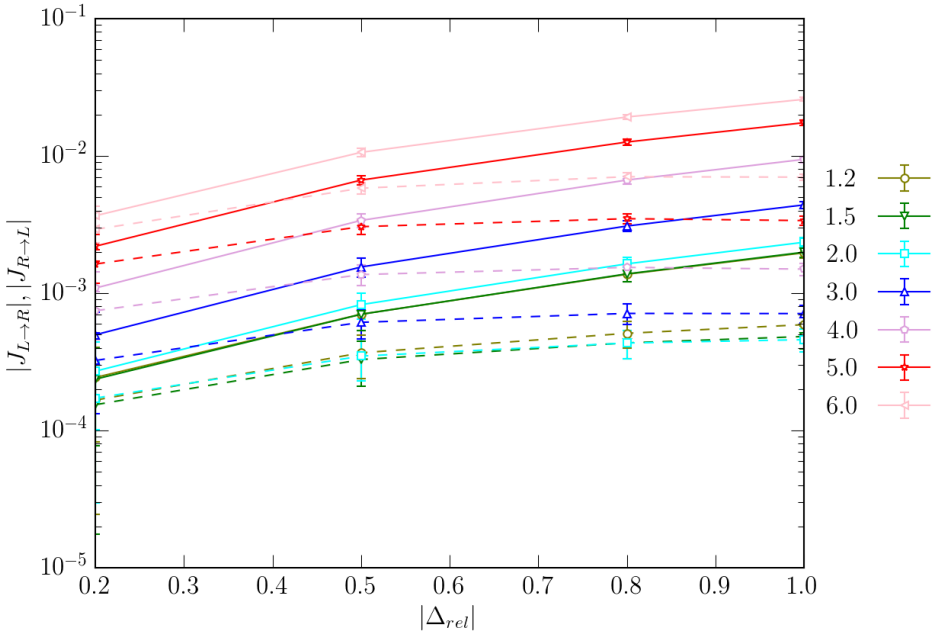

Figure 4.22: Linear-log plot of the heat current against $|\Delta_{rel}|$ for different values of μ for the TSQC. The parameters of the chains are $k_L = 1.0$, $A_L = 1.0$, $\lambda = 5.0$, $k_\mu = 0.1$, while for the baths we have $T_m = 1.0$. The solid and dashed lines correspond to $|J_{R\to L}|$ and $|J_{L\to R}|$ respectively.

From figure 4.21, we can see that $|J_{L\to R}|$ have a minimum near $\mu = 2.0$ when $|\Delta_{rel}| = 1.0$, and for lower temperature differences the minimum appears for lower values of μ. In contrast, $|J_{R\to L}|$ is strictly increasing with μ. For any value of μ, both currents are strictly increasing with $|\Delta_{rel}|$.

For fixed μ, the rectification increases with $|\Delta_{rel}|$. In figure 4.23 it is shown that, for $|\Delta_{rel}| = 0.2$, R is maximal at $\mu = 2.0$. As $|\Delta_{rel}|$ increases, the maximum shifts larger values of μ, being located at $\mu = 4.0$ for $|\Delta_{rel}| = 1.0$. See also figures 4.24 and 4.25.

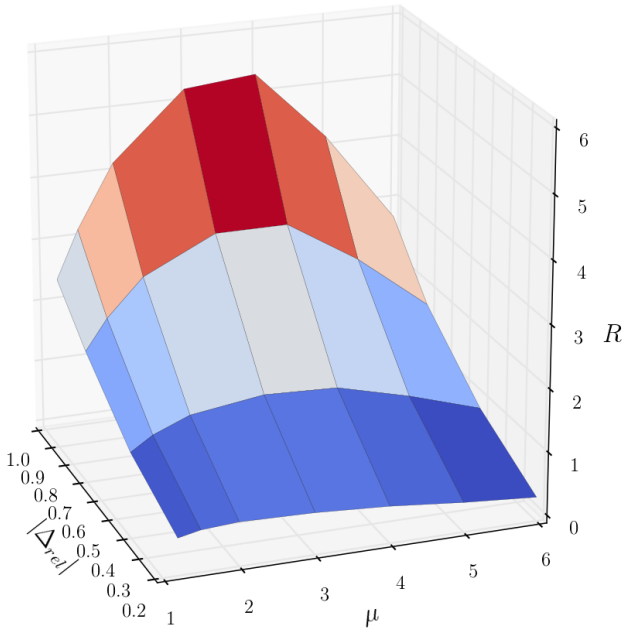

Figure 4.23: Surface plot of rectification coefficient against $(|\Delta_{rel}|, \mu)$ for the TSQC. The parameters of the chains are $k_L = 1.0$, $A_L = 1.0$, $\lambda = 5.0$, $k_\mu = 0.1$, while for the baths we have $T_m = 1.0$.

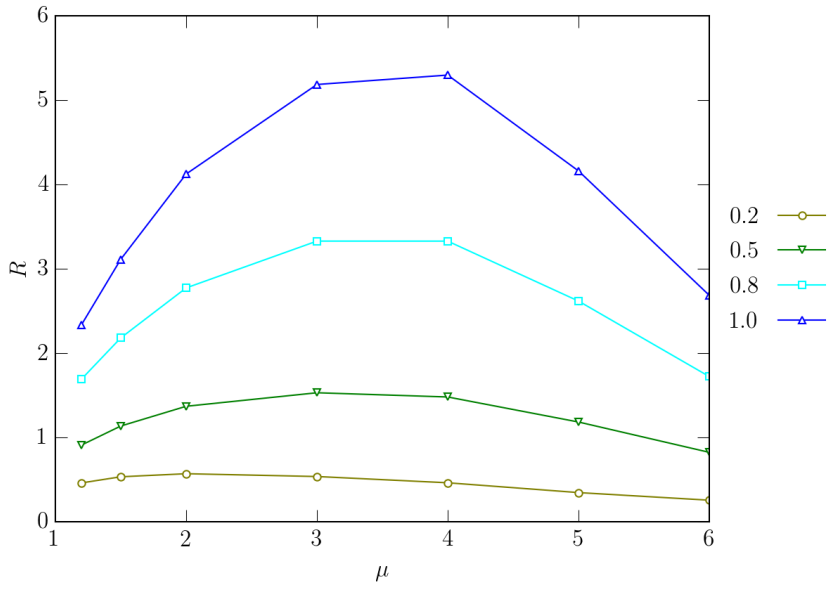

Figure 4.24: Linear plot of the rectification coefficient against μ, for different values of $|\Delta_{rel}|$, for the TSQC. The parameters of the chains are $k_L = 1.0$, $A_L = 1.0$, $\lambda = 5.0$, $k_\mu = 0.1$, while for the baths we have $T_m = 1.0$.

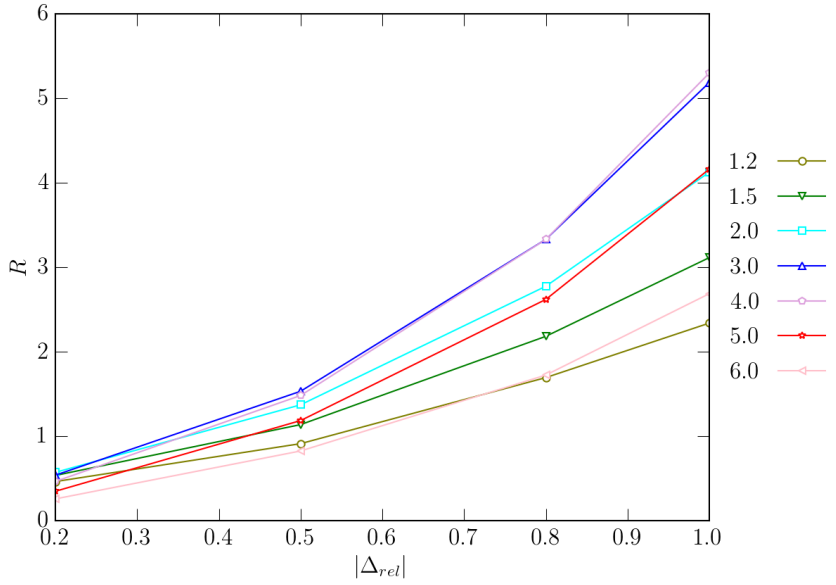

Figure 4.25: Linear plot of the rectification coefficient against $|\Delta_{rel}|$, for different values of μ, for the TSQC. The parameters of the chains are $k_L = 1.0, A_L = 1.0, \lambda = 5.0, k_\mu = 0.1$, while for the baths we have $T_m = 1.0$.

Finally, we look at the dynamics for different values of T_m, at fixed $|\Delta_{rel}|$. In this case, $k_L = 1.0, A_L = 1.0, \lambda = 5.0, k_\mu = 0.2, |\Delta_{rel}| = 1.0$.

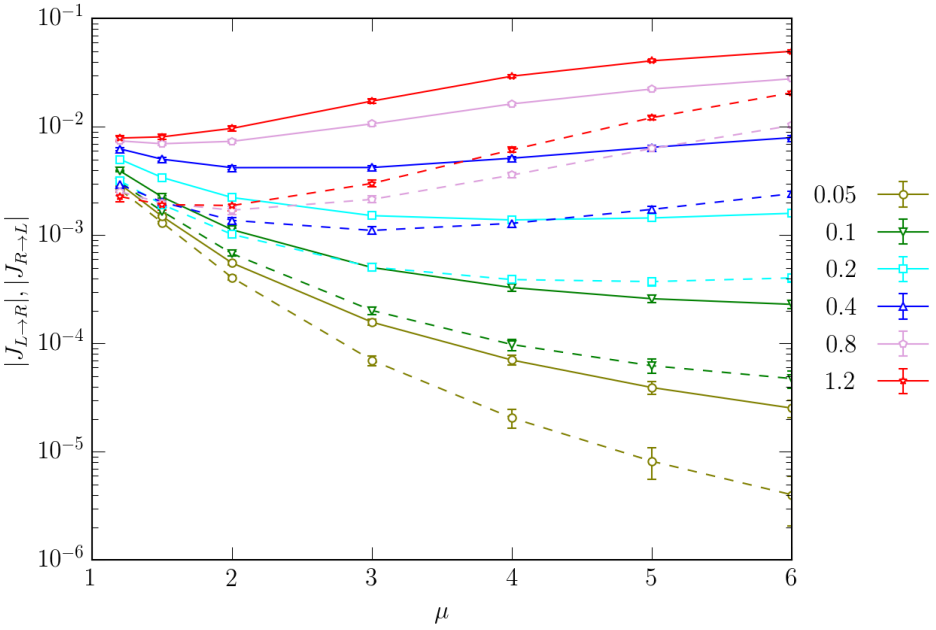

Figure 4.26: Linear-log plot of the heat current against μ, for different values of T_m, for the TSQC. The parameters of the chains are $k_L = 1.0, A_L = 1.0, \lambda = 5.0, k_\mu = 0.2$, while for the baths we have $|\Delta_{rel}| = 1.0$. The solid and dashed lines correspond to $J_{R\to L}$ and $J_{L\to R}$ respectively.

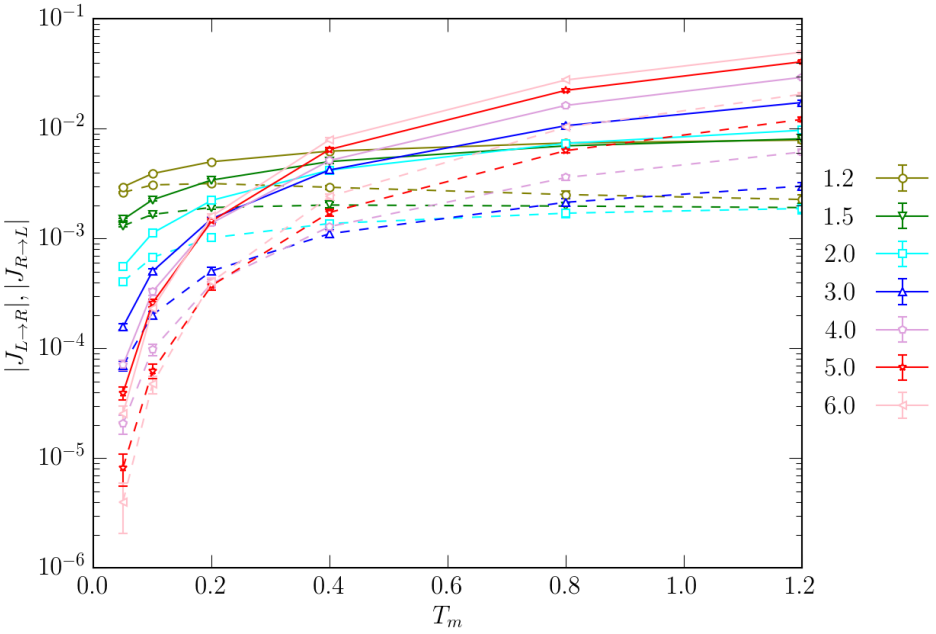

Figure 4.27: Linear-log plot of the heat current against T_m, for different values of μ, for the TSQC. The parameters of the chains are $k_L = 1.0, A_L = 1.0, \lambda = 5.0, k_\mu = 0.2$, while for the baths we have $|\Delta_{rel}| = 1.0$. The solid and dashed lines correspond to $J_{R\to L}$ and $J_{L\to R}$ respectively.

The higher the average temperature, the higher the heat currents (since $|T_L - T_R| = T_m|\Delta_{rel}|$ and Δ_{rel} is fixed). However, if $T_m < 0.2$, the heat currents actually decrease with μ, in stark contrast with the previous cases.

For higher temperatures, the heat current seems to have a minimum that depends on its direction. As an example, $|J_{L\to R}|$ have a minimum at $\mu = 1.2$ for $T_m = 1.2$, while $|J_{R\to L}|$ have a minimum at $\mu = 2.0$ for the same temperature.

In figure 4.28, we can see that the dependency of R with (μ, T_m) is very non-trivial. A saddle point appears near $T_m \approx 1.1$ and $\mu \approx 2.3$, indicating the overlap of regions with very different dependencies of R in (μ, T_m). The cuts of the surface $R = R(\mu, T_m)$, shown in figures 4.29 and 4.30, make this even clearer.

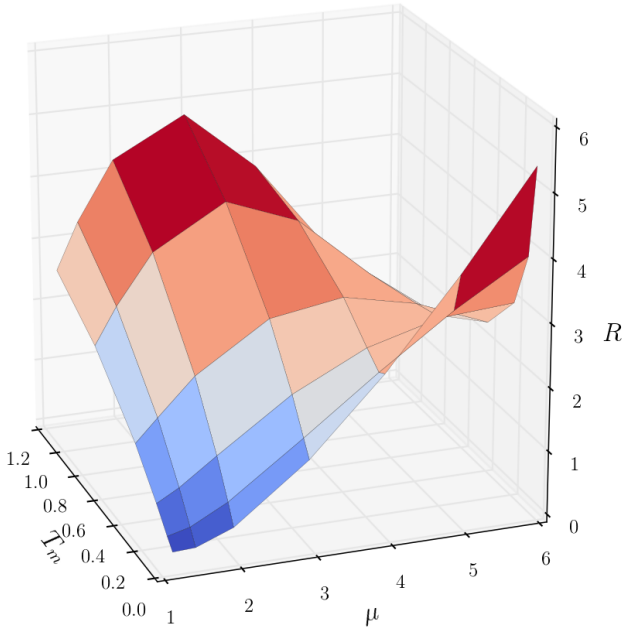

Figure 4.28: Surface plot of rectification coefficient against (T_m, μ) for the TSQC. The parameters of the chains are $k_L = 1.0, A_L = 1.0, \lambda = 5.0, k_\mu = 0.2$, while for the baths we have $|\Delta_{rel}| = 1.0$.

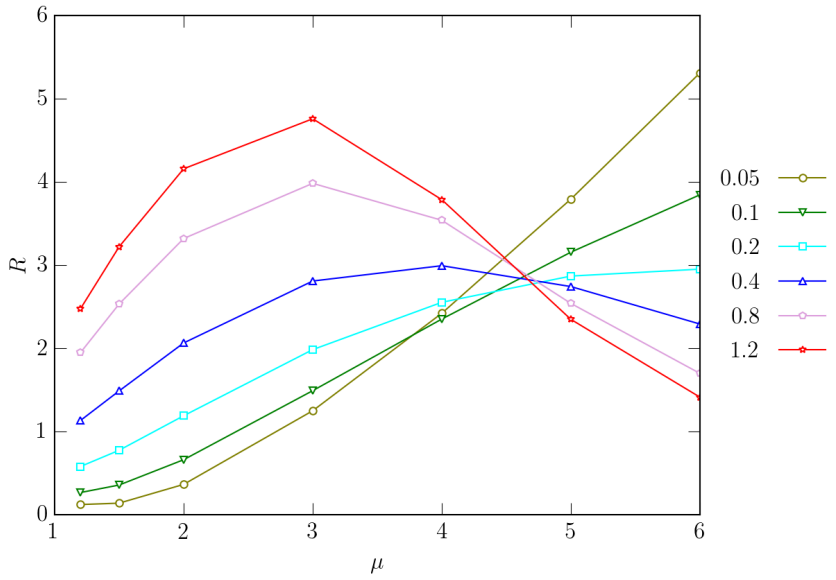

Figure 4.29: Linear plot of the rectification coefficient against μ, for different values of T_m, for the TSQC. The parameters of the chains are $k_L = 1.0, A_L = 1.0, \lambda = 5.0, k_\mu = 0.2$, while for the baths we have $|\Delta_{rel}| = 1.0$.

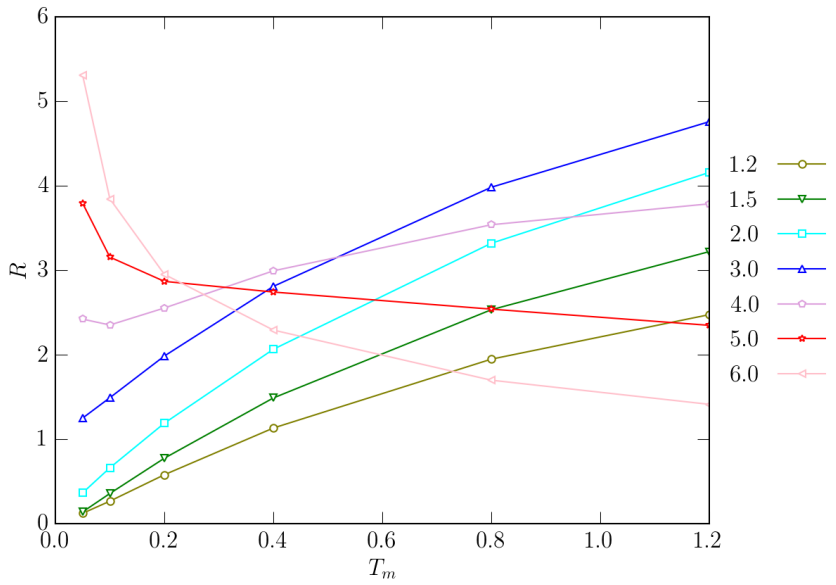

Figure 4.30: Linear plot of the rectification coefficient against μ, for different values of Δ_{rel}, for the TSQC. The parameters of the chains are $k_L = 1.0, A_L = 1.0, \lambda = 5.0, k_\mu = 0.2$, while for the baths we have $|\Delta_{rel}| = 1.0$.

For lower values of T_m, it seems that R always increases with μ, but for higher values we have a maximum. These maxima show at lower values of μ as we increase T_m.

4.4 Final remarks

In this chapter, our study of the thermal diode was divided in three parts. First we wanted to understand the properties of the diode with harmonic inter-segment interaction, for both the ϕ^4 and Frenkel-Kontorova chains.

Firstly, for the ϕ^4 model, it was shown that the rectification increases with the asymmetry A_L/A_R, indicating it hampers the phonon band overlap of the two segments.

Secondly, the effect of the heat bath temperatures was analyzed for both models. We have seen that the average temperature T_m increases the heat currents, but not necessarily the rectification. A maximal value of the rectification for the Frenkel-Kontorova model, when plotted as a function of T_m, was observed (in the analyzed case, $T_m = 0.2$). In contrast, for the ϕ^4 model, the rectification generally increased with T_m.

Another interesting observation, when comparing both models, was the preferred direction for the rectification. For the ϕ^4 chain, we have seen a preferred direction from the lower anharmonic amplitude to the higher one, while the Frenkel-Kontorova chain was the opposite.

Thirdly, as a contribution of this work, not found in the literature, the effect of the interfacial interaction nonlinearity, together with the heat baths temperatures, was analyzed on the ϕ^4 model.

In most cases, we noticed that there was a maximal value of the rectification, as a function of the exponent μ, depending on the parameters of the system. In particular, when the inter-segment potential amplitude decreases, the rectification increases, while the maximum occurs for larger values of μ (see figure 4.18).

The rectification also increases with $|\Delta_{rel}|$ (see figure 4.23), while the value of μ for maximal rectification slightly increases (from 2 to 4).

This occurs for $T_m \approx 1$, but for lower temperatures the behavior changes (see figure 4.28).

5
Conclusions

The motivation for this work was the growing interest in nanoscale thermal rectification, after the theoretical proposal by Terraneo, Peyrard and Casati, in 2002, [8] and the experimental confirmation by Chang, Okawa, Majumdar and Zettl, in 2006 [1]. This phenomenon also has a plethora of interesting possible applications, as discussed in chapter 1 [26].

However, many questions about thermal diodes are still unanswered, and few theoretical results exist [65]. Since it is still an emerging field, most results rely on computer simulations, although the number of experimental realizations is growing.

In this work, we first reviewed the simpler problem of heat conduction in a chain of particles, interacting harmonically. This was done to build some understanding of the systems to be studied for the thermal diode.

To obtain normal heat conduction, we added an anharmonic on-site potential in the chain, and studied two cases, the Frenkel-Kontorova potential and the ϕ^4 potential. The main reason for this choice is that the former is bounded, while the latter is unbounded.

We have seen that the relative values between the anharmonic potential amplitude, the harmonic potential amplitude, and the mean temperature of the baths, establish if the system will in fact conduct heat. This makes sense if we think in terms of the vibrations of the particles.

According to the literature [36, 39], the conductivity of both models depends on the temperature ($\kappa = \kappa(T)$), and we have observed this on the slight curvature of their heat profiles for higher number of particles in the chain.

For the thermal diode, we divided the previous chains in two segments, and defined different values for the amplitudes of the potentials on both sides, creating an asymmetry. Then we observed how different parameters changed the rectification of this new system. The interpretation in terms of the dynamics of the particles was not as simple, since the thermal diode is analyzed mostly in terms of heat currents, which depend more on the covariance between neighboring particles than on their individual vibrations.

When fixing the inter-segment potential as harmonic, we have seen ev-

idences that higher asymmetries, A_L/A_R, decrease the phonon band overlap between the segments. The temperature of the heat baths also affects the magnitude of the rectification, with higher temperatures increasing the rectification for the ϕ^4 potential (which is unbounded), while having an optimal value in the case of the Frenkel-Kontorova one (which is bounded). In this case, it was interesting to observe that the preferred heat current direction changed for each model. In the ϕ^4 chain, currents from the segment with lower anharmonic amplitude to the higher one are higher, while in the Frenkel-Kontorova chain the inverse occurs.

Finally, this work's original contribution to the literature was looking at how a non-linear inter-segment interaction changes the previous results. In most cases, when looking at the rectification R as a function of the interaction exponent μ, we found that there was a maximal value different from two.

Bibliography

[1] CHANG, C. W.; OKAWA, D.; MAJUMDAR, A.; ZETTL, A. **Science**. Solid-state thermal rectifier, journal, v.314, p. 1121–1124, 2006.

[2] KOBAYASHI, W.; TERAOKA, Y.; TERASAKI, I. **Applied Physics Letters**. An oxide thermal rectifier, journal, v.95, p. 171905, 2009.

[3] TIAN, H.; XIE, D.; YANG, Y.; REN, T.; ZHANG, G.; WANG, Y.; ZHOU, C.; PENG, P.; WANG, L.; LIU, L. **Scientific Reports**. A novel solid-state thermal rectifier based on reduced graphene oxide, journal, v.2, p. 523, 2012.

[4] MARTÍNEZ-PÉREZ, M. J.; FORNIERI, A.; GIAZOTTO, F. **Nature Nanotechnology**. Rectification of electronic heat current by a hybrid thermal diode, journal, v.10, p. 303–307, 2015.

[5] TSO, C.; CHAO, C. Y. **International Journal of Heat and Mass Transfer**. Solid-state thermal diode with shape memory alloys, journal, v.93, p. 605–611, 2016.

[6] SHRESTHA, R.; LUAN, Y.; LUO, X.; SHIN, S.; ZHANG, T.; SMITH, P.; GONG, W.; BOCKSTALLER, M.; LUO, T.; CHEN, R.; HIPPALGAONKAR, K.; SHEN, S. **Nature Communications**. Dual-mode solid-state thermal rectification, journal, v.11, p. 4346, 2020.

[7] KASPRZAK, M.; SLEDZINSKA, M.; ZALESKI, K.; IATSUNSKYI, I.; ALZINA, F.; VOLZ, S.; SOTOMAYOR TORRES, C. M.; GRACZYKOWSKI, B. **Nano Energy**. High temperature silicon thermal diode and switch, journal, v.78, p. 105261, 2020.

[8] TERRANEO, M.; PEYRARD, M.; CASATI, G. **Physical Review Letters**. Controlling the energy flow in nonlinear lattices: A model for a thermal rectifier, journal, v.88, p. 4, 2002.

[9] LIENHARD IV, J. H.; LIENHARD V, J. H. **A heat transfer textbook**. Fifth. ed., Phlogiston Press, 2019.

[10] TRUESDELL, C. A. **The tragicomical history of thermodynamics 1822-1854**. 1st. ed., Springer-Verlag, 1980.

[11] NUSSENZVEIG, H. M. **Curso de física básica. fluidos, oscilações e ondas, calor.**, volume 2. 4a. ed., São Paulo, Brasil: Editora Blucher, 2002.

[12] GONDAR, J. L.; CIPOLATTI, R. **Iniciação à física matemática: Modelagem de processos e métodos de solução**. Coleção Matemática e Aplicações. 2a. ed., Brasil: Instituto Nacional de Matemática Pura e Aplicada - IMPA, 2011.

[13] ASHCROFT, N. W.; MERMIN, N. D. **Solid state physics**. 1st. ed., California, USA: Brooks/Cole, Cengage Learning, 1976.

[14] LEPRI, S.; LIVI, R.; POLITI, A. **Physics Reports**. Thermal conduction in classical low-dimensional lattices, journal, v.377, p. 1–80, 2003.

[15] PEIERLS, R. E. **Quantum theory of solids**. Oxford University Press, 1955.

[16] RIEDER, Z.; LEBOWITZ, J. L.; LIEB, E. **Journal of Mathematical Physics**. Properties of a harmonic crystal in a stationary nonequilibrium state, journal, v.8, p. 1073–1078, 1967.

[17] CÂNDIDO, M. M.; M. MORGADO, W. A.; DUARTE QUEIRÓS, S. M. **Brazilian Journal of Physics**. Eliminating the Cuspidal Temperature Profile of a Non-equilibrium Chain, journal, v.47, p. 366–375, 2017.

[18] PROSEN, T.; CAMPBELL, D. K. **Physical Review Letters**. Momentum conservation implies anomalous energy transport in 1D classical lattices, journal, v.84, p. 2857–2860, 2000.

[19] CASATI, G.; FORD, J.; VIVALDI, F.; VISSCHER, W. M. **Physical Review Letters**. One-dimensional classical many-body system having a normal thermal conductivity, journal, v.52, p. 1861–1864, 1984.

[20] MIMNAGH, D. J. R.; BALLENTINE, L. E. **Physical Review E**. Thermal conductivity in a chain of alternately free and bound particles, journal, v.56, p. 5332–5342, 1997.

[21] PROSEN, T.; ROBNIK, M. **Journal of Physics A: Mathematical and General**. Energy transport and detailed verification of Fourier heat law in a chain of colliding harmonic oscillators, journal, v.25, p. 3449–3472, 1992.

[22] HU, B.; LI, B.; ZHAO, H. **Physical Review E**. Heat conduction in one-dimensional chains, journal, v.57, p. 2992–2995, 1998.

[23] HU, B.; LI, B.; ZHAO, H. **Physical Review E**. Heat conduction in one-dimensional nonintegrable systems, journal, v.61, p. 3828–3831, 2000.

[24] LEPRI, S.; LIVI, R.; POLITI, A. **Chaos: An Interdisciplinary Journal of Nonlinear Science**. Studies of thermal conductivity in Fermi–Pasta–Ulam-like lattices, journal, v.15, p. 015118, 2005.

[25] LI, B.; WANG, L.; CASATI, G. **Physical Review Letters**. Thermal diode: Rectification of heat flux, journal, v.93, p. 184301, 2004.

[26] WEHMEYER, G.; YABUKI, T.; MONACHON, C.; WU, J.; DAMES, C. **Applied Physics Reviews**. Thermal diodes, regulators, and switches: Physical mechanisms and potential applications, journal, v.4, p. 041304, 2017.

[27] LI, N.; REN, J.; WANG, L.; ZHANG, G.; HÄNGGI, P.; LI, B. **Reviews of Modern Physics**. Phononics: Manipulating heat flow with electronic analogs and beyond, journal, v.84, p. 1045–1066, 2012.

[28] SKLAN, S. R. **AIP Advances**. Splash, pop, sizzle: Information processing with phononic computing, journal, v.5, p. 053302, 2015.

[29] OLIVARES, C.; ANTENEODO, C. **Physical Review E**. Role of the range of the interactions in thermal conduction, journal, v.94, p. 042117, 2016.

[30] CHEN, S.; PEREIRA, E.; CASATI, G. **EPL (Europhysics Letters)**. Ingredients for an efficient thermal diode, journal, v.111, p. 30004, 2015.

[31] CHEN, D.; AUBRY, S.; TSIRONIS, G. P. **Physical Review Letters**. Breather mobility in discrete ϕ^4 nonlinear lattices, journal, v.77, p. 4, 1996.

[32] AOKI, K.; LUKKARINEN, J.; SPOHN, H. **Journal of Statistical Physics**. Energy transport in weakly anharmonic chains, journal, v.124, p. 1105–1129, 2006.

[33] SAVIN, A. V.; GENDELMAN, O. V. **Physical Review E**. Heat conduction in one-dimensional lattices with on-site potential, journal, v.67, p. 041205, 2003.

[34] DHAR, A. **Advances in Physics**. Heat transport in low-dimensional systems, journal, v.57, p. 457–537, 2008.

[35] LEFEVERE, R.; SCHENKEL, A. **Journal of Statistical Mechanics: Theory and Experiment**. Normal heat conductivity in a strongly pinned chain of anharmonic oscillators, journal, v.2006, p. L02001–L02001, 2006.

[36] LI, N.; LI, B. **Physical Review E**. Parameter-dependent thermal conductivity of one-dimensional ϕ^4 lattice, journal, v.76, p. 011108, 2007.

[37] GILLAN, M. J. **Journal of Physics C: Solid State Physics**. Transport in the Frenkel-Kontorova model. I. Diffusion and single-particle motion, journal, v.18, p. 4885–4902, 1985.

[38] GILLAN, M. J.; HOLLOWAY, R. W. **Journal of Physics C: Solid State Physics**. Transport in the Frenkel-Kontorova model. II. The diffusion coefficient, journal, v.18, p. 4903–4921, 1985.

[39] GILLAN, M. J.; HOLLOWAY, R. W. **Journal of Physics C: Solid State Physics**. Transport in the Frenkel-Kontorova model. III. Thermal conductivity, journal, v.18, p. 5705–5720, 1985.

[40] PAUL, J.; GENDELMAN, O. **Physics Letters A**. Kapitza resistance in basic chain models with isolated defects, journal, v.384, p. 126220, 2020.

[41] NOSÉ, S. **The Journal of Chemical Physics**. A unified formulation of the constant temperature molecular dynamics methods, journal, v.81, p. 511–519, 1984.

[42] EVANS, D. J.; HOLIAN, B. L. **The Journal of Chemical Physics**. The Nosé–Hoover thermostat, journal, v.83, p. 4069–4074, 1985.

[43] HOOVER, W. G. **Physical Review A**. Canonical dynamics: Equilibrium phase-space distributions, journal, v.31, p. 1695–1697, 1985.

[44] NELSON, E. **Dynamical theories of Brownian motion**. Second. ed., Princeton University Press, 2001.

[45] LEMONS, D. S.; GYTHIEL, A. **American Journal of Physics**. Paul Langevin's 1908 paper "on the theory of Brownian motion" ["sur la théorie du mouvement brownien," C. R. Acad. Sci. (Paris) 146 , 530–533 (1908)], journal, v.65, p. 1079–1081, 1997.

[46] SEKIMOTO, K. **Stochastic energetics**. Springer-Verlag, 2010.

[47] RISKEN, H. **The Fokker-Planck equation, methods of solution and applications**. Second. ed., Berlin, Germany: Springer-Verlag, 1989.

[48] VAN KAMPEN, N. G. **Stochastic processes in physics and chemistry**. 3rd. ed., Amsterdam, The Netherlands: Elsevier, 2007.

[49] VAN KAMPEN, N.; OPPENHEIM, I. **Physica A: Statistical Mechanics and its Applications**. Brownian motion as a problem of eliminating fast variables, journal, v.138, p. 231–248, 1986.

[50] UHLENBECK, G. E.; ORNSTEIN, L. S. **Physical Review**. On the theory of the Brownian motion, journal, v.36, p. 823–841, 1930.

[51] SALINAS, S. R. A. **Introdução à física estatística**. 2a. ed., São Paulo, Brasil: Editora da Universidade de São Paulo, 2013.

[52] TOMÉ, T.; DE OLIVEIRA, M. J. **Dinâmica estocástica e irreversibilidade**. 2a. ed., São Paulo, Brasil: Editora da Universidade de São Paulo, 2014.

[53] OKSENDAL, B. **Stochastic differential equations: An introduction with applications**. Sixth. ed., Springer, 2003.

[54] SHREVE, S. E.; KARATZAS, I. **Brownian motion and stochastic calculus**. Second. ed., Springer, 1998.

[55] STEELE, J. M. **Stochastic calculus and financial applications**. Springer-Verlag, 2001.

[56] LE GALL, J. **Brownian motion, martingales, and stochastic calculus**. Springer-Verlag, 2016.

[57] MCQUARRIE, D. A. **Statistical mechanics**. University Science Books, 2000.

[58] BILLINGSLEY, P. **Probability and measure**. 3rd. ed., John Wiley & Sons, 1995.

[59] CHEN, S.; DONADIO, D.; BENENTI, G.; CASATI, G. **Physical Review E**. Efficient thermal diode with ballistic spacer, journal, v.97, p. 030101, 2018.

[60] DHAR, A.; LEBOWITZ, J. L. **Physical Review Letters**. Effect of phonon-phonon interactions on localization, journal, v.100, p. 134301, 2008.

[61] AOKI, K.; KUSNEZOV, D. **Annals of Physics**. Nonequilibrium statistical mechanics of classical lattice ϕ^4 field theory, journal, v.295, p. 50–80, 2002.

[62] AOKI, K.; KUSNEZOV, D. Bulk properties of anharmonic chains in strong thermal gradients: Non-equilibrium ϕ^4 theory, journal, p. 7, 2000.

[63] HU, B.; YANG, L. **Chaos: An Interdisciplinary Journal of Nonlinear Science**. Heat conduction in the Frenkel–Kontorova model, journal, v.15, p. 015119, 2005.

[64] TSIRONIS, G. P.; BISHOP, A. R.; SAVIN, A. V.; ZOLOTARYUK, A. V. **Physical Review E**. Dependence of thermal conductivity on discrete breathers in lattices, journal, v.60, p. 6610–6613, 1999.

[65] PEREIRA, E. **Physical Review E**. Requisite ingredients for thermal rectification, journal, v.96, p. 012114, 2017.

[66] WHITE, F. M. **Mecânica dos fluidos**. Sixth. ed., AMGH Editora Ltda., 2011.

[67] LEMOS, N. A. **Convite à física matemática**. First. ed., Brasil: Editora Livraria da Física, 2013.

[68] HIRSCH, M. W.; SMALE, S.; DEVANEY, R. L. **Differential equations, dynamical systems, and an introduction to chaos**. 3rd. ed., Elsevier, 2013.

[69] PLATEN, E.; KLOEDEN, P. E. **Numerical solution of stochastic differential equations**. Springer-Verlag, 1999.

[70] HANSEN, J. A.; PENLAND, C. **Monthly Weather Review**. Efficient approximate techniques for integrating stochastic differential equations, journal, v.134, p. 3006–3014, 2006.

[71] QUARTERONI, A.; SACCO, R.; SALERI, F. **Numerical mathematics**. Second. ed., Springer, 2007.

[72] HAIRER, E.; WANNER, G. **Solving ordinary differential equations II: Stiff and differential-algebraic problems**. Second. ed., Springer-Verlag, 1996.

[73] GIORDANO, N. J. **Computational physics**. Prentice-Hall, Inc., 1997.

[74] CHAPRA, S. C. **Métodos numéricos aplicados com matlab para engenheiros e cientistas**. Third. ed., AMGH Editora Ltda., 2012.

[75] GALASSI, M. **GNU Scientific Library Reference Manual**.

[76] CHARNET, R.; FREIRE, C. A. D. L.; CHARNET, E. M. R.; BONVINO, H. **Análise de modelos de regressão linear**. Second. ed., Editora da Unicamp, 2015.

[77] VIRTANEN, P.; GOMMERS, R.; OLIPHANT, T. E.; HABERLAND, M.; REDDY, T.; COURNAPEAU, D.; BUROVSKI, E.; PETERSON, P.; WECKESSER, W.; BRIGHT, J.; VAN DER WALT, S. J.; BRETT, M.; WILSON, J.; MILLMAN, K. J.; MAYOROV, N.; NELSON, A. R. J.; JONES, E.; KERN, R.; LARSON, E.; CAREY, C. J.; POLAT, İ.; FENG, Y.; MOORE, E. W.; VANDERPLAS, J.; LAXALDE, D.; PERKTOLD, J.; CIMRMAN, R.; HENRIKSEN, I.; QUINTERO, E. A.; HARRIS, C. R.; ARCHIBALD, A. M.; RIBEIRO, A. H.; PEDREGOSA, F.; VAN MULBREGT, P.; SCIPY 1.0 CONTRIBUTORS, . **Nature Methods**. SciPy 1.0: fundamental algorithms for scientific computing in Python, journal, v.17, p. 261–272, 2020.

A
Numerical solutions

In the previous chapter, we defined models that should reproduce normal heat conduction (see section 2.4) and heat current rectification (see section 2.5). Now, we want to know how to solve the equations of motion laid out before.

Since both models use a Langevin thermostat, they have the implicit assumption that the dynamical variables q_n, v_n are random variables. This means we have to solve a system of stochastic differential equations (SDEs). Two difficulties make this highly non-trivial. Due to the particle-particle interaction, the n equations (one for each particle) are coupled, and due to on-site potentials, the equations are nonlinear and cannot be decoupled. We do not even know if these systems have analytical solutions. These problems motivate us to use numerical methods.

Whatever analytical form the solution may or may not have, its numerical values surely depend on the choice of parameters for the system. Which brings forth the question, what are realistic choices for such systems?

This clearly depends on the units we are working with, bringing another difficulty forward. Instead of spending much time with this discussion, we will try to bypass it entirely by redefining our equations in a non-dimensional form. Thus, before discussing the numerical methods we use for solving each system of SDEs considered in the previous chapter, we will redefine those models in a way that the dynamic variables and constants of the model have no units.

A.1
Nondimensionalization

Nondimensionalization is a common tactic in the field of fluid mechanics[66]. Using non-dimensional equations not only helps bring forward physical insights, it also gives solutions that do not depend on the scale of a system. Hence such solutions are transferable to different scales, if the physical phenomena in question are still the same.

Just like in that field, here we will focus on nondimensionalizing directly the equations of motion, instead of beginning over from a Hamiltonian description of the system.

Two examples of this process were already discussed before. In section 2.4, we showed how one can think of q_n as a dimensionless variable in the scale of the lattice separation a. We also discussed how the temperatures would be thought of in units of energy, since the Boltzmann constant k_B is just an artifice for changing units of temperature to units of energy. The temperature of the heat baths were then redefined as $T_L \to k_B T_L$ and $T_R \to k_B T_R$.

The nondimensionalization process then just consists of dividing and multiplying our variables by factors of scale, redefining them as their non-dimensional counterparts. In the following arguments, we will use the notation $[z]$ to represent what is the unit of a variable z.

Let us first define three factors of scale, Θ_1 for the displacement from equilibrium, Θ_2 for the time and Θ_3 for the mass, and use those to redefine our dynamic variables q_n, v_n, the system evolution time t, and the particles mass. The non-dimensional versions of our variables will be

$$m_n^* = \frac{m_n}{\Theta_3}, \tag{A-1}$$

$$q_n^* = \frac{q_n}{\Theta_1}, \tag{A-2}$$

$$v_n^* = \frac{v_n}{(\Theta_1/\Theta_2)}, \tag{A-3}$$

$$t^* = \frac{t}{\Theta_2}, \tag{A-4}$$

which will be substituted in the equations of motion for each model. When looking at the equations for the particles of the bulk ($\{n = 2, 3, \ldots, N-1\}$), this is enough. However, for the particles in contact with the heat baths ($n = 1, N$), we have one more term that needs to be adapted to a non-dimensional version, and that is the random noise.

The random noise dW_t actually has dimensions of square root of time, while $\epsilon(t)$ has dimensions of time to the power of minus half.

To see why that is the case, take the Wiener process $W(t)$. One of the defining properties of such a random process is that its increments are independent and identically distributed Gaussian variables. We write, as we did in section 2.2,

$$\langle \Delta W(t) \Delta W(t') \rangle = \delta(t - t'), \tag{A-5}$$

to find the units of $\Delta W(t)$. The Dirac delta function $\delta(z)$ has units of the inverse of its argument, since its defining property [67] is that

$$\int_{\infty}^{\infty} g(z)\delta(z)dz = g(0), \tag{A-6}$$

for an arbitrary function $g(z)$. A function always has the same dimension, independent of the value of its argument, so $[g(z)] = [g(0)]$. The ensemble

average does not add any dimension to a variable, since it is defined as

$$\langle z \rangle \doteq \int_{\mathbb{R}} z p(z) dz, \tag{A-7}$$

where $p(z)$ is a probability density function, hence $[p(z)] = 1/[z]$. This means that $[\langle z \rangle] = [z]$.

Now, from equations A-5, A-6 and A-7, we see that $[\Delta W(t)] = [t]^{1/2}$. Since we argued in section 2.2 that $\epsilon(t)$ is analogous to what would be dW_t/dt, then $[\epsilon(t)] = [\Delta W(t)]/[t] = [t]^{-1/2}$.

This means that to nondimensionalize $\epsilon(t)$, we need to define $\epsilon^*(t) = \Theta_2^{1/2}\epsilon(t)$. However, notice that we are using another time variable, t^*, and so we should actually write

$$\epsilon^*(t^*) = \Theta_2^{1/2}\epsilon(\Theta_2 t^*), \tag{A-8}$$

which not only has no dimensions, but also has unit variance. To see this, we use another property of the Dirac delta function [67], namely

$$\delta(\alpha z) = \frac{1}{|\alpha|}\delta(z). \tag{A-9}$$

Substituting equations A-9 and A-8 in equation A-5, we recover the property

$$\langle \epsilon^*(t^*)\epsilon^*(t'^*) \rangle = \delta(t^* - t'^*). \tag{A-10}$$

Now we use what we discussed here, inside the equations of motion. The arguments will not change much for both cases.

A.1.1 Homogeneous chain

We will substitute the scale groups in each equation of motion. The first ones are trivial,

$$\frac{dq_n^*}{dt^*} = v_n^*, \tag{A-11}$$

since they are just the definition of velocity, and for the initial conditions $q_n^*(0) = q_{n,0}^*,\ v_n^*(0) = v_{n,0}^*$.

Then, for the particles of the bulk, we write

$$\frac{\Theta_1/\Theta_2}{\Theta_2}\frac{dv_n^*}{dt^*} = -\frac{k\Theta_1}{m_n^*\Theta_3}(2q_n^* - q_{n-1}^* - q_{n+1}^*) - \frac{1}{m_n^*\Theta_3}\frac{dV}{dq_n}, \tag{A-12}$$

$$\frac{dv_n^*}{dt^*} = -\frac{k\Theta_2^2}{m_n^*\Theta_3}(2q_n^* - q_{n-1}^* - q_{n+1}^*) - \frac{\Theta_2^2}{m_n^*\Theta_3\Theta_1}\frac{dV}{dq_n}, \tag{A-13}$$

where the force due to the on-site potential have to be rewritten in terms of q_n^*. This is is obtained through $V^*(q_n^*) = V(\Theta_1 q_n^*)$, giving

$$\frac{dV}{dq_n} = \frac{1}{\Theta_1}\frac{dV}{dq_n^*}. \tag{A-14}$$

Thus, for the ϕ^4 chain, we have

$$\frac{dV}{dq_n} = A_Q\Theta_1^3 q_n^{*3}, \tag{A-15}$$

while for the FK chain,

$$\frac{dV}{dq_n} = \frac{A_{FK}}{a_s}\sin\left(\frac{2\pi\Theta_1}{a_s}q_n^*\right). \tag{A-16}$$

Notice that the on-site potential force term in equation A-13 already defines a nondimensional force, since $\Theta_3\Theta_1/\Theta_2^2$ has dimensions of force. So we did not need to define a nondimensional V, equation A-13 (together with equation A-14) already defined it for us, $V^* = \Theta_2^2 V/\Theta_3\Theta_1^2$.

Now we just nondimensionalize the equations of motion for the particles in contact with the heat baths ($n = 1, N$),

$$\frac{dv_n^*}{dt^*} = -\frac{k\Theta_2^2}{m_n^*\Theta_3}q_n^* - \frac{k\Theta_2^2}{m_n^*\Theta_3}(q_n^* - q_{n\pm1}^*) - \frac{\Theta_2^2}{m_n^*\Theta_3\Theta_1}\frac{dV}{dq_n} - \gamma\Theta_2 v_n^* + \frac{\Theta_2^2}{\Theta_1}\sqrt{\frac{2\gamma T_n}{m_n^*\Theta_3\Theta_2}}\,\epsilon_n^*(t^*), \tag{A-17}$$

where if $n = 1$, then $T_n = T_L$, $\epsilon_n^*(t^*) = \epsilon_L^*(t^*)$ and we use the plus sign for the second term in the right-hand side of the equation, $q_n^* - q_{n+1}^*$, while if $n = N$, then $T_n = T_R$, $\epsilon_n^*(t^*) = \epsilon_R^*(t^*)$ and we have $q_n^* - q_{n-1}^*$.

We then redefine all our parameters,

$$k^* = \frac{k\Theta_2^2}{\Theta_3}, \tag{A-18}$$

$$A_Q^* = \frac{A_Q\Theta_1^2\Theta_2^2}{\Theta_3}, \tag{A-19}$$

$$A_{FK}^* = \frac{A_{FK}\Theta_2^2}{a_s\Theta_3\Theta_1}, \tag{A-20}$$

$$a_s^* = \frac{a_s}{\Theta_1}, \tag{A-21}$$

$$\gamma^* = \gamma\Theta_2, \tag{A-22}$$

$$T_L^* = \frac{\Theta_2^2 T_L}{\Theta_1^2\Theta_3}, \tag{A-23}$$

$$T_R^* = \frac{\Theta_2^2 T_R}{\Theta_1^2\Theta_3}, \tag{A-24}$$

and the equations will have the exact same analytical form they had before, but changing all variables and parameters to their non-dimensional version.

A.1.2 Thermal diode

The discussion on nondimensionalizing the thermal diode equations of motion is similar to the one on heat conduction. We just need to take care to separate the left and right segment parameters, and to nondimensionalize an extra parameter for the interface particles, k_μ.

The list of non-dimensional parameters will be

$$k_L^* = \frac{k_L \Theta_2^2}{\Theta_3}, \tag{A-25}$$

$$k_R^* = \frac{k_R \Theta_2^2}{\Theta_3}, \tag{A-26}$$

$$A_{Q,L}^* = \frac{A_{Q,L} \Theta_1^2 \Theta_2^2}{\Theta_3}, \tag{A-27}$$

$$A_{Q,R}^* = \frac{A_{Q,R} \Theta_1^2 \Theta_2^2}{\Theta_3}, \tag{A-28}$$

$$A_{FK,L}^* = \frac{A_{FK,L} \Theta_2^2}{a_s \Theta_3 \Theta_1}, \tag{A-29}$$

$$A_{FK,R}^* = \frac{A_{FK,R} \Theta_2^2}{a_s \Theta_3 \Theta_1}, \tag{A-30}$$

$$a_s^* = \frac{a_s}{\Theta_1}, \tag{A-31}$$

$$\gamma^* = \gamma \Theta_2, \tag{A-32}$$

$$T_L^* = \frac{\Theta_2^2 T_L}{\Theta_1^2 \Theta_3}, \tag{A-33}$$

$$T_R^* = \frac{\Theta_2^2 T_R}{\Theta_1^2 \Theta_3}. \tag{A-34}$$

$$\tag{A-35}$$

For the parameter k_μ, we take a look at the interfacial interaction term, that show on the equations of particles $n = N/2, N/2+1$ as

$$-\frac{k_\mu}{m_n} \mathrm{sgn}\left(q_n - q_{n\pm1}\right) \left|q_n - q_{n\pm1}\right|^{\mu-1}, \tag{A-36}$$

where the signal inside the displacement index is positive for $n = N/2$ and negative for $n = N/2+1$.

Before, we implicitly used the assumption that the scale groups $\Theta_1, \Theta_2, \Theta_3$ were non-zero, but now we will also assume that they are positive. Then substituting $q_n \to \Theta_1 q_n^*$, using the fact that $\mathrm{sgn}\left(\alpha z\right) = \mathrm{sgn}\left(z\right)$ if $\alpha > 0$, and multiplying by the scale factor $\left(\Theta_1/(\Theta_3\Theta_2^2)\right)^{-1}$ (due to the left-hand side of equations 2-63 and 2-64), we get the non-dimensional parameter

$$k_\mu^* = \frac{k_\mu \Theta_1^{\mu-2} \Theta_2^2}{\Theta_3}, \tag{A-37}$$

so that the interfacial interaction now has the form

$$-\frac{k_\mu^*}{m_n^*}\mathrm{sgn}\left(q_n^*-q_{n\pm1}^*\right)\left|q_n^*-q_{n\pm1}^*\right|^{\mu-1}. \tag{A-38}$$

A.1.3
Advantages of nondimensionalization

Using the non-dimensional version of our equations of motion, we can reduce the number of parameters needed to define our system. In fact, since the scale factors $\Theta_1, \Theta_2, \Theta_3$ are completely arbitrary, we can choose them so that some adimensional constants are 1.0, effectively taking them out of the equations. As an example, assume all particles have equal mass ($m_n = m$, for $n = 1, 2, \ldots, N$), then choose $\Theta_1 = a_s = a$, $\Theta_2 = 1/\gamma$, and $\Theta_3 = m$. This gives $m_n^* = m^* = 1.0$, $a^* = a_s^* = 1.0$, and $\gamma^* = 1.0$, so these three parameters are always one unit, and we do not need to specify them anymore.

The effect they have on the system is also embedded in the other parameters, so when we choose A_Q^*, we are actually choosing A_Q with respect to $m\gamma^2/a^2$, since in this case

$$A_Q^* = \frac{A_Q}{m\gamma^2/a^2}. \tag{A-39}$$

We could also choose the scale factors in such a way as to remove the effect of m, k and the temperatures, effectively making their nondimensional version equal to one. However, it is not possible to make $T_L^* = 1$ and $T_R^* = 1$ simultaneously, by this choice, because of the restrictions $m^* = 1$ and $k^* = 1$. We can only choose three parameters to remove.

So, let the average temperature be $T_m = (T_L + T_R)/2$, and choose Θ_1, Θ_2 and Θ_3 so that $T_m^* = 1.0$. When this is done, the anharmonic amplitude of the ϕ^4 chain will be

$$A_Q^* = \frac{A_Q T_m}{k^2}, \tag{A-40}$$

and so the nondimensional group $A_Q T_m/k^2$ should determine the behavior of the QC model.

Also, since from here on out we will mainly use the non-dimensional equation of motion, we will not bother to write the asterisk for the non-dimensional constants and variables. Always consider that none of them have dimensions.

A.2
Stochastic numerical integration

Before diving in the stochastic version of numerical integration methods, let us first remind the basic ideas for a system of ordinary differential equations

(ODEs). Let the system be described as

$$\frac{d\vec{x}}{dt} = f(\vec{x}, t), \tag{A-41}$$

where $\vec{x}$ are independent variables and t is the time. The solution for this problem is a function $\vec{x} = \vec{x}(t)$ that satisfies the system of ODEs considered.

The idea behind the numerical integration of a system along a time interval $[0, t_{max}]$ is to define a partition of such interval, $0 < t_1 < \ldots < t_l < \ldots < t_{max}$, and try to approximate the true function points $(\vec{x}(t_n), t_n)$ by some sequence $(\vec{y}_n, t_n)$ [68, 69]. Each numerical schema then defines a way to partition the interval, and with that, compute this sequence in an iterative way.

Stochastic integration schemes work in the same way. They try to, in some sense, approximate the true points of a stochastic process, (X_{t_n}, t_n), by some sequence of random variables, (Y_{t_n}, t_n). The true process $X(t)$ is defined by a system of stochastic differential equations (SDEs), namely

$$\frac{d\vec{x}}{dt} = \vec{a}(\vec{x}, t) + G(\vec{x}, t)\vec{\epsilon}(t), \tag{A-42}$$

where G is the matrix for the amplitude of the noise term of each component of $\vec{x}$, the noise itself being a vector of Wiener processes $\vec{\epsilon}$ with unit variance.

In this case, we can look at how well a numerical method approaches the original solutiong pathwise (called strong convergence), or at how well it approximates the moments of the process (called weak convergence) [69]. These are commonly discussed in terms of the time step employed. We will not discuss them at length here, restraining ourselves on citing convergence results from the literature.

It is interesting to just try and adapt the classical methods for stochastic problems, because they are easier to understand and generally uses less computations. The methods discussed here are then the stochastic Euler method and the stochastic Runge-Kutta method [69, 70]. In what follows, we will partition the time interval for the simulation in fixed width sub-intervals, $t_l - t_{l-1} = \delta t$, for all $l = 0, 1, 2, \ldots, \max$.

A.2.1 Euler scheme

The deterministic Euler method consists of approaching the evolution of the system by a Taylor series truncated at the linear terms at each step

$$\vec{x}(t_n + \tau) \approx \vec{x}(t_n) + \delta t \left(\frac{d\vec{x}}{dt}\right)_{t=t_n}, \tag{A-43}$$

the derivative being given by the ordinary differential equation itself.

When the time step goes to zero, $\delta t \to 0$, the approximate solution is known to converge under certain weak assumptions on the ODEs [71] and thus it is expected that for small enough δt and a fixed time interval such a method works reasonably well.

However, the Euler scheme is not stable. This means that, if we do not choose δt small enough, then as the time interval increases, the numerical algorithm diverges from the true solution [72], and the error increases indefinitely. For some systems of ODEs, such a time step may be impossible to choose.

In the case of the one-dimensional harmonic oscillator, whatever the time step chosen, the system will always diverge for higher time intervals [73]. Physically, the energy of the system increases indefinitely, just due to the choice of numerical scheme.

The stochastic Euler method is similar, although the definition of a Taylor series in the framework of stochastic calculus has some changes [69]. From section A.1, we know that the random noise $\epsilon(t)$ is of the order of $O(t^{1/2})$, thus we scale the time step for the Euler scheme accordingly.

For solving the Langevin equation by itself [52], the stochastic Euler method is thus

$$v_{n+1} = v_n - (\delta t)\gamma v_n + \sqrt{(\delta t)\Gamma}\xi_n, \tag{A-44}$$

$$x_{n+1} = x_n + (\delta t)v_n, \tag{A-45}$$

where ξ_n is a sequence of independent and identically distributed (i.i.d.) random variables sampled from a Gaussian distribution $N(0,1)$. The general case, for a system of SDEs, does not present any difficulties. It can be written [69] as

$$\vec{x}_{n+1} = \vec{x}_n + \delta t\vec{a}(\vec{x}_n, t_n) + \delta t G(\vec{x}_n, t_n)\vec{\xi}_n, \tag{A-46}$$

with $\vec{\xi}_n$ now being sampled from a multivariate normal distribution with no correlation terms ($N(\vec{0}, \mathbb{I})$, where $\mathbb{I}$ is the identity matrix). This is the same as sampling each component of $\vec{\xi}_n$, independently, from a Gaussian distribution.

This scheme is known to generally have strong convergence of order $(\delta t)^{1/2}$ [69], which is different to its deterministic case, when it converges with order (δt) [71].

A.2.2 Runge-Kutta scheme

The Runge-Kutta family of methods are the most commonly used algorithms for the numerical solution of deterministic systems of ODEs. This

is due to the fact that they can attain accuracy of higher orders in the time step without using higher-order derivatives [74].

These schemae are multi-step methods, with iteration algorithm given by

$$\vec{u}_{n+1} = \vec{u}_n + \vec{\phi}(\delta t), \tag{A-47}$$

where ϕ depends on the function f evaluated on many different points. The increment function ϕ is written as a series

$$\vec{\phi} = \sum_j^m a_j \vec{K}_j, \tag{A-48}$$

with each a_j being a constant that depends on which Runge-Kutta algorithm is being used. The terms $\vec{K}_j$ are functions of the form

$$\vec{K}_j = \vec{f}\left(t_n + p_{j-1}\delta t, \vec{u}_n + \delta t \sum_{i=1}^{j-1} q_{j-1,i}\vec{K}_i\right), \tag{A-49}$$

where $p_0 = 0$, and the $p_j, q_{j-1,i}$ are constants that also depend on the specific method used.

All constants $a_j, p_j, q_{j-1,i}$, are commonly chosen to increase the accuracy of the method. We will not reproduce here the way this is done.

The most commonly used scheme used in this family of schemae is the fourth order Runge-Kutta method [74], where the constants are such that

$$\begin{aligned}
\vec{u}_{n+1} &= \vec{u}_n + \frac{\delta t}{6}\left(\vec{K}_1 + 2\vec{K}_2 + 2\vec{K}_3 + \vec{K}_4\right), && \text{(A-50)}\\
\vec{K}_1 &= \vec{f}(t_n, \vec{u}_n) && \text{(A-51)}\\
\vec{K}_2 &= \vec{f}(t_n + \frac{1}{2}\delta t, \vec{u}_n + \frac{\delta t}{2}\vec{K}_1) && \text{(A-52)}\\
\vec{K}_3 &= \vec{f}(t_n + \frac{1}{2}\delta t, \vec{u}_n + \frac{\delta t}{2}\vec{K}_2) && \text{(A-53)}\\
\vec{K}_4 &= \vec{f}(t_n + \delta t, \vec{u}_n + \delta t\vec{K}_3), && \text{(A-54)}
\end{aligned}$$

which have global truncation error of the order $O((\delta t)^4)$.

Like the Euler scheme, the fourth-order Runge-Kutta scheme is not stable [71], although the value of δt, such that its approximation diverges indefinitely, is generally higher. In the case of the one-dimensional harmonic oscillator, it is possible to choose a δt so that the Runge-Kutta approximation step error is bounded.

To adapt this method to a stochastic version, we will follow ref. [70], where they add a random noise term for each computation of the functions $\vec{K}_j$. The stochastic fourth order Runge-Kutta method will then read

$$\vec{u}_{n+1} = \vec{u}_n + \frac{\delta t}{6}\left(\vec{K}_1 + 2\vec{K}_2 + 2\vec{K}_3 + \vec{K}_4\right) + \frac{1}{6}\left(M_1 + 2M_2 + 2M_3 + M_4\right)\vec{\xi}_n, \tag{A-55}$$

where

$$\begin{aligned}
\vec{K}_1 &= \vec{f}(t_n, \vec{u}_n), && \text{(A-56)}\\
\vec{K}_2 &= \vec{f}(t_n + \frac{1}{2}\delta t, \vec{u}_n + \frac{\delta t}{2}\vec{K}_1 + \frac{1}{2}M_1\vec{\xi}_n), && \text{(A-57)}\\
\vec{K}_3 &= \vec{f}(t_n + \frac{1}{2}\delta t, \vec{u}_n + \frac{\delta t}{2}\vec{K}_2 + \frac{1}{2}M_2\vec{\xi}_n), && \text{(A-58)}\\
\vec{K}_4 &= \vec{f}(t_n + \delta t, \vec{u}_n + \delta t\vec{K}_3 + M_3\vec{\xi}_n), && \text{(A-59)}\\
M_1 &= G(t_n, \vec{u}_n), && \text{(A-60)}\\
M_2 &= G(t_n + \frac{1}{2}\delta t, \vec{u}_n + \frac{\delta t}{2}\vec{K}_1 + \frac{1}{2}M_1\vec{\xi}_n), && \text{(A-61)}\\
M_3 &= G(t_n + \frac{1}{2}\delta t, \vec{u}_n + \frac{\delta t}{2}\vec{K}_2 + \frac{1}{2}M_2\vec{\xi}_n), && \text{(A-62)}\\
M_4 &= G(t_n + \delta t, \vec{u}_n + \delta t\vec{K}_3 + M_3\vec{\xi}_n), && \text{(A-63)}
\end{aligned}$$

and as was the case for the Euler scheme, $\vec{\xi}_n$ is sampled from a $N(\vec{0}, \mathbb{I})$ distribution. This method reproduces Stratonovich calculus, and has strong convergence of order δt [70].

The fourth-order stochastic Runge-Kutta algorithm is the main one used in the literature of heat conduction and thermal diodes, in great part due to being the most common deterministic scheme and having good accuracy. Due to this, we also use the Runge-Kutta algorithm.

A.3 Pseudo-random number generator

In both the Euler and Runge-Kutta schemae, a sequence of random vectors, $\vec{\xi}_n$, is sampled from the distribution $N(\vec{0}, \mathbb{I})$. To be able to do that computationally, we use pseudo-random number generators.

This is done by using a deterministic algorithm, from which we get a sequence of numbers (from a starting seed) that behaves randomly [73]. Good algorithms will then produce numbers that are non-correlated and uniformly distributed. Also, different seeds should give non-correlated sequences.

Then, to simulate a random variable with any given probability distribution, it is possible to define a random variable $Y = g(X)$, where X is uniformly distributed, that have the wanted distribution [73].

In this work, we use the GNU Scientific Library [75] to generate random numbers, by means of the Mersenne Twister generator. In the models discussed in this work, only two seeds are necessary (one for each heat bath). We then

number each simulation sample as l (see chapter 3), with $l = 1, 2, \ldots \mathcal{N}$, and use $2l$ and $2l + 1$ as the seeds.

A.4 Simulation parameters

We have four models to choose the parameters, QC, FKC, TSQC, and TSFKC. However, it is simple to see how the TSQC and TSFKC models are just generalizations of the QC and FKC models, respectively. We can actually get the latter by choosing $\mu = 2.0$, $A_L = A_R$ and $k_L = k_R = k_\mu$ in the former. This means that in all simulations, we can use the same equations of motion but with a suitable choice of parameters.

In all the simulations, all particles have the same mass, so $m_n = m$ for $n = 1, 2, \ldots, N$. As a simplifying assumption, the scale factors are chosen so that all cases also have $m = 1.0$, $\gamma = 1.0$, and $a = a_s = 1.0$.

The velocity and momentum of a particle are related by $v_n = p_n/m_n$, but since in our case we assume unit masses, both will have the same value. This means that we can interpret the equations of motion interchangeably in terms of the velocities or the momenta, and the heat current can be calculated using the velocities.

Beyond that, instead of inputting the parameters directly in the simulation, we define some closely related ones that give us deeper physical understanding of the system. This was also done in order to more closely follow the work by Li, Wang and Casati [25].

Thus, to begin with, we define the mean temperature between the baths as $T_m = (T_L + T_R)/2$, and the temperature difference relative to T_m is given by $\Delta_{rel} = (T_L - T_R)/T_m$. These definitions can be rewritten as

$$T_L = T_m \left(1 + \frac{\Delta T_{rel}}{2}\right), \tag{A-64}$$

$$T_R = T_m \left(1 - \frac{\Delta T_{rel}}{2}\right). \tag{A-65}$$

The ratio between the force strengths of the left and right segments of the chain is considered to be constant and equal to λ, so $\lambda = k_R/k_L = A_R/A_L$. For the homogeneous systems QC and FKC, $\lambda = 1.0$ always.

It is also important to define the parameters of the numerical algorithm, which are the integration time step δt, the total simulation time t_{max} (being δt multiplied by the total number of steps in the simulation) and the number of independent sample paths $\mathcal{N}$ in the ensemble on which we will take thermodynamic averages.

For each sample path, we measure the kinetic temperature and the heat current along the chain as a time average after an interval of time we call the transient time t_{trans}.

The last parameter to take in consideration is the number of particles in the chain, N. For the two-segment models, each segment always has $N/2$ particles.

B
Linear regression of temperature profiles

When simulating heat conduction, a purely harmonic particle chain gives a flat temperature profile. To obtain the linear profile expected by Fourier's law, when κ does not depend on the temperature, in this work we add an anharmonic on-site potential, so that the system does not conserve momentum.

However, the exact temperature profile depends on the parameters of the chain. Some choices of parameters still give a flat profile, due to the harmonic interaction dominating the dynamics (we show this in chapter 3).

Thus, it is natural to question ourselves when the transition happens, from mainly harmonic behavior to normal conduction. To try to see this happening, we check the slope of the temperature profile for each choice of parameters. This slope is calculated by using least-squares linear regression [76], specifically the SciPy implementation [77], on the chain, excluding the particles in contact with the heat baths (to avoid the Kapitza resistance discontinuity).

Here we show the results of the linear regression when varying the number of particles N in the chain, for both models. How well the linear regression describes the data is given by the determination coefficient [76], r^2, that is calculated by squaring the correlation between the particle number i/N and the temperature $T(i/N)$.

B.1
ϕ^4 model varying N

In the following figures, we give the results of the linear regression for the ϕ^4 model. The values for the number of particles N, the determination coefficient r^2, the slope and the intercept, are given in the legend. In most cases, the temperature profile shows a clear convexity, but it is so small that the $r^2 > 0.9$, showing a good linear approximation. So using the slope to see when the profile stop being flat should be a good approximation.

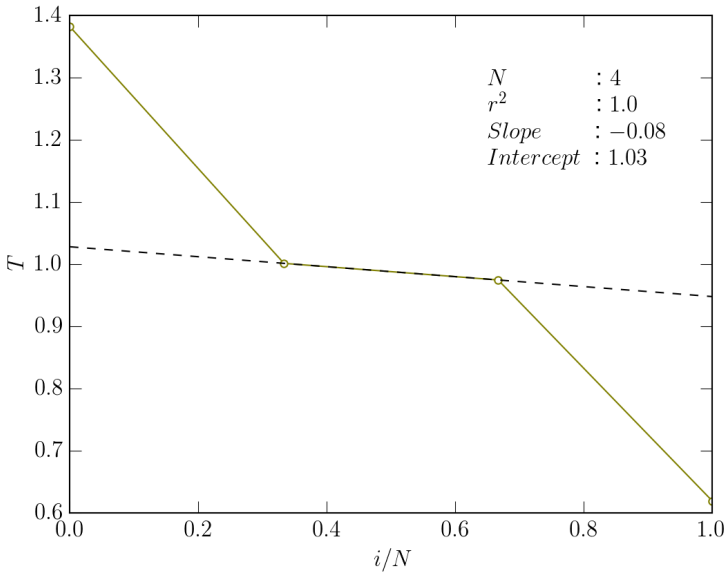

Figure B.1: Linear regression, for the ϕ^4 model of heat conduction, with $N = 4$, $A_Q = 1.0$, $k = 1.0$, $T_m = 1.0$ and $\Delta_{rel} = 1.0$. The dashed line is the regression, while the solid line is the simulated points.

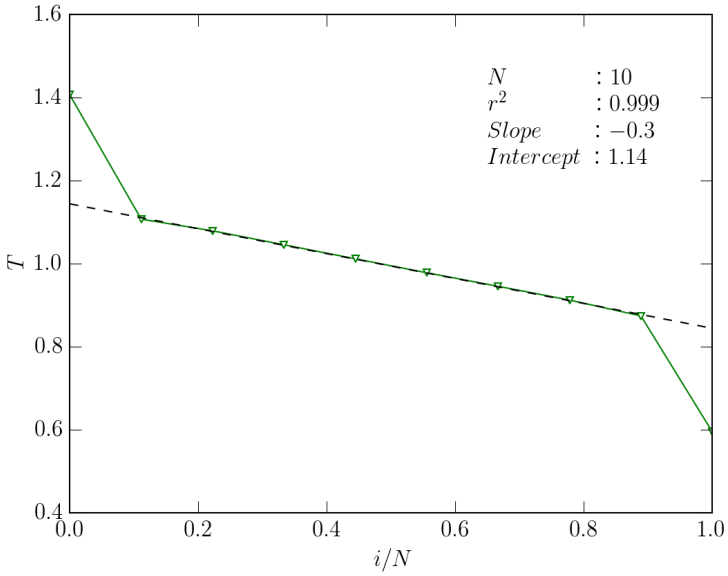

Figure B.2: Linear regression, for the ϕ^4 model of heat conduction, with $N = 10$, $A_Q = 1.0$, $k = 1.0$, $T_m = 1.0$ and $\Delta_{rel} = 1.0$. The dashed line is the regression, while the solid line is the simulated points.

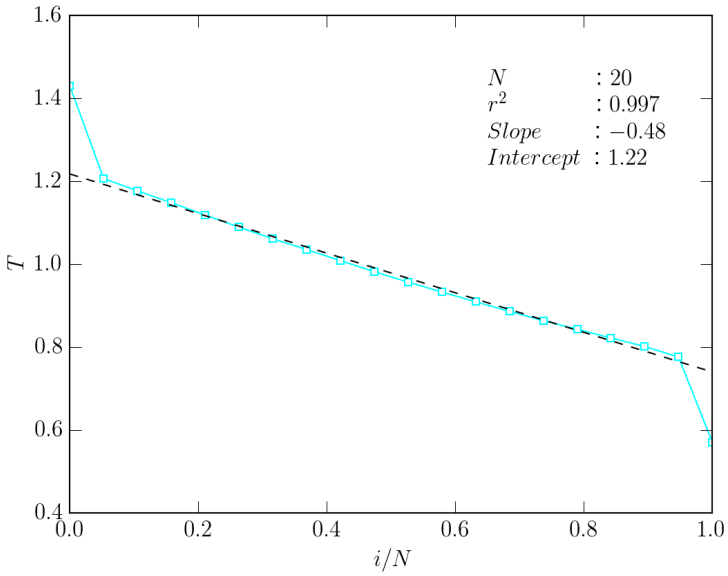

Figure B.3: Linear regression, for the ϕ^4 model of heat conduction, with $N = 20$, $A_Q = 1.0$, $k = 1.0$, $T_m = 1.0$ and $\Delta_{rel} = 1.0$. The dashed line is the regression, while the solid line is the simulated points.

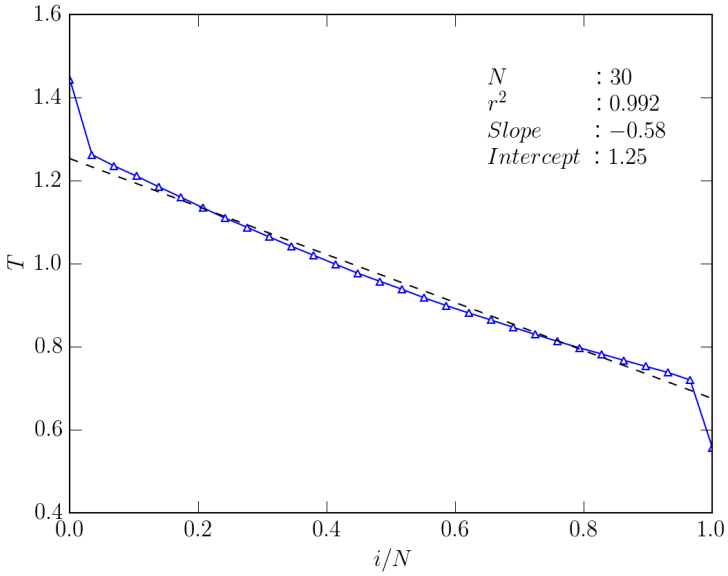

Figure B.4: Linear regression, for the ϕ^4 model of heat conduction, with $N = 30$, $A_Q = 1.0$, $k = 1.0$, $T_m = 1.0$ and $\Delta_{rel} = 1.0$. The dashed line is the regression, while the solid line is the simulated points.

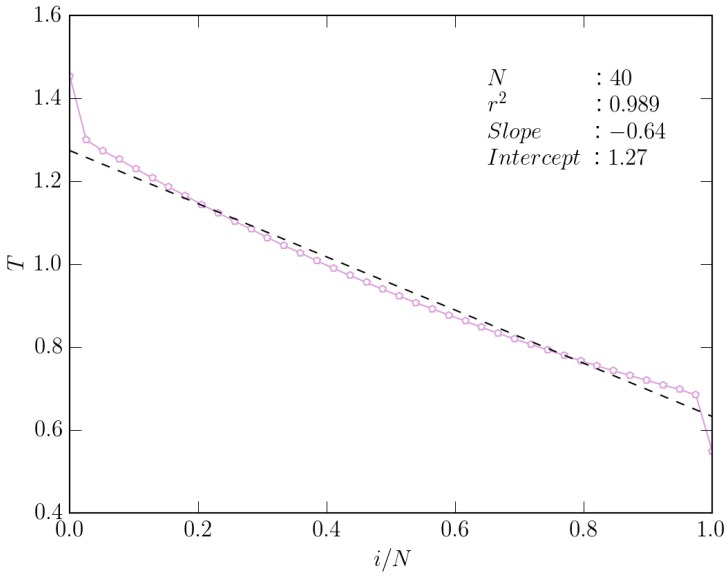

Figure B.5: Linear regression, for the ϕ^4 model of heat conduction, with $N = 40$, $A_Q = 1.0$, $k = 1.0$, $T_m = 1.0$ and $\Delta_{rel} = 1.0$. The dashed line is the regression, while the solid line is the simulated points.

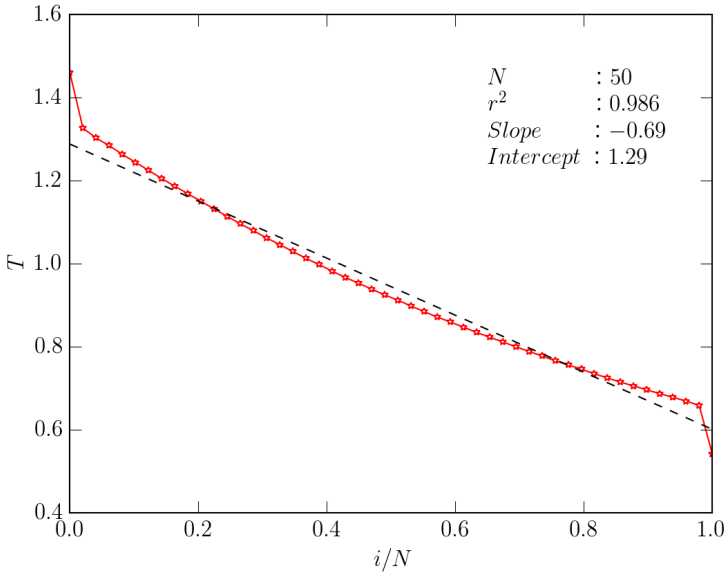

Figure B.6: Linear regression, for the ϕ^4 model of heat conduction, with $N = 10$, $A_Q = 1.0$, $k = 1.0$, $T_m = 1.0$ and $\Delta_{rel} = 1.0$. The dashed line is the regression, while the solid line is the simulated points.

B.2
Frenkel-Kontorova model varying N

Linear regression results for the Frenkel-Kontorova model. As for the ϕ^4 mode, N, r^2, the slope and the intercept, are shown in each figure. The temperature profiles in this case also show a clear convexity, although, for the linear approximation, we have $r^2 > 0.9$, because the curvature is small.

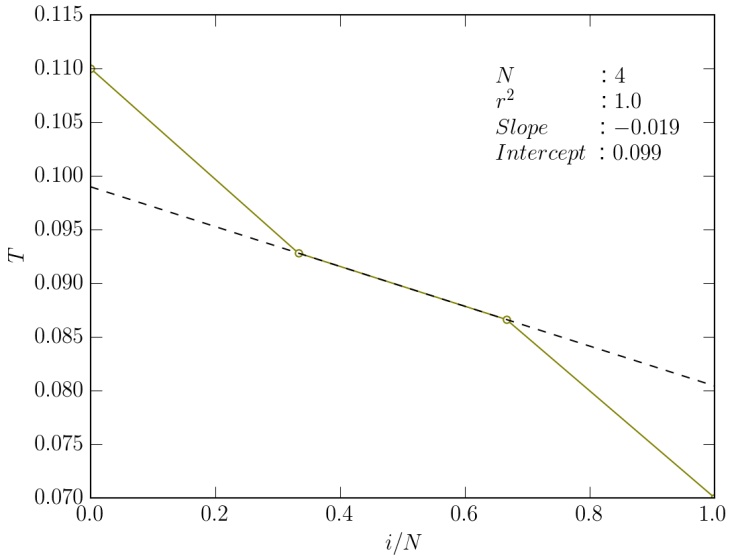

Figure B.7: Linear regression, for the Frenkel-Kontorova model of heat conduction, with $N = 4$, $A_Q = 5/2\pi$, $k = 1.0$, $T_m = 0.09$ and $\Delta_{rel} = 0.5$. The dashed line is the regression, while the solid line is the simulated points.

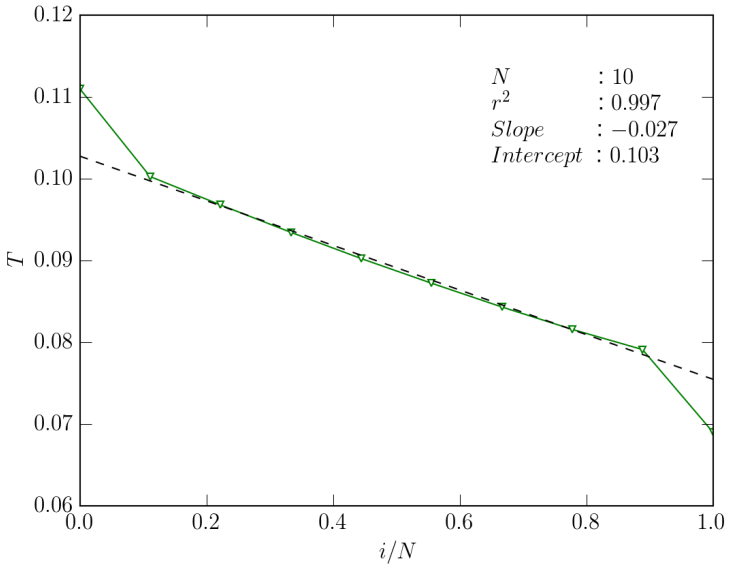

Figure B.8: Linear regression, for the Frenkel-Kontorova model of heat conduction, with $N = 10$, $A_Q = 5/2\pi$, $k = 1.0$, $T_m = 0.09$ and $\Delta_{rel} = 0.5$. The dashed line is the regression, while the solid line is the simulated points.

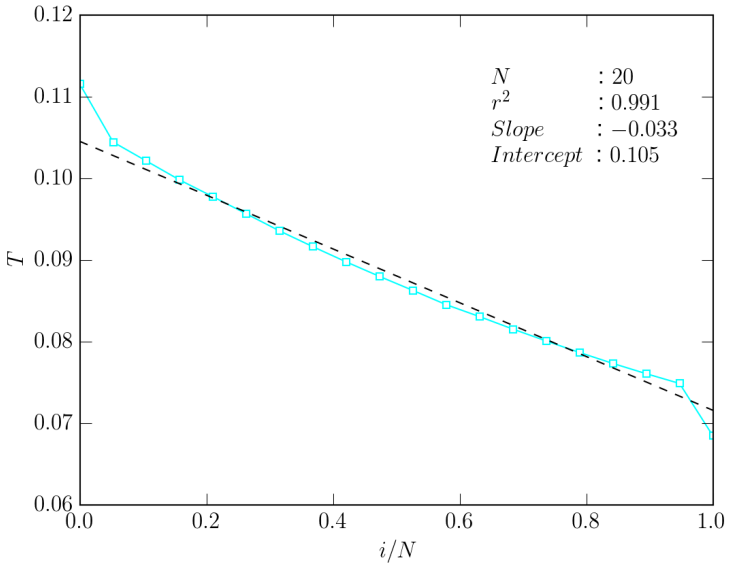

Figure B.9: Linear regression, for the Frenkel-Kontorova model of heat conduction, with $N = 20$, $A_Q = 5/2\pi$, $k = 1.0$, $T_m = 0.09$ and $\Delta_{rel} = 0.5$. The dashed line is the regression, while the solid line is the simulated points.

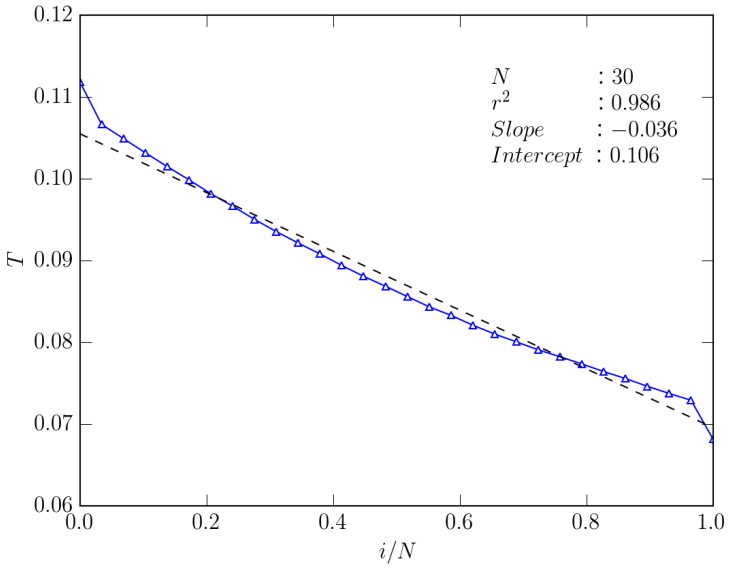

Figure B.10: Linear regression, for the Frenkel-Kontorova model of heat conduction, with $N = 30$, $A_Q = 5/2\pi$, $k = 1.0$, $T_m = 0.09$ and $\Delta_{rel} = 0.5$. The dashed line is the regression, while the solid line is the simulated points.

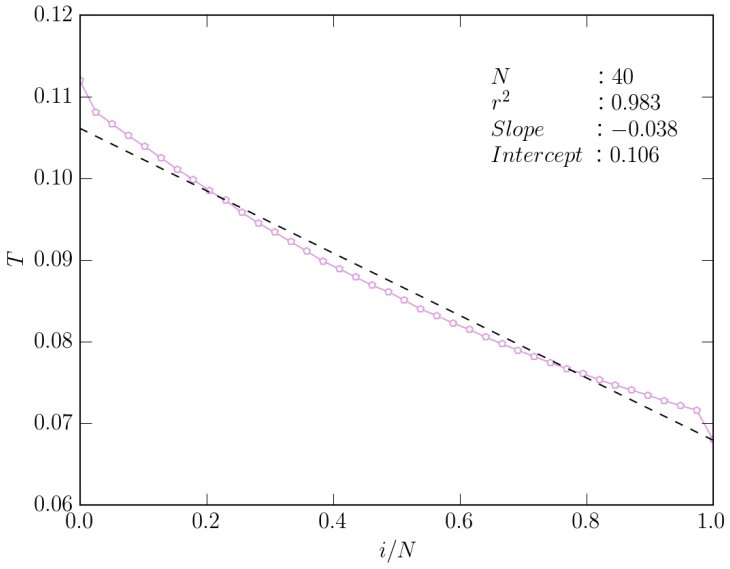

Figure B.11: Linear regression, for the Frenkel-Kontorova model of heat conduction, with $N = 40$, $A_Q = 5/2\pi$, $k = 1.0$, $T_m = 0.09$ and $\Delta_{rel} = 0.5$. The dashed line is the regression, while the solid line is the simulated points.

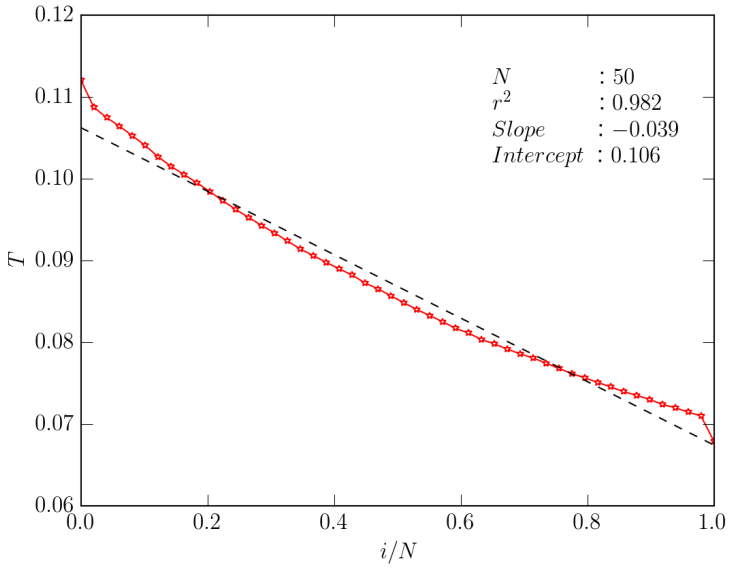

Figure B.12: Linear regression, for the Frenkel-Kontorova model of heat conduction, with $N = 50$, $A_Q = 5/2\pi$, $k = 1.0$, $T_m = 0.09$ and $\Delta_{rel} = 0.5$. The dashed line is the regression, while the solid line is the simulated points.